11-15-2017

Nonlinear Model-Based Control for Neuromuscular Electrical Stimulation

Ruzhou Yang
Louisiana State University and Agricultural and Mechanical College

NONLINEAR MODEL-BASED CONTROL FOR NEUROMUSCULAR ELECTRICAL STIMULATION

A Dissertation

Submitted to the Graduate Faculty of the
Louisiana State University and
Agricultural and Mechanical College
in partial fulfillment of the
requirements for the degree of
Doctor of Philosophy

in

The Department of Mechanical Engineering

by
Ruzhou Yang
B.S., Mechanical Engineering, Southwest Jiao Tong University, China, 2011
December 2017

Acknowledgements

I would like to express sincere appreciation to my advisor, Dr. Marcio de Queiroz, who opened a magic window and kept guiding me to such a fascinating area of nonlinear control theory and applications. Without his guidance and persistent help, this dissertation would not have been possible. I would also like to thank my committee members, Dr. Hunter Gilbert, Dr. Wanjun Wang, and Dr. Mark Boyer, for their time and valuable suggestions and comments. I am also thankful to the LSU Department of Mechanical and Industrial Engineering for their financial support. My gratitude also goes to my parents, my best friends, Dr. Zhichao Xue and Milad Khaledyan, and my love, Xin Zhou for their selfless help and support. Finally, I cannot forget to thank AcFun, Amazon, Bilibili, Facebook, YouTube and Zhihu. It was their company and service that encouraged me to keep going on my research during all these tough days.

Table of Contents

List of Figures

Abstract

Neuromuscular electrical stimulation (NMES) is a technology where skeletal muscles are externally stimulated by electrodes to help restore functionality to human limbs with motor neuron disorder. This dissertation is concerned with the model-based feedback control of the NMES quadriceps muscle group-knee joint dynamics. A class of nonlinear controllers is presented based on various levels of model structures and uncertainties. The two main control techniques used throughout this work are backstepping control and Lyapunov stability theory.

In the first control strategy, we design a model-based nonlinear control law for the system with the exactly known passive mechanical that ensures asymptotical tracking. This first design is used as a stepping stone for the other control strategies in which we consider that uncertainties exist. In the next four control strategies, techniques for adaptive control of nonlinearly parameterized systems are applied to handle the unknown physical constant parameters that appear nonlinearly in the model. By exploiting the Lipschitzian nature or the concavity/convexity of the nonlinearly parameterized functions in the model, we design two adaptive controllers and two robust adaptive controllers that ensure practical tracking.

The next set of controllers are based on a NMES model that includes the uncertain muscle contractile mechanics. In this case, neural network-based controllers are designed to deal with this uncertainty. We consider here voltage inputs without and with saturation. For the latter, the Nussbaum gain is applied to handle the input saturation.

The last two control strategies are based on a more refined NMES model that accounts for the muscle activation dynamics. The main challenge here is that the activation state is unmeasurable. In the first design, we design a model-based observer that directly estimates the unmeasured state for a certain activation model. The second design introduces a nonlinear filter with an adaptive control law to handle parametric uncertainty in the activation dynamics. Both the observer- and

filter-based, partial-state feedback controllers ensure asymptotical tracking.

Throughout this dissertation, the performance of the proposed control schemes are illustrated via computer simulations.

Chapter 1 Introduction

1.1 Motivation

Neuromuscular electrical stimulation (NMES), or functional electrical stimulation (FES), refers to a promising technique where skeletal muscles are externally stimulated in order to restore functional tasks in persons with movement disorders [111]. The idea behind NMES stems from the principle of voluntary muscle contraction of human beings. Skeletal muscles —the main part of human voluntary muscles— are controlled by the central nervous system on their contraction. Signals in the form of action potentials are sent by the brain through the nervous system to specialized cells (motor neurons) that cause a series of chemical reactions and an ion exchange through the fiber membrane in a specialized junction (synapse). This transient change in membrane potential is the action potential. This condition promotes the release of Ca^{2+} ions, which invokes cross-bridge formation and innervates the muscle fibers. The cross-bridge cycle repeats itself as long as the action potential exists. When the stimulation stops, the Ca^{2+} ions return back into the sarcoplasmic reticulum, preventing cross-bridge formation in the relaxed state [43, 89]. When upper motor neuron diseases occur (e.g., stroke and spinal cord injuries [112]), the action potentials are prevented from being sent to the corresponding motor neuron due to nervous system dysfunctions. This has motivated the idea of directly delivering a series of artificial, external electrical stimuli to the neural tissue to generate the desired response of the nerve and help restore the muscle-limb functionality. This is accomplished via skin or implanted electrodes which upon voltage excitation produce muscle contraction and consequently joint torque and limb motion.

As a key technology for realizing neuroprosthetic devices, NMES is an active area of investigation in the biomedical and rehabilitation engineering research communities. In the early 1960s, FES was used for the first time on the quadriceps and glutei muscles via surface electrodes

to assist standing without additional mechanical bracing for people with selected central nervous system (CNS) damage [54, 72]. In the following decades, NMES has been shown to restore lower extremity function in paraplegia patients [25, 35, 65, 81]. Implanted neuroprostheses have been in clinical use for several essential activities, such as breathing and urinating, to improve the lives of people with spinal cord injury [92, 93]. In 1996, multichannel implanted stimulators with epineural and/or epimyisal electrodes were developed in several research projects [94] to provide a higher level of selectivity and modulation of muscle stimulation [29]. In more recent studies, NMES is reported to have been used in the rehabilitation of patients with congestive heart failure as a new training method for avoiding dyspnea, a side effect that can be brought during conventional exercise-training modalities [114]. The rapid development of NMES techniques has lead to the combination of FES and motorized lower extremity exoskeletons [60], including the ReWalk system [27], Mina [88], and the Vanderbilt exoskeleton [28]. Related researches on hybrid FES/electric motor gait restoration devices can be found in [8, 42, 59, 100].

Control of NMES systems is a challenging problem because the system dynamics are nonlinear and highly uncertain. This is due to a variety of reasons, including the unkown full mechanism of muscle force generation, muscle fatigue, stimulus response time delay, changing muscle geometry under electrodes in non-isometric conditions, and limited force production in the stimulated muscles [102, 109, 112]. In light of these challenges, researchers continue to investigate effective NMES control strategies as outlined in the literature review that follows.

1.2 Literature Review

Due to its challenging nature, the NMES control problem has served as a platform throughout the years for the application of numerous control theoretical methods.

1.2.1 Non-Model-Based Control

In many NMES applications in physical therapy clinics, open-loop control [29, 46, 82, 118] is used because of its simplicity. Traditional linear feedback methods such as a PID control have

also been applied [1, 61, 68, 69, 78]. As was reported in [51, 107], the above approaches either fail to guarantee closed-loop stability or produce unsatisfactory results. Additionally, trial-and-error adjustments to control parameters during experimentation inevitably increase the number of experiments and fatigue of the patient. An early review of NMES control methods can be found in [18].

1.2.2 NMES Dynamics

One impediment for the application of more sophisticated feedback control techniques is the difficulty in understanding and modeling the nonlinear physiological and mechanical dynamics of muscle stimulation, activation and contraction. One of the first modeling results is Hill's work in the 1930's [47], which was based on input-output data obtained from experiments. The activated muscle was represented by a lumped-parameter model consisting of a contractile element (CE) surrounded by "passive" connective tissue both in series and parallel. More specifically, equations were proposed representing CE tension-length and CE force-velocity relationships. Since Hill's work, the identification and modeling of muscle dynamics has received considerable attention from various research groups; see, for example, [23, 24, 26, 29, 34, 44, 45, 76, 70, 101, 108, 115]. In [29, 76, 115], the human lower-limb dynamics was modeled using a pendulum-like experiment where the limb was moved against gravity and then dropped while the knee joint angle and torque were measured. In [23], a Hill-based model was used for the human musculotendon system but with a reverse-order recruitment dynamics for the FES system and a new heterogeneous model structure for the CE. In [34], the off-line identification of lower leg passive dynamics was considered and a nonlinear elastic term was reported to improve the prediction capability of the model. In [44, 45], Hatze proposed a high-order nonlinear musculotendon model where 50 parameters were required to describe the motion of a single joint. This model was reported to effectively describe many nonlinear behaviors [123, 135]. Reviews of muscle dynamics modeling and identification can be found in [57, 103, 123, 132].

1.2.3 Model-Based Control

As one would expect, the development of model-based NMES controllers has grown with the better understanding of the NMES dynamics. This body of work includes adaptive control [3, 13, 63], sliding mode control [51, 60], robust control [83, 110, 111], backstepping control [107], optimal control [22, 121, 113, 117], neural network control [41, 104, 112, 109], and fuzzy logic control [102]. In [3], a low-dimensional adaptive controller was proposed for a redundant hybrid neuroprosthesis by first transforming the original muscle stimulation dynamics into a lower-dimensional system with principal component analysis. Bernotas et al. [13] designed a discrete-time adaptive controller based for a electrically-stimulated cat tibialis anterior muscles, and its performance was evaluated on the basis of the stability and response to step, ramp and sinusoidal inputs. Jezernik et al. [51] designed a sliding mode controller that accounted for the second-order Ca^{2+} dynamics. In [110], a dynamic robust control was designed to compensate for uncertainties in the muscle-knee joint mechanical dynamics and stimulation dynamics. In [112, 109], system uncertainties were handled by employing a neural network-based controller. Some control schemes have been proposed to account for the system state/input time delay and muscle fatigue. For example, input time delay was compensated using Lyapunov-Krasovski functionals combined with robust controllers in [4, 5, 83, 98, 111]. A known, constant input delay was compensated by a predictor-based hybrid controller in [55]. Sharma and co-workers [12, 60, 59] showed that muscle fatigue of lower limbs during walking or swinging can be attenuated and delayed by a motor assist from a neuroprosthestic system using the feedback linearization technique. A model predictive controller and a second-order sliding mode controller were proposed in [12] and [60], respectively, after the muscle-joint model was linearized.

1.2.4 Adaptive Control for Nonlinearly Parametrized Systems

The NMES mechanical dynamics contains uncertain parameters that appear nonlinearly in the elastic and damping terms, i.e., it is a *nonlinearly parametrized* system. This makes the

use of adaptive control more difficult since classical adaptive schemes require the unknown parameters to appear linearly in the system model. As a result, most advanced NMES controllers that compensate for modeling uncertainties compensate for functional uncertainties; e.g., the neural network controllers in [41, 104, 112, 109] and the robust-like controllers in [51, 111]. One can argue that if the uncertainties are only parametric in nature, then such controllers are unnecessarily complex and conservative. Note that the adaptive controller in [63] assumes the NMES mechanical parameters appear linearly, while the adaptive controllers of [3, 13] use the update law to tune control parameters, not unknown plant parameters.

The design of adaptive controllers for nonlinearly parametrized systems is a nontrivial task. Since the mid 1990's, some researchers have worked in this area and devised many interesting results. For example, [91] proposed an adaptation scheme for stabilization of systems with concave parameterizations. In [11], a min-max adaptive controller was designed for first-order nonlinear systems with concave/convex parameterizations which ensures tracking with prescribed precision. This result was extended in [62] to second-order nonlinear systems with extended matching condition. The concave/convex parameterization assumption of [11, 62] was removed in [77] to allow all nonlinear parameterizations where the parameters lie in a known compact set and appear through additive, continuous, scalar, nonlinear functions. In [86], it was shown how to convexify nonlinear parameterizations to enable the use of adaptive controllers for convexly parameterized nonlinear systems. The work in [33] proposed a semi-adaptive stabilization control law for convexly parameterized systems that switches between adaptive and robust controllers. In [87], an adaptive control for multilinearly parameterized systems was introduced that combines convex and concave reparameterizations to ensure stability. A simple, adaptive stabilization controller with a linear-in-parameter-like structure was designed in [50] for systems satisfying the extended matching condition with Lipschitzian parameterizations.

1.2.5 Adaptive Control for Systems with Unknown Control Coefficients

In comparison to the uncertain nonlinearly parametrized mechanical dynamics, the unknown muscle contractile and activation dynamics bring no less challenges. As is shown in Chapter 2 of this dissertation, the contractile and activation dynamics leads to functional uncertainties in the input channel. Therefore, the NMES adaptive control problem considering contractile and activation dynamics can be categorized as a system with unknown control coefficients.

The control of strict-feedback systems has attracted a wealth of ideas since the backstepping technique was proposed in [53] and extended in [67]. In [67], the adaptive backstepping technique was extended to strict-feedback systems with unknown, constant control coefficients. For the case where the control coefficients are unknown state-related functions, approximation-based adaptive control has been employed. The function approximation capability of neural networks were combined with adaptive control techniques in [39, 71, 96, 119, 125, 134] to retain the closed-loop stability properties in the presence of functional uncertainties. When applying neural networks to directly approximate the unknown control coefficient functions, the problem of loss of controllability inevitably arises because the approximated gains can approach to zero due to the neural network (NN) parameter adaptation. To overcome the singularity problem, [134] proposed a NN controller that incorporates an integral-type Lyapunov function where the signs and upper bounds of the control coefficients were assumed known. The use of the upper bound can potentially increase the control magnitude and lead to control saturation. In [39], a direct adaptive NN controller was introduced without the integral-type Lyapunov function but with more strict structural assumptions on the control coefficient; viz., the unknown control coefficient function is independent of certain system states. This assumption was relaxed in [119]; however, knowledge of the lower and upper bounds on the control coefficients were required. An alternative way to handle the singularity problem is to apply switching control [48, 49, 64, 130]. In [130],

a discontinuous, switching NN controller was proposed for single-input/single-output feedback linearizable systems where closed-loop stability was ensured by high gain feedback. Hysteresis switching strategies were introduced in [64] to avoid the singularity problem for fully linearizable systems; however, the control could cause chattering. The control discontinuity was removed in [49], where a smooth switching scheme between an adaptive linearizing control and a robust control around the singularity was applied.

In the context of NMES control, [17, 112, 121] used a dynamic robust controller combined with a NN feedforward term to deal with the unknown control coefficient and other modeling uncertainties. These results required high gain feedback to ensure stability. In [107], an online approximation of the nonlinear muscle contractile function was performed by a Normalized Radial Basis Function network which was then used in the backstepping control. In [2], a continuous switching between a NN controller with a single neuron and a sliding mode controller coupled to a recurrent NN was presented. Although the singularity problem was not an issue in [2] since the unknown control coefficient was simply estimated by a function without any adaptation, closed-loop stability was not guaranteed due to the optimization-based backpropagation learning algorithm of the recurrent NN.

1.2.6 Adaptive Control for Systems with Input Saturation

Like many practical systems, NMES control is subject to control input saturation. That is, the input signals are naturally constrained by physical limits; e.g., the stimulus voltage is limited to a range of values, or the pulse width of the stimulus signals delivered by electrodes is required to be non-negative and upper bounded. A control strategy that does not account for input saturation may result in degraded performance or loss of stability [116]. The input saturation problem is more challenging when an adaptive control scheme is used. In [36], it was mentioned that input saturation can have an adverse effect on the parameter update laws, leading to the deterioration of the control performance even in the unsaturated region.

In the past several decades, numerous design and analysis methods for adaptive control with input saturation were developed. For linear systems, two approaches are often used [14, 15, 136]. The first approach aims at minimizing the effects of input saturation by adding a compensation term to the *nominal* control (i.e., control design without considering input saturation) [136, 31]. The second approach is to correct the inconsistency between the controller output and the states of the controller by modifying the controller inputs [9, 10, 15, 56]. For nonlinear systems, the so-called *Nussbaum gain* has been used to handle input saturation [16, 36, 74, 122, 137, 138]. The Nussbaum gain was originally proposed in [90] during the design of an adaptive controller for a class of first-order linear systems without a priori knowledge of the sign of the control coefficients. Since then this method has been broadly used in adaptive control of systems with unknown control directions or unknown control coefficients [38, 73, 79, 129]. The Nussbaum gain is applicable when the derivative of the saturated input function is involved. In [122], two robust adaptive backstepping controllers with Nussbaum-type gains were proposed and closed-loop stability was proven by utilizing the properties of the Nussbaum functions. In [122], the saturated input was approximated by the hyperbolic tangent function plus an uncertainty, and the control design required an input filter that increased the system order. In [137], the Mean Value theorem was cleverly applied to avoid increasing the system order while using Nussbaum functions in the backstepping design process.

Few results exist in the NMES control literature that deal with input saturation. To the author's best knowledge, the first consideration of input saturation was in [51], where a sliding mode control was designed for a NMES model represented by the second-order passive dynamics and the second-order Ca^{2+} concentration dynamics. However, the control input in [51] was not assured to remain within the amplitude constraints. In [109], the NMES system with input saturation was considered including the first-order muscle fatigue dynamics and the first-order

activation dynamics. Unfortunately, closed-loop stability was only validated in the unsaturated region. Similar to [109], the more recent papers [6, 7] released an unsuccessful attemption to prove closed-loop stability regardless of the consideration of input saturation.

1.3 Dissertation Organization

We begin by introducing in Chapter 2 the full-order dynamic model of the quadriceps muscle group-knee joint stimulation system, which is composed of three subsystems: the passive mechanical dynamics, the knee joint contractile mechanics, and the muscle activation dynamics. Simplified versions of this full-order model will be used in the control designs of the following chapters.

In Chapter 4, a nonlinear tracking control strategy is proposed for the passive mechanical dynamics only where all nonlinear functions and parameters are assumed known. The control design is based on the backstepping technique [67], and an integral-type Lyapunov function is used to prove asymptotic tracking without violating the physical limits on the knee joint angular position. The purpose of this controller is to present the basic control design procedure that will be later extended to account for model uncertainties and more complete system models.

In Chapter 5, two solutions to the NMES *adaptive* tracking control problem with nonlinear parameterization are presented. We again consider only the passive mechanical dynamics. In Section 5.1, we use the approach in [50] to exploit the Lipschitzian parameterization of the NMES mechanical model to compensate for parametric uncertainties. The resulting discontinuous adaptive control ensures asymptotic tracking for angular position of the knee joint without violating its physical limits. In Section 5.2, we propose an alternative solution to the adaptive tracking control problem for the nonlinearly parametrized limb dynamics. Here, we take explicit advantage of the concavity or convexity of the model functions with respect to the nonlinear parameters. The foundation for the second design is the adaptive strategy introduced in [9, 62]; however, we introduce a few modifications to simplify the resulting control algorithm. Since our

mechanics dynamics are of order two, we first employ a filtered tracking error [21] to convert it into a first-order system. We also bypass the min-max optimization procedure since our main control objective is closed-loop stability. Finally, we utilize a simple projection algorithm on some of the parameter estimates which facilitates the Lyapunov stability analysis and control implementation. The adaptive control in this section is continuous and shown to ensure practical tracking for the angular position/velocity of the limb. Simulation results are provided to demonstrate the performance of both adaptive controllers. The main contribution of this chapter is that, to the best our of knowledge, the proposed adaptive controls are the first to directly account for the nonlinearly parameterized dynamics of the human shank-knee joint. The work in this chapter appeared in [126, 127].

In Chapter 6, we present two *robust adaptive* tracking control designs for the nonlinearly parameterized shank dynamics in the presence of disturbance torques based on the strategies proposed in Chapter 5. Our first design modifies the discontinuous adaptive control in Section 5.1 by replacing the signum function with a hyperbolic tangent function. A robust term is applied to handle the disturbance torques and the error caused by the function replacement. The second robust adaptive controller is based on the concavity or convexity of the model functions. Different from the adaptive approach in Section 5.2, we simplify the design of the tuning functions by removing the numerical solution of some nonlinear functions to alleviate the computational burden. For both controllers, we prove practical tracking for the angular position of the shank. A verification of the control performance is provided in the form of computer simulations, where the proposed control algorithms are compared with the dynamic robust control from [112]. The main contributions of this chapter are: 1) The robust adaptive techniques can compensate for external disturbances and unmodeled elastic effects; and 2) Both control laws are continuous, which is required for further control design extension and implementations.

In Chapter 7, we propose two NN-based control strategies for the NMES dynamic model where the passive mechanical dynamics and the unknown muscle contractile mechanics are considered simultaneously. The first design is based on the integral-type Lyapunov function proposed in [134] that avoids the singularity problem in the control coefficient estimation. The NN approximation is used to estimate all uncertainties in the dynamics while initial condition sensitivity is attenuated by modifying the integral-type Lyapunov function. We then propose a new NN-based controller that accounts for input saturation. The second control law is based on the Nussbaum gain and is capable of handling the input saturation without performance degradation. Both controllers ensure practical tracking for the shank position. Again, the control performance is illustrated by computer simulations. The contributions of this chapter include: 1) High gain feedback is not required for compensating for the uncertainties in the NMES model; 2) Large control input transients can be attenuated; and 3) We rigorously account for input saturation in the control design and analysis.

In Chapter 8, we augment the NMES model from Chapter 7 with the muscle activation dynamics. Under the assumption that the state of the activation dynamics is unmeasurable, we present two *partial-state* feedback control strategies for stabilizing the resulting, third-order NMES model. In the first design, we assume exact model knowledge and use a model-based state observer to estimate the unmeasurable state. A model-based controller based on the estimated state is formulated to guarantee asymptotic tracking. In the second design, we consider that muscle activation dynamics is subject to parametric uncertainty. In this case, we apply a filter design inspired by [67] coupled with an adaptive control law to again prove asymptotic tracking. Simulations are conducted to demonstrate the performance of the filter-based partial-state feedback controller. The contribution of this chapter is that a rigorous stability analysis is conducted for combined observer/filter-controller system.

Finally, conclusions and directions for future work are presented in Chapter 9.

Chapter 2 Muscle-Joint Stimulation Dynamics

The foundation of any model-based controller is an accurate mathematical model of the dynamic system under control. In the case of the NMES system, the derivation of such a model is virtually hard to achieve even for a single muscle-joint dynamics of the human shank due to the complex relationships of the electrical stimulus-muscle activation, muscle length-force, contraction velocity-force, and muscle-joint stiffness and damping effects. In this chapter, we present the full-order, nonlinear physiological and mechanical dynamics of the quadriceps muscle group-knee joint stimulation based on what is known in the literature. The resulting full-order model has order four with some of its terms being determined empirically via experimentation.

2.1 Overview

This section provides an overview of the nature of the electrically-stimulated quadriceps muscle-joint system. The physiological and mechanical phenomena includes two levels: passive dynamics and active dynamics. The *passive dynamics,* also known as the body-segmental mechanical dynamics, represents the macroscopic body-segment movements governed by Newton's second law. Similar to most robot manipulator dynamics, passive dynamics in muscle-joint systems describes the relationship between the torque and joint angle by a second-order differential equation including elastic, viscous (damping), and gravitational joint moments. The control input of the passive dynamics is the torque applied to the joint. See Figure 2.1(c) for a block diagram of the passive dynamics.

The active dynamics, on the other hand, describes the generation of the joint torque from the electrode stimulus. These dynamics include two distinct mechanisms that interact to determine the force developed by the quadriceps muscle group: 1) the activation dynamics and 2) the contractile mechanics. For a patient suffering a disconnection between the quadriceps motor neurons and CNS, the activation dynamics refers to the release of nerve action potentials by means of NMES,

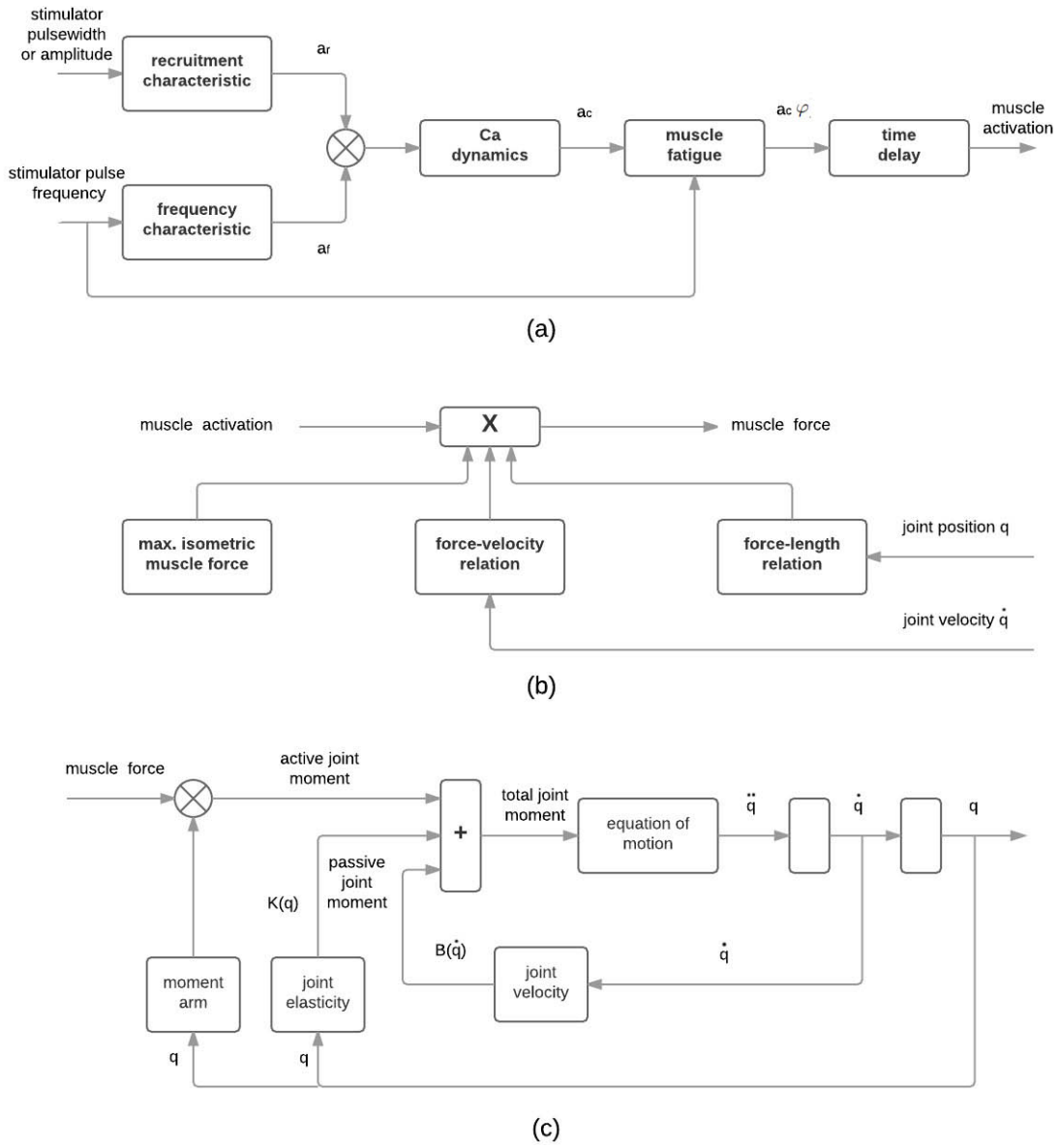

Figure 2.1: (a) the activation dynamics; (b) contractile mechanics; (c) passive dynamics.

which affects the muscle force by the state of muscle activation. Although NMES is often regarded as "muscle stimulation", the electrical stimulus activates the motor neurons rather than muscle fibers because the threshold for electrical stimulation of the motor axons is far below that of the muscle fibers [84]. In NMES, pulsed currents are applied as stimulus input signals. Each pulse releases a separate action potential in the neurons that are depolarized above the threshold [103]. Muscle force output is determined by the pulse amplitude, pulse duration, pulse frequency, and the muscle fatigue state [17]. Pulse amplitude and duration determine the total number of motor neurons that are recruited and is referred to as spatial summation. Each pulse can cause a twitch in the muscle fibers. An interesting phenomenon occurs when a subsequent pulse is applied before the previous twitch finishes. In this case, the two twitches superimpose and a higher muscle force is generated. This effect is often called temporal summation. When the pulse frequency is higher than a threshold called fusion frequency, a continuous muscle force output can be achieved [17]. However, a higher frequency may cause faster muscle fatigue. Therefore, modulation of the pulse amplitude and width is usually used in NMES control while the pulse frequency is kept constant and as low as possible to maintain a continuous force output [93]. The muscle activation status is consequently considered as the product of the spatial summation (a nonlinear recruitment curve of the pulse duration/amplitude-activation relationship) and the temporal summation (a nonlinear frequency-activation relationship), which serve as an input to the Ca^{2+} dynamics [45]. A fatigue model can be incorporated given that the muscle fatigue state increases with rising pulse frequency. The time delay factor can also be taken into consideration given the finite conduction velocities in the membrane system and delays from the chemical reactions involved [102]. See Figure 2.1(a) for a block diagram of the activation dynamics.

Contractile mechanics determines the forces generated in response to changes in muscle length when the level of activation remains constant [57]. The contractile mechanics in quadriceps are

computed as a function of the maximum isometric muscle force (the contraction force tested under the condition of constant muscle length), a normalized force-length relationship, and a normalized force-velocity relationship. The interactions between the contractile mechanics and the activation dynamics were studied in [57], although the full nature of these interactions is not fully understood. Specifically, the contractile mechanics is known to change dramatically based on the level of activation, but the activation dynamics itself is affected by the contractile mechanics via a feedback mechanism. Since this feedback interaction is poorly understood, it is not considered here. See Figure 2.1(b) for a block diagram of the contractile mechanics.

2.2 Mathematical Model

The full dynamic model of the quadriceps muscle group is presented in this section. For simplicity, the quadriceps muscle group is considered as a single muscle.

2.2.1 Passive Dynamics

Based on the principles introduced in previous Section 2.1, we consider the following musculoskeletal passive dynamics for the shank using the leg extension machine from [29, 34, 111]

$$J\ddot{q} + K(q) + B(\dot{q}) + G(q) = \tau \tag{2.1}$$

where $q(t) \in \mathbb{R}$ represents the shank angular position about the knee joint,

$$K(q) = k_1 \exp(-k_2 q)(q - q_0) \tag{2.2}$$

is the elastic moment,

$$B(\dot{q}) = b_1 \dot{q} + b_2 \tanh(b_3 \dot{q}) \tag{2.3}$$

denotes the damping moment,

$$G(q) = mgl \sin(q) \tag{2.4}$$

is the gravitational moment, $\tau \in \mathbb{R}$ is the torque created by electrode stimulation of the quadricep muscles, J and m represent the constant inertia and mass of the shank/machine combination, respectively, and l is the distance between the knee joint and center of the mass of

the shank/machine. All elastic parameters k_i and damping parameters b_i in (2.2) and (2.3) are positive and constant. The leg extension machine in [29, 34, 111] was designed with the user in sitting position such that the vertical position for the free-swinging shank is $q = 0$, and $q > 0$ when the knee joint extends (see Figure 2.2). Note that the human knee joint is not capable of moving beyond the following approximate limits

$$|q(t)| < \frac{\pi}{2}, \ \forall t \geq 0. \tag{2.5}$$

Also, notice that the elastic moment $K(q)$ does not vanish at $q = 0$ because of the existence of a non-zero, resting knee angle q_0 [29].

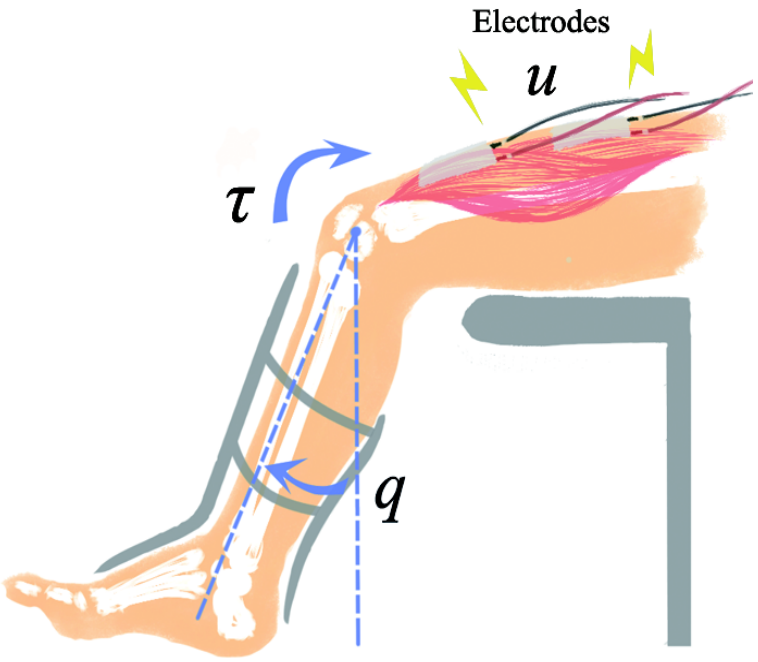

Figure 2.2: Depiction of the lower limb with electrode stimulation of the quadriceps muscle.

2.2.2 Contractile Mechanics

The torque acting on the knee joint is generated through the muscle tendon contraction force F_T by

$$\tau = \varsigma(q) F_T \tag{2.6}$$

where $\varsigma(q) \in \mathbb{R}$ is the moment arm that changes with the extension and flexion of the shank. The work in [102, 66] showed that the moment arm of the quadriceps muscle can be modeled by the

following continuously differentiable, positive, bounded function

$$\varsigma(q) = n_1 \exp\left(-n_2 q^2\right) \sin(q) + n_3, \tag{2.7}$$

where all n_i are positive constants. Note that the derivative of (2.7) with respect to q is also bounded. The force produced by the tendon is modeled as [102]

$$F_T = F \cos a_q(q) \tag{2.8}$$

where $F \in \mathbb{R}$ is the force generated by muscle fibers, $a_q(q)$ is the pennation angle between the tendon and the direction of the muscle fibers. Note that $a_q(q)$ is a continuously differentiable, positive, monotonic, bounded function with bounded first derivative [105]. The muscle force $F(q, \dot{q}, t)$ is defined as [102, 109]

$$F = F_m \eta_l(q)\, \eta_v(q, \dot{q})\, \varphi(t)\, a_c(t), \tag{2.9}$$

where $F_m \in \mathbb{R}$ is the constant maximum isometric muscle force, $\varphi(t) \in \mathbb{R}$ is the muscle fatigue state, $a_c(t) \in \mathbb{R}$ is the intermediate normalized muscle activation state, the nonlinear functions $\eta_l(q) \in \mathbb{R}$ and $\eta_v(q, \dot{q}) \in \mathbb{R}$ represent the normalized force-length and normalized force-velocity relations, respectively, defined as [102, 44]

$$\eta_l = \exp\left(-\left(\frac{\bar{l} - 1}{\varepsilon}\right)^2\right) \tag{2.10}$$

$$\eta_v = m_1 \arctan(m_2 \bar{v} + m_3) + m_4, \tag{2.11}$$

where $\bar{l} \in \mathbb{R}$ is the muscle length normalized with respect to the optimal muscle length l_{opt} (the muscle length at $F = F_m$), i.e., $\bar{l} = l_m / l_{opt}$ with $l_m = C + \int_0^q \varsigma(q) dq$, $C > 0$ being the muscle length, ε is called the shape factor, $\bar{v}$ is the muscle velocity normalized with respect to the maximum muscle contraction velocity $v_{\max}$, i.e., $\bar{v} = v / |v_{\max}|$ with $v = dl_m/dt$ denoting the muscle velocity such that $v < 0$ for muscle contraction. This accounts for the phenomena where the muscle force monotonically decreases when the contraction velocity increases and approaches zero as the contraction velocity is approaches $v_{\max}$. The muscle velocity v is related to the knee

angle q and angular velocity $\dot{q}$ by [102]

$$v = \dot{q}\varsigma(q). \tag{2.12}$$

2.2.3 Activation Dynamics

The muscle activation state can be modeled as a critically-damped, second-order linear system representing the release and absorption of Ca^{2+}. In [107], this critically-damped response was approximated by the following first-order equation for simplicity

$$\dot{a}_c = -wa_c + wa_r(u_w)a_f(u_f) \tag{2.13}$$

where $w > 0$ is the unknown time constant for Ca^{2+} dynamics, and $u_w(t), u_f(t) \in \mathbb{R}$ are the pulse width and pulse frequency modulation signals evoked from the external stimulation device, respectively. The nonlinear functions $a_r : \mathbb{R} \rightarrow [0,1]$ and $a_f : \mathbb{R} \rightarrow [0,1]$, which represent the recruitment process and frequency characteristic relations, respectively, are given by [101]

$$\begin{aligned} a_r(u_w) &= \rho_1[(u_w - u_{thr})\arctan(c_{thr}(u_w - u_{thr})) \\ &\quad - (u_w - u_{sat})\arctan(c_{sat}(u_w - u_{sat}))] + \rho_2 \end{aligned} \tag{2.14}$$

$$a_f(u_f) = \frac{(\upsilon u_f)^2}{1 + (\upsilon u_f)^2} \tag{2.15}$$

where $u_{thr} \in \mathbb{R}$ and $u_{sat} \in \mathbb{R}$ denote the pulse width values corresponding to the threshold and saturation, respectively (i.e., the minimum pulse width for which muscle contraction is observed when the shank is at rest position and at fully extended position, respectively), $c_{thr} \in \mathbb{R}, c_{sat} \in \mathbb{R}$ are positive constants selected to adjust the curvatures of the recruitment curve in the threshold and saturation areas , $\rho_1, \rho_2 \in \mathbb{R}$ are positive constants that scale the recruitment curve to ensure that $a_r(0) = 0$ and $a_r(u_w \rightarrow \infty) \rightarrow 1$, and f$\upsilon \in \mathbb{R}$ is the constant shape factor. Note that (2.14) is monotonic and continuous for all u_{thr}. Therefore, u_w can be uniquely determined by

$$u_w = a_r^{-1} \quad \text{for } 0 < a_r < 1 \tag{2.16}$$

where a_r^{-1} is the inverse function of (2.14). Since a constant and low pulse frequency u_f is

typically used during NMES control to delay the muscle fatigue, we consider $a_f(u_f) = B$ where $B \in (0,1)$ is a constant. From (2.13) and (2.14), it can be shown that $a_c(t) \in [0,1]$ for all $t \geq 0$.

The muscle fatigue variable $\varphi(t)$ is given by the following first-order differential equation [102, 101]

$$\dot{\varphi} = \frac{\lambda(u_f)}{T_f}(\varphi_{\min} - \varphi)a_c + \frac{1}{T_r}(1-\varphi)(1-\lambda(u_f)a_c) \tag{2.17}$$

where $T_f, T_r > 0$ are unknown time constants for the fatigue and the recovery phase in the quadriceps, respectively, $\varphi_{\min} \in [0,1]$ is an unknown constant representing the minimum fatigue state, $\lambda(u_f)$ is a function of the stimulation frequency defined as

$$\lambda(u_f) = 1 - \beta + \beta\left(\frac{u_f}{100}\right)^2, \quad \text{for } u_f < 100 \text{ Hz} \tag{2.18}$$

where $0 < \beta < 1$ is a constant shape factor. Notice that since $u_f(t)$ is considered a constant, $\lambda(u_f)$ from (2.18) is constant as well, and $\lambda(u_f) \in (0,1)$. Since $a_c(t) \in [0,1]$ for $t \geq 0$, it then can be shown that $\varphi \in [\varphi_{\min}, 1]$. Specifically, $\varphi = 1$ when the muscle is fully rested, and $\varphi = \varphi_{\min}$ when the muscle is fully fatigued [109].

The time delay of the muscle response to the stimulus is not considered in this dissertation. Readers are referred to [52, 83] and the references therein for information on the time delay issue.

Chapter 3 Mathematical Background

This chapter presents some mathematical definitions, notations, and results that will be used in the rest of the dissertation.

3.1 Lipschitzian Functions

The definition of a Lipschitzian function followed by the statement of a useful related lemma from [131] are presented below.

Definition 1 The function $f(x,\lambda) : \mathbb{R} \times \mathbb{R} \to \mathbb{R}$ is said to be *Lipschitzian* in λ if there is a continuous function $0 \leq L(x) < \infty$ such that

$$\left| f(x,\lambda) - f\left(x,\bar{\lambda}\right) \right| \leq L(x) \left| \lambda - \bar{\lambda} \right| \tag{3.1}$$

where $\bar{\lambda} \in \mathbb{R}$.

Lemma 1 For any $\eta \in \mathbb{R}$ and Lipschitzian function $f(x,\lambda)$, the following inequality holds

$$\eta f(x,\lambda) \leq \eta \left[f\left(x,\bar{\lambda}\right) + \text{sgn}(\eta) L(x) \left| \lambda - \bar{\lambda} \right| \right] \tag{3.2}$$

where $\text{sgn}(\cdot)$ is the signum function and $L(x)$ is the Lipschitz bounding function from Definition .

3.2 Convex and Concave Functions

Definition 2 A C^1 function $f(\lambda) : \mathbb{R} \to \mathbb{R}$ is said to be *convex* on $\Theta = [\lambda_{\min}, \lambda_{\max}]$ if

$$f(\mu\lambda_1 + (1-\mu)\lambda_2) \leq \mu f(\lambda_1) + (1-\mu) f(\lambda_2), \tag{3.3}$$

and *concave* if

$$f(\mu\lambda_1 + (1-\mu)\lambda_2) \geq \mu f(\lambda_1) + (1-\mu) f(\lambda_2), \tag{3.4}$$

$\forall \lambda_1, \lambda_2 \in \Theta$ and $\forall \mu \in [0,1]$.

Lemma 2 For any C^1 function $f(\lambda) : \mathbb{R} \to \mathbb{R}$ that is convex on Θ:[1]

$$f'(\lambda_{\min}) \leq f'(\lambda) \leq f'(\lambda_{\max}), \ \forall \lambda \in \Theta. \tag{3.5}$$

If the function is concave, then

$$f'(\lambda_{\min}) \geq f'(\lambda) \geq f'(\lambda_{\max}), \ \forall \lambda \in \Theta. \tag{3.6}$$

The following is a corollary to Lemma 2, whose proof is given in the Appendix B.

Corollary 3 For any C^1 function $f(\lambda) : \mathbb{R} \to \mathbb{R}$ that is convex on $\Theta = [\lambda_{\min}, \lambda_{\max}]$ and for any $\lambda \in \Theta$,

$$f(\lambda) - f(\lambda_{\min}) + (\lambda_{\min} - \lambda) f'(\lambda_{\min}) \geq 0 \tag{3.7a}$$

$$f(\lambda) - f(\lambda_{\max}) + (\lambda_{\max} - \lambda) f'(\lambda_{\min}) \leq 0. \tag{3.7b}$$

If the function is concave, then

$$f(\lambda) - f(\lambda_{\min}) + (\lambda_{\min} - \lambda) f'(\lambda_{\min}) \leq 0 \tag{3.8a}$$

$$f(\lambda) - f(\lambda_{\max}) + (\lambda_{\max} - \lambda) f'(\lambda_{\min}) \geq 0. \tag{3.8b}$$

The proof of Corollary 3 can be found in Appendix B.

3.3 Neural Networks

For feedback control purposes, the *function approximation property* of neural networks is of key importance. The two-layer NN is the simplest to have this property and thus will be used in this work.

Theorem 4 [19, 71] Let $f : \mathbb{R}^n \to \mathbb{R}^m$ be a continuous function. Then, there exists a two-layer NN such that

$$f(x) = W^\top S\left(V^\top \bar{x}\right) + \delta(x), \ \forall x \in \Theta, \tag{3.9}$$

[1] The proof of Lemma 2 is omitted since the results can be easily verified by graphical means.

where Θ is a compact set, $\bar{x} = [x^\top, 1]^\top$ is the input vector, $V = [v_1, , ..., v_L] \in \mathbb{R}^{(n+1)\times L}$ is the input-to-activation layer weight matrix, $W \in \mathbb{R}^{L\times m}$ is the activation layer-to-output layer weight matrix**,** $L > 1$ represents the number of activation layer neurons,

$$S\left(V^\top \bar{x}\right) = \left[s\left(v_1^\top \bar{x}\right), ..., s\left(v_{L-1}^\top \bar{x}\right), 1\right]^\top \in \mathbb{R}^L$$

is the activation layer with the sigmoid function

$$s\left(x\right) = \frac{1}{1+e^{-\sigma x}},\ \sigma > 0, \tag{3.10}$$

and $\delta\left(x\right)$ is the NN approximation error satisfying $\left\|\delta\left(x\right)\right\| < \bar{\delta}$, which decreases as L increases.

In the following, let $\left\|\cdot\right\|_F$ denote the Frobenius norm of a matrix, $\left\|\cdot\right\|$ the 2-norm of a vector, and $\left\|\cdot\right\|_1$ the 1-norm of a vector.

Lemma 5 [133] For NN approximator (3.9), the estimation error can be expressed as

$$\hat{W}^\top S\left(\hat{V}^\top \bar{y}\right) - W^\top S\left(V^\top \bar{y}\right) = \tilde{W}^\top\left(\hat{S} - \hat{S}'\hat{V}^\top \bar{y}\right) + \hat{W}^\top \hat{S}'\tilde{V}^\top \bar{y} + d_u,$$

where $\hat{S} = S\left(\hat{V}^\top \bar{y}\right)$, $\hat{S}' = \text{diag}\{\hat{s}_1', \hat{s}_2', ..., \hat{s}_L'\}$ with $\hat{s}_i' = s'\left(v_i^\top \bar{y}\right) = d[s\left(x\right)]/dx|_{x=v_i^\top \bar{y}}$, $i = 1, ..., L$, and the residual term d_u is bounded by

$$\left|d_u\right| \leq \left\|V\right\|_F \left\|\bar{y}\hat{W}^\top \hat{S}'\right\|_F + \left\|W\right\| \left\|\hat{S}'\hat{V}^\top \bar{y}\right\| + \left\|W\right\|_1.$$

3.4 Nussbaum Function

Definition 3 Any continuous function $N : \mathbb{R} \to \mathbb{R}$ is a function of *Nussbaum* type if it has the following properties

$$\lim_{s\to\infty} \sup \frac{1}{s}\int_0^s N\left(\zeta\right) d\zeta = +\infty \tag{3.11a}$$

$$\lim_{s\to\infty} \inf \frac{1}{s}\int_0^s N\left(\zeta\right) d\zeta = -\infty. \tag{3.11b}$$

In this dissertation, the even Nussbaum function

$$N\left(\zeta\right) = \zeta^2 \cos\left(\omega\zeta\right) \tag{3.3}$$

will be used, where $\omega > 0$ is a control gain.

Lemma 6 [38, 122] Let $V(t)$ and $\zeta(t)$ be continuous functions defined on $[0, t_f)$ with $V(t) \geq 0$, $\forall t \in [0, t_f)$, and $N(\zeta)$ be the even Nussbaum function in (3.3). If the following inequality holds

$$V(t) \leq c_0 + e^{-c_1 t} \int_0^t \left[g(\tau) N(\zeta) + 1 \right] \dot{\zeta}(\tau) e^{c_1 \tau} d\tau, \ \forall t \in [0, t_f),$$

where $c_0, c_1 > 0$ are constants and $g(t)$ is a time-varying parameter which takes values in the unknown interval $I = [l^-, l^+]$ with $0 \notin I$, then $V(t)$, $\zeta(t)$, and $\int_0^t g(t) N(\zeta) \dot{\zeta} d\tau$ must be bounded on $[0, t_f)$.

The proof of Lemma 6 can be found in [122] when $\omega = \pi/2$ in (3.3). For any $\omega = n\pi$ with $n > 0$, the proof is similar and hence not shown in this report.

3.5 Other

Lemma 7 [95] The inequality

$$0 \leq |\eta| - \eta \tanh\left(\frac{\eta}{\varepsilon}\right) \leq c\varepsilon \tag{3.4}$$

holds for any $\varepsilon > 0$ and any $\eta \in \mathbb{R}$, where $c = 0.2758$.

Lemma 8 For matrices $A, B \in \mathbb{R}^{m \times n}$, the following relation holds

$$\text{tr}\left\{A^\top A\right\} + \text{tr}\left\{B^\top B\right\} \geq -2\text{tr}\left\{A^\top B\right\}, \tag{3.5}$$

where tr$\{\cdot\}$ denotes the matrix trace.

Finally, the following definitions will be used for notation simplification. For any vector $y = \{y_i\} \in \mathbb{R}^n$ where $y_i \in [y_{i\min}, y_{i\max}]$,

$$|y| := \{|y_i|\}, \quad y_{\max} := \{y_{i\max}\}, \quad \text{and} \quad y_{\min} := \{y_{i\min}\}. \tag{3.6}$$

Chapter 4 Model-Based Control: The Basic Idea

Tackling the NMES control problem for the full-order dynamic model described in Chapter 2 in a rigorous manner is very difficult. Thus, most results in the literature make the problem tractable by considering reduced-order system models. We follow the same approach here and consider only the passive dynamics in this chapter with subsequent chapters accounting for some of the other subsystems.

4.1 Problem Statement

Consider the passive dynamics in (2.1) rewritten as follows

$$J\ddot{q} + h\left(q, \dot{q}\right) = \tau \tag{4.1}$$

where

$$h\left(q, \dot{q}\right) = K\left(q\right) + B\left(\dot{q}\right) + G\left(q\right) \tag{4.2}$$

and τ is the control input. Our control objective is to design $\tau = \tau(q, \dot{q}, t)$ to asymptotically track any bounded C^2 reference trajectory $q_d\left(t\right)$ satisfying $\sup\left|q_d\left(t\right)\right| < \pi/2$ and $(\dot{q}_d(t), \ddot{q}_d(t)) \in \mathcal{L}_\infty$ without violating the constraint in (2.5). We assume for now that no uncertainties exist in (4.1).

To construct our controller, we define the tracking error as

$$e = q - q_d\,. \tag{4.3}$$

By defining $p = \inf q_d(t)$ and $P = \sup q_d(t)$ and imposing the following constraint

$$-\frac{\pi}{2} - P < e < \frac{\pi}{2} - p, \tag{4.4}$$

we ensure (2.5) holds.

4.2 Backstepping Control Design

The backstepping control design approach [67] for (4.1) involves two steps.

Step 1:

Let

$$z_1 = e \tag{4.5}$$

and write the z_1-dynamics as

$$\dot{z}_1 = \dot{e} = \alpha + z_2 \tag{4.6}$$

where

$$z_2 = \dot{e} - \alpha \tag{4.7}$$

and α is a virtual control signal to be designed.

Define the following positive-definite function

$$V_1(z_1) = \int_0^{z_1} \frac{s}{(s-a)(b-s)} ds \tag{4.8}$$

where

$$a = -\frac{\pi}{2} - P \quad \text{and} \quad b = \frac{\pi}{2} - p. \tag{4.9}$$

This choice of "barrier" function stems from the need to satisfy (4.4). That is, note that

$$V_1(z_1) \to \infty \text{ as } z_1 \to a, b. \tag{4.10}$$

Taking the derivative of (4.8) along (4.6) yields

$$\begin{aligned} \dot{V}_1 &= \frac{z_1 \dot{z}_1}{(z_1 - a)(b - z_1)} \\ &= \frac{z_1 z_2}{(z_1 - a)(b - z_1)} + \frac{z_1 \alpha}{(z_1 - a)(b - z_1)}. \end{aligned} \tag{4.11}$$

By designing

$$\alpha = -c_1 z_1 (z_1 - a)(b - z_1) \tag{4.12}$$

where $c_1 > 0$ is a control gain, we obtain

$$\dot{V}_1 = -c z_1^2 + \frac{z_1 z_2}{(z_1 - a)(b - z_1)}. \tag{4.13}$$

Step 2:

The dynamics of the error variable (4.7) is given by

$$\begin{aligned} J\dot{z}_2 &= J(\ddot{e} - \dot{\alpha}) \\ &= \tau - h(q, \dot{q}) - J(\ddot{q}_d + \dot{\alpha}) \end{aligned} \tag{4.14}$$

where (4.7), (4.1) and (4.3) were used,

$$\dot{\alpha} = c_1 \dot{e} \left[3z_1^2 - 2\left(a+b\right) z_1 + ab \right]. \tag{4.15}$$

We now define the positive-definite function

$$V\left(z_1, z_2\right) = V_1 + \frac{1}{2} J z_2^2, \tag{4.16}$$

whose derivative along (4.14) is given by

$$\dot{V} = -cz_1^2 + \frac{z_1 z_2}{\left(z_1 - a\right)\left(b - z_1\right)} + z_2 \left[\tau - h\left(q, \dot{q}\right) - J\left(\ddot{q}_d + \dot{\alpha}\right) \right]. \tag{4.17}$$

We now are ready to present our main result of this chapter.

Theorem 9 The model-based control law

$$\tau = -c_2 z_2 + h + J\left(\ddot{q}_d + \dot{\alpha}\right) - \frac{z_1}{\left(z_1 - a\right)\left(b - z_1\right)}, \tag{4.18}$$

where $c_2 > 0$ is a control gain, ensures $(e, \dot{e}) = 0$ is asymptotically stable (AS) and the boundedness of all other signals.

Proof. Substituting (4.18) into (4.17) yields

$$\dot{V}\left(z_1, z_2\right) = -c_1 z_1^2 - c_2 z_2^2, \tag{4.19}$$

which implies that $\dot{V}$ is negative definite. Therefore, $V\left(z_1, z_2\right)$ is a Lyapunov function and $\left(z_1, z_2\right) = 0$ is AS [58]. Since $\alpha(z_1 = 0) = 0$, we know from (4.5) and (4.7) that $(e, \dot{e}) = 0$ is AS. Since $(q_d(t), \dot{q}_d(t), \ddot{q}_d(t)) \in \mathcal{L}_\infty$ by design, we know $\dot{q}(t) \in \mathcal{L}_\infty$. Therefore, we know from (4.15) and (4.18) that $\tau(t) \in \mathcal{L}_\infty$. Finally, it follows from (4.1) that $\ddot{q}\left(t\right) \in \mathcal{L}_\infty$. ■

Chapter 5 Adaptive Control

In this chapter, we consider that the parameters in (2.1) are *uncertain*. To deal with this parametric uncertainty, we will formulate two *adaptive* control laws. What makes the adaptive NMES design challenging is that fact that some of the parameters appear *nonlinearly* in the model. In the first adaptive control strategy, we will take advantage of the Lipschitzian nature of the functions where the parameters appear and apply the discontinuous adaptive control design proposed in [50]. In the second design, we will take explicit advantage of the concavity or convexity of the model functions with respect to the nonlinear parameters, and a continuous adaptive controller with tuning functions inspired by [11] is proposed.

5.1 Discontinuous Adaptive Controller

In this section, we present a solution to the NMES adaptive tracking control problem with nonlinear parametrization. We consider only the dynamics of the human shank-knee joint model. Our design uses the approach in [50] to exploit the Lipschitzian parameterization of the NMES mechanical model to compensate for parametric uncertainties. Our adaptive control ensures asymptotic tracking for the angular position and velocity of the shank movement.

5.1.1 Problem Statement

Similar to Section 4.1, our control objective is to design $\tau = \tau(q, \dot{q}, t)$ to asymptotically track any bounded C^2 reference trajectory $q_d(t)$ satisfying $\sup |q_d(t)| < \pi/2$ and $(\dot{q}_d(t), \ddot{q}_d(t)) \in \mathcal{L}_\infty$ but under the constraint that all parameters in (2.1) are uncertain. For the sake of the subsequent adaptive design, (2.2) will be separated into the sum of two distinct terms, i.e.,

$$K(q) = k_1 \exp(-k_2 q)\, q - k_3 \exp(-k_4 q), \tag{5.1}$$

where $k_3 = k_1 q_0$ and $k_4 = k_2$. We assume the parameters that appear nonlinearly in (2.1)-(2.4), viz., k_2, k_4, and b_3, lie in a known compact set. This assumption is required because our Lipschitz bounding functions L will be designed based on the convexity/concavity of the nonlinear functions

in $K(q)$ and $B(\dot{q})$. The assumption may be unnecessary if other choices for L are made.

To quantify the parametric uncertainty, we define the estimate of the unknown parameter $\bullet$ or unmeasurable state $\bullet(t)$ to be $\hat{\bullet}(t)$ with the corresponding parameter estimation error being denoted by $\tilde{\bullet}(t) = \hat{\bullet}(t) - \bullet$ or $\tilde{\bullet}(t) = \hat{\bullet}(t) - \bullet(t)$. Finally, if parameter $\bullet$ lies in a compact set, then $\bullet \in [\bullet_{\min}, \bullet_{\max}]$ where $\bullet_{\min}$ and $\bullet_{\max}$ are known positive constants.

5.1.2 Control Design

We will again follow the backstepping procedure introduced in Section 4.2. Step 1 of the design process will be identical to the one for the model-based controller since the uncertain parameters do not appear in this step. That is, we use the same Lyapunov function candidate (4.8) and, as a result, the same virtual control signal α given by (4.12).

In Step 2, we rewrite (4.14) as

$$J\dot{z}_2 = \tau - W(q, \dot{q}, t)\theta + \sum_{i=1}^{3} \sigma_i f_i(x_i, \lambda_i) \tag{5.2}$$

where

$$W = \begin{bmatrix} \dot{q} & g\sin(q) & \ddot{q}_d + \dot{\alpha}_1 \end{bmatrix}, \tag{5.3}$$

$\theta = [b_1, ml, J]^\top$, $\sigma_1 = k_1$, $\sigma_2 = k_3$, and $\sigma_3 = b_2$ denote the parameters that appear linearly in (4.14), $\lambda_1 = k_2$, $\lambda_2 = k_4$, and $\lambda_3 = b_3$ are the parameters that appear nonlinearly, $x_1 = x_2 = q$, and $x_3 = \dot{q}$, and

$$f_1(x_1, \lambda_1) = -q\exp(-k_2 q), \quad f_2(x_2, \lambda_2) = \exp(-k_4 q), \quad f_3(x_3, \lambda_3) = -\tanh(b_3 \dot{q}). \tag{5.4}$$

We now introduce the positive-definite, radially unbounded function

$$V_2 = V_1 + \frac{1}{2} J z_2^2 + \frac{1}{2}\left(\tilde{\theta}^\top \Gamma^{-1} \tilde{\theta} + \sum_{i=1}^{3} \gamma_i^{-1} \tilde{\sigma}_i^2 + \sum_{i=1}^{3} \beta_i^{-1} \tilde{\Lambda}_i^2 \right) \tag{5.5}$$

where $\Gamma > 0 \in \mathbb{R}^{3\times 3}$ is constant and diagonal, $\gamma_i, \beta_i > 0$ are constants, and

$$\Lambda_i = (\lambda_i - \lambda_{i\min})\,\sigma_i. \tag{5.6}$$

After taking the derivative of (5.5) along (5.2), we obtain

$$\begin{aligned}\dot{V}_2 &= -c_1 z_1^2 + \frac{z_1 z_2}{(z_1 - a)(b - z_1)} + z_2 \left(\tau - W(q, \dot{q}, t)\theta + \sum_{i=1}^{3} \sigma_i f_i(x_i, \lambda_i) \right) \\ &\quad + \tilde{\theta}^\top \Gamma^{-1} \dot{\hat{\theta}} + \sum_{i=1}^{3} \gamma_i^{-1} \tilde{\sigma}_i \dot{\hat{\sigma}}_i + \sum_{i=1}^{3} \beta_i^{-1} \tilde{\Lambda}_i \dot{\hat{\Lambda}}_i \end{aligned} \tag{5.7}$$

where (4.13) was used. Applying Lemma 1 to (5.7) yields

$$\begin{aligned}\dot{V}_2 &\leq -c_1 z_1^2 + \frac{z_1 z_2}{(z_1 - a)(b - z_1)} + z_2 (\tau - W(q, \dot{q}, t)\theta) \\ &\quad + \sum_{i=1}^{3} z_2 \left[\sigma_i f_i(x_i, \lambda_{i\min}) + \text{sgn}(z_2) L_i(x_i) \Lambda_i \right] \\ &\quad + \tilde{\theta}^\top \Gamma^{-1} \dot{\hat{\theta}} + \sum_{i=1}^{3} \gamma_i^{-1} \tilde{\sigma}_i \dot{\hat{\sigma}}_i + \sum_{i=1}^{3} \beta_i^{-1} \tilde{\Lambda}_i \dot{\hat{\Lambda}}_i. \end{aligned} \tag{5.8}$$

In Appendix A, we prove the existence of the Lipschitz bounding functions $L_i(x_i)$.

The main result of this section is given in the following theorem.

Theorem 10 The adaptive control law

$$\begin{aligned}\tau &= -c_2 z_2 - \frac{z_1}{(z_1 - a)(b - z_1)} - \sum_{i=1}^{3} \text{sgn}(z_2) L_i(x_i) \hat{\Lambda}_i + W(q, \dot{q}, t)\hat{\theta} \\ &\quad - \sum_{i=1}^{3} f_i(x_i, \lambda_{i\min}) \hat{\sigma}_i, \end{aligned} \tag{5.9}$$

where $c_2 > 0$ is a control gain and

$$\begin{aligned}&\dot{\hat{\theta}} = -\Gamma W(q, \dot{q}, t) z_2, \quad \dot{\hat{\sigma}}_i = \gamma_i z_2 f_i(x_i, \lambda_{i\min}), \\ &\dot{\hat{\Lambda}}_i = \beta_i z_2 \text{sgn}(z_2) L_i(x_i), \end{aligned} \tag{5.10}$$

ensures that

$$(e(t), \dot{e}(t)) \to 0 \text{ as } t \to \infty \tag{5.11}$$

and all signals are bounded.

Proof. Substituting (5.9) and (5.10) into (5.8) gives

$$\dot{V}_2 \leq -c_1 z_1^2 - c_2 z_2^2. \tag{5.12}$$

Given the form of (5.5) and (5.12), we can invoke Corollary 2 of [32][2] to show that that ($z_1(t)$, $z_2(t)$, $\tilde{\theta}(t)$, $\tilde{\sigma}_i(t)$, $\tilde{\Lambda}_i(t)$)$\in \mathcal{L}_\infty$ and $(z_1(t) = e(t), z_2(t)) \rightarrow 0$ as $t \rightarrow \infty$. From (4.12), we know that $\alpha(z_1(t)) \rightarrow 0$ as $t \rightarrow \infty$; therefore, we have that $\dot{e}(t) \rightarrow 0$ as $t \rightarrow \infty$ from (4.7). From (4.15), it is clear that $\dot{\alpha}(t) \in \mathcal{L}_\infty$. The boundedness of $\hat{\theta}$, $\hat{\sigma}_i$, and $\hat{\Lambda}_i$ are obvious from the definition of the parameter estimate and estimate error. Since $(q_d(t), \dot{q}_d(t)) \in \mathcal{L}_\infty$, we know that $(q(t), \dot{q}(t)) \in \mathcal{L}_\infty$. The boundedness of $W(q, \dot{q}, t)$, $f_i(x_i, \lambda_{i\,\min})$, and $L_i(x_i)$ are clear from (5.3), (5.4), and (A.7)-(A.9). We can now use (5.9) to see that $\tau(t) \in \mathcal{L}_\infty$ and (5.10) to show that the adaptation laws are bounded. Finally, we know $\ddot{q}(t) \in \mathcal{L}_\infty$ from (2.1). ■

5.1.3 Simulation

The performance of the proposed adaptive controller is illustrated via a simulation. The system parameters in (2.1) were set to

$$\begin{gathered} J = 0.39 \text{ kg-m}^2\text{/rad}, b_1 = 0.6 \text{ kg-m}^2\text{/(rad-s)}, b_2 = 0.1 \text{ kg-m}^2\text{/(rad-s)}, \\ b_3 = 45 \text{ s/rad}, k_1 = 7.9 \text{ kg-m}^2\text{/(rad-s}^2\text{)}, k_2 = 1.68 \text{ 1/rad}, \\ k_3 = 6.21 \text{ kg-m}^2\text{/s}^2, k_4 = 1.81 \text{ 1/rad}, ml = 1.09 \text{ kg-m}. \end{gathered} \tag{5.13}$$

The compact sets for the nonlinear parameters were chosen as follows

$$\begin{aligned} [k_{2\,\min}, k_{2\,\max}] &= [k_{4\,\min}, k_{4\,\max}] = [1.0, 2.5] \text{ 1/rad} \\ [b_{3\,\min}, b_{3\,\max}] &= [40, 105] \text{ s/rad}. \end{aligned}$$

The reference trajectory was set to

$$q_d(t) = \frac{7\pi}{24} + \frac{\pi}{8}\left(1 - e^{-0.4t}\right) \sin \omega t \text{ rad},$$

where $\omega = 0.6\pi + 0.5\pi / \left[\cosh\left(0.6\left(t - 10\right)\right)\right]$, which leads to to the parameters in (4.9) being $a = -2.88$ rad and $b = 1.05$ rad. The initial conditions for the states were $q(0) = 0.8$ rad and $\dot{q}(0) = -0.3$ rad/s, while all parameter estimates were initialized to zero. The control and adaptation gains were selected by trial-and-error and set to $c_1 = 3$, $c_2 = 5$, $\Gamma = \text{diag}\{1, 1, 0.5\}$,

[2] The differential equation governing the closed-loop dynamics has a discontinuous right-hand side due to (5.9) and (5.10). Therefore, the proof of stability requires the use of a LaSalle-Yoshizawa-like theorem for nonsmooth systems.

$\gamma_1 = 1.5$, $\gamma_2 = 2$, $\gamma_3 = 3$, $\beta_1 = \beta_2 = 2$, and $\beta_3 = 0.6$.

Figure 5.1 shows $q_d(t)$ versus $q(t)$ and the corresponding position tracking error. Figure 5.2 shows $\dot{q}_d(t)$ versus $\dot{q}(t)$ and the control input, where the discontinuity of the control input can be observed.

The parameter estimates $\hat{\theta}(t)$, $\hat{\sigma}_i(t)$, and $\hat{\Lambda}_i(t)$ are given in Figures 5.3, 5.4, and 5.5, respectively. All parameter estimates are bounded under the adaptation.

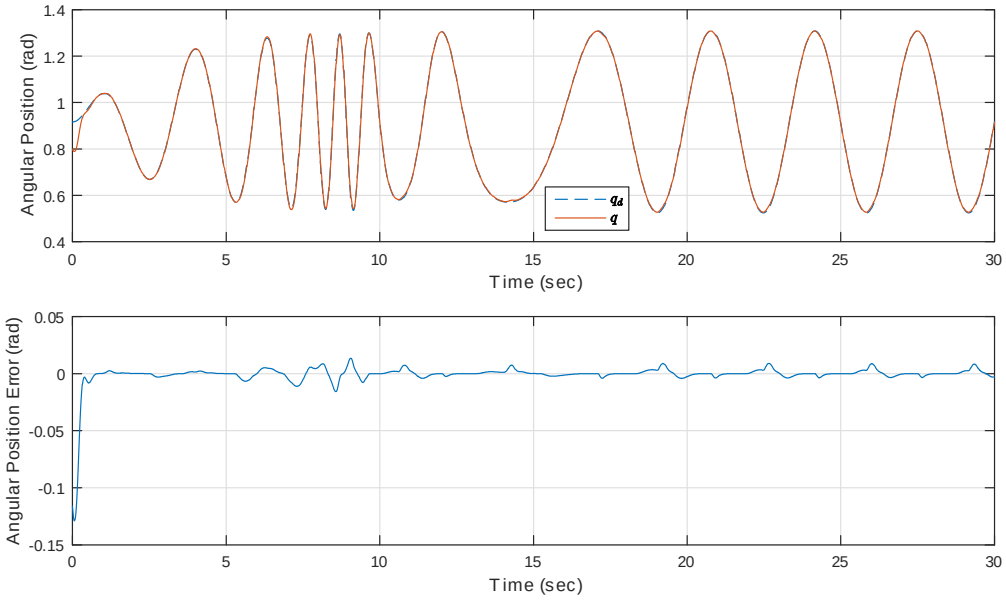

Figure 5.1: Top plot: $q_d(t)$ versus $q(t)$; Bottom plot: tracking error $e(t)$

5.2 Continuous Adaptive Controller

In this section, we propose an alternative solution to the adaptive tracking control problem for the nonlinearly parametrized limb dynamics which leads to a *continuous* control law. This is done by exploiting the concavity or convexity of the functions in (2.1) with respect to the nonlinear parameters. The design in this section is founded on the adaptive strategy introduced in [11, 62].

5.2.1 Problem Statement

The control objective in this section is identical to the one in Section 5.1.1. To facilitate the control design, we introduce the filtered tracking error [21]

$$r = \dot{e} + \mu e, \tag{5.14}$$

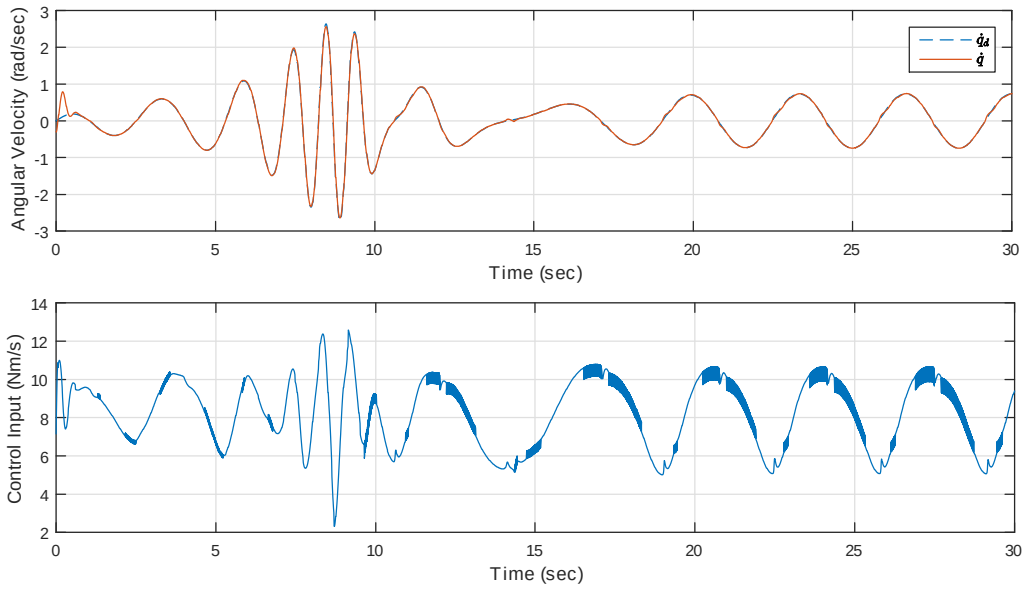

Figure 5.2: Top plot: $\dot{q}_d(t)$ versus $\dot{q}(t)$; Bottom plot: control input $\tau(t)$.

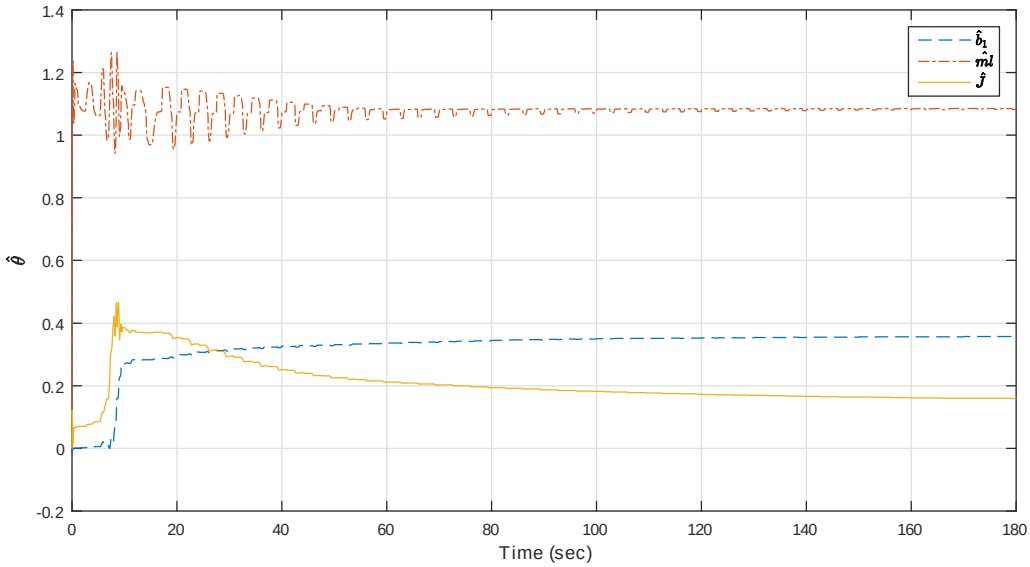

Figure 5.3: Parameter estimate $\hat{\theta}(t)$.

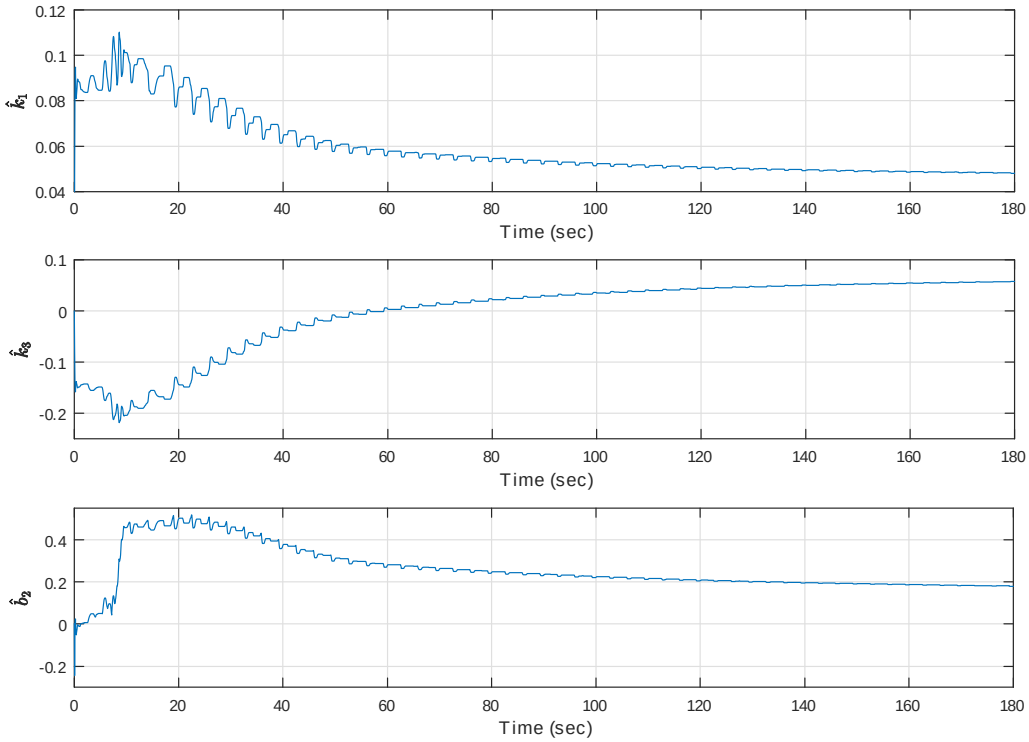

Figure 5.4: Parameter estimate $\hat{\sigma}\,(t)$.

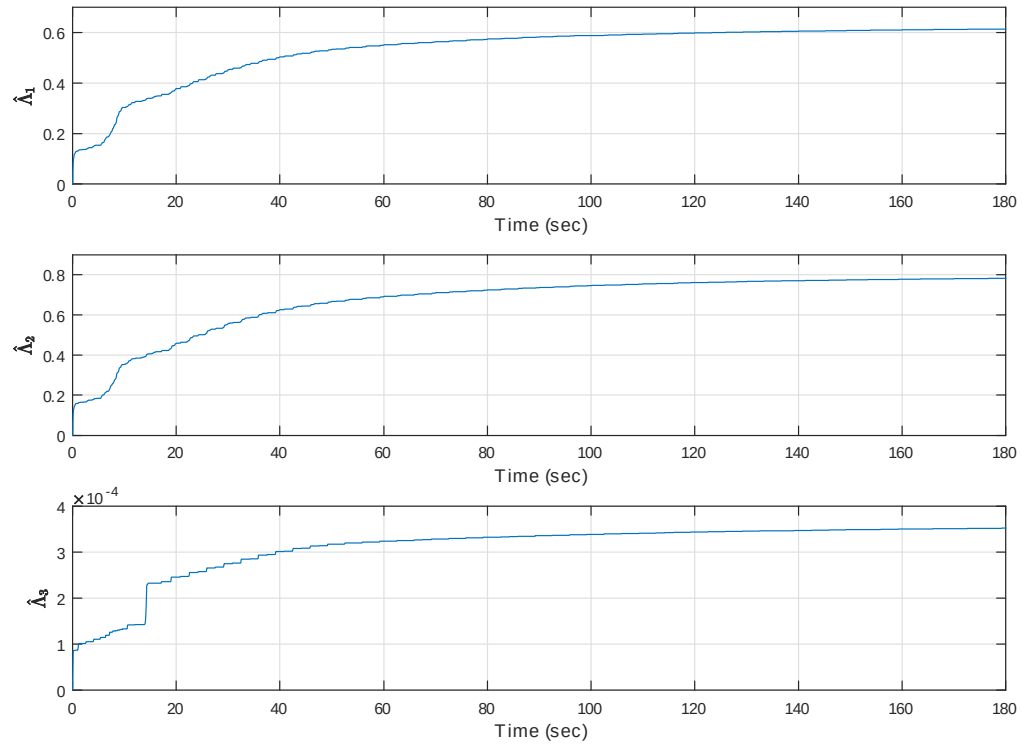

Figure 5.5: Parameter estimate $\hat{\Lambda}\,(t)$.

where e was defined in (4.3) and $\mu > 0$ is a user-defined control gain, and the following tuning error [11]

$$r_\epsilon = r - \epsilon S(\frac{r}{\epsilon}), \tag{5.15}$$

where $\epsilon > 0$ is another user-defined control parameter and $S(\cdot)$ is the saturation function

$$S(y) = \begin{cases} 1, & y \geq 1 \\ y, & |y| < 1 \\ -1, & y \leq -1. \end{cases} \tag{5.16}$$

Note that (5.15) has a dead-zone; thus, if $r_\epsilon = 0$, then $|r| \leq \epsilon$ and if $|r_\varepsilon| \leq \eta$, then $|r| \leq \varepsilon + \eta$. Also, since (5.14) represents a stable linear system with input r and output e, if $\lim_{t\to\infty} |r(t)| < \epsilon$ then (see Theorem 2.13 in [85])

$$\lim_{t\to\infty} |e(t)| < \frac{\epsilon}{\mu}. \tag{5.17}$$

When ϵ/μ can be made arbitrarily small, we refer to (5.17) as *practical tracking* [97].

5.2.2 Control Design

We begin the design by rewriting the system dynamics (2.1)-(2.4) in terms of (5.14):

$$J\dot{r} = \tau + J\left(\mu\dot{e} - \ddot{q}_d\right) - B\left(\dot{q}\right) - K(q) - G\left(q\right). \tag{5.18}$$

After segregating the linear parameterizations from the nonlinear ones in (5.18), we have

$$J\dot{r} = \tau + W(q, \dot{q}, t)\theta - \sum_{i=1}^{3} \phi_i f_i\left(x_i, \lambda_i\right) \tag{5.19}$$

where $W = [\mu\dot{e} - \ddot{q}_d \quad -\dot{q} \quad -g\sin(q)]$, $\theta = [J \quad b_1 \quad ml]^\intercal$, $\phi_1 = k_1$, $\phi_2 = k_3$, $\phi_3 = b_2$, $\lambda_1 = k_2$, $\lambda_2 = k_4$, $\lambda_3 = b_3$, $x_1 = x_2 = q$, $x_3 = \dot{q}$, $f_1 = q\exp\left(-k_2 q\right)$, $f_2 = -\exp(-k_4 q)$, and $f_3 = \tanh\left(b_3\dot{q}\right)$. If $\Theta_i = [\lambda_{i\min}, \lambda_{i\max}]$ is a known compact set, note that f_1 is convex on Θ_1 for $q \geq 0$ and concave for $q < 0$, f_2 is concave on Θ_2 for all q, and f_3 is concave on Θ_3 for $\dot{q} \geq 0$ and convex for $\dot{q} < 0$.

We propose the following certainty equivalence-type control law to stabilize (5.19)

$$\tau = -k_c r - W\hat{\theta} + \sum_{i=1}^{3} \hat{\phi}_i f_i(x_i, \hat{\lambda}_i) + \tau_a, \tag{5.20}$$

where $k_c > 0$ is a control gain, and u_a is an additional control signal to be specified later. The

main design challenge here is constructing the adaptation laws for the nonlinear parameterizations $\hat{\lambda}_i$. Our solution is stated in the following theorem.

Theorem 11 The adaptive control law (5.20) with

$$\dot{\hat{\theta}} = \Gamma W^{\intercal} r_{\epsilon}, \tag{5.21}$$

$$\dot{\hat{\phi}}_i = -\gamma_i r_{\epsilon} \hat{f}_i, \tag{5.22}$$

$$\dot{\hat{\lambda}}_i = -\beta_i r_{\epsilon} \omega_i \left(\hat{\lambda}_i - \lambda_{i\,\min}\right)\left(\lambda_{i\,\max} - \hat{\lambda}_i\right),\ \hat{\lambda}_i(0) \in \Theta_i, \tag{5.23}$$

$$\begin{aligned} &\omega_1 = f_1'(x_1, \lambda_{1\,\min}),\ \omega_2 = f_2'(x_2, \lambda_{2\,\max}), \\ &\omega_3 = \frac{f_{3\,\max} - f_{3\,\min}}{\lambda_{3\,\max} - \lambda_{3\,\min}} \end{aligned} \tag{5.24}$$

$$\tau_a = -S(\frac{r}{\epsilon}) \sum_{i=1}^{3} a_i^*, \tag{5.25}$$

if $r \geq 0$:

$$a_1^* = \begin{cases} -\phi_{1\,\max}\left[f_{1\,\min} - \hat{f}_1 + \left(\hat{\lambda}_1 - \lambda_{1\,\min}\right)\omega_1\right] \text{ if } q \geq 0 \\ -\phi_{1\,\max}\left[f_{1\,\max} - \hat{f}_1 + \left(\hat{\lambda}_1 - \lambda_{1\,\max}\right)\omega_1\right] \text{ if } q < 0, \end{cases} \tag{5.26}$$

$$a_2^* = -\phi_{2\,\max}\left[f_{2\,\min} - \hat{f}_2 + \left(\hat{\lambda}_2 - \lambda_{2\,\min}\right)\omega_2\right], \tag{5.27}$$

$$a_3^* = \begin{cases} -\phi_{3\,\max}\left[f_{3\,\max} - \hat{f}_3 + \left(\hat{\lambda}_3 - \lambda_{3\,\max}\right)\omega_3\right] \text{ if } \dot{q} \geq 0 \\ -\phi_{3\,\max}\left[\bar{f}_3 - \hat{f}_3 + \left(\hat{\lambda}_3 - \bar{\lambda}_3\right)\omega_3\right] \text{ if } \dot{q} < 0, \end{cases} \tag{5.28}$$

if $r < 0$:

$$a_1^* = \begin{cases} \phi_{1\,\max}\left[f_{1\,\max} - \hat{f}_1 + \left(\hat{\lambda}_1 - \lambda_{1\,\max}\right)\omega_1\right] \text{ if } q \geq 0 \\ \phi_{1\,\max}\left[f_{1\,\min} - \hat{f}_1 + \left(\hat{\lambda}_1 - \lambda_{1\,\min}\right)\omega_1\right] \text{ if } q < 0, \end{cases} \tag{5.29}$$

$$a_2^* = \phi_{2\,\max}\left[f_{2\,\max} - \hat{f}_2 + \left(\hat{\lambda}_2 - \lambda_{2\,\max}\right)\omega_2\right], \tag{5.30}$$

$$a_3^* = \begin{cases} \phi_{3\max}\left[\bar{f}_3 - \hat{f}_3 + \left(\hat{\lambda}_3 - \bar{\lambda}_3\right)\omega_3\right] \text{ if } \dot{q} \geq 0 \\ \phi_{3\max}\left[f_{3\min} - \hat{f}_3 + \left(\hat{\lambda}_3 - \lambda_{3\min}\right)\omega_3\right] \text{ if } \dot{q} < 0, \end{cases} \tag{5.31}$$

where $\Gamma \in \mathbb{R}^{3\times 3}$ is diagonal and positive definite, $\gamma_i, \beta_i > 0$, $f_i' = \partial f_i/\partial \lambda_i$, $f_{i\max} = f_i(x_i, \lambda_{i\max})$, $f_{i\min} = f_i(x_i, \lambda_{i\min})$, $\hat{f}_i = f_i(x_i, \hat{\lambda}_i)$, and $\bar{f}_3 = f_3(x_3, \bar{\lambda}_3)$ such that $\bar{\lambda}_3 \in \Theta_3$ satisfies $f_3'(x_3, \bar{\lambda}_3) = \omega_3$,[3] ensures the boundedness of all closed-loop signals and practical tracking in the sense of (5.17).

Before we prove Theorem 11, a few comments and preliminary results are in order. First, despite the switching between (5.26)-(5.28) and (5.29)-(5.31), the adaptive control law is continuous due to the presence of the multiplicative saturation function in (5.25). Second, the form of (5.24)-(5.31) was inspired by the min-max optimization strategy in [77]. However, we use specific forms for ω_i and a_i^* rather than the generalized ones in [77] which were meant to minimize the amplitude of (5.25). Third, the projection-type algorithm in (5.23) ensures $\hat{\lambda}_i(t) \in \Theta_i \ \forall t \geq 0$ since the update law is turned off when $\hat{\lambda}_i(t) = \lambda_{i\min}$ or $\lambda_{i\max}$. This fact is needed in Lemma 12 below.

Lemma 12 For any $\lambda_i, \hat{\lambda}_i \in \Theta_i$ and $\phi_i > 0$, if f_i is convex on Θ_i, then

$$\begin{aligned} &\phi_i\left[f_i - \hat{f}_i + \left(\hat{\lambda}_i - \lambda_i\right) f_{i\min}'\right] \geq \phi_{i\max}\left[f_{i\min} - \hat{f}_i\right. \\ &\left. + \left(\hat{\lambda}_i - \lambda_{i\min}\right) f_{i\min}'\right] \end{aligned} \tag{5.32}$$

and

$$\begin{aligned} &\phi_i\left[f_i - \hat{f}_i + \left(\hat{\lambda}_i - \lambda_i\right)\left(\tfrac{f_{i\max} - f_{i\min}}{\lambda_{i\max} - \lambda_{i\min}}\right)\right] \geq \phi_{i\max}\left[\bar{f}_i - \hat{f}_i\right. \\ &\left. + \left(\hat{\lambda}_i - \bar{\lambda}_i\right)\left(\tfrac{f_{i\max} - f_{i\min}}{\lambda_{i\max} - \lambda_{i\min}}\right)\right] \end{aligned} \tag{5.33}$$

where $f_{i\min}' = f_i'(x_i, \lambda_{i\min})$, $f_{i\max}' = f_i'(x_i, \lambda_{i\max})$, and $\bar{\lambda}_i$ satisfies the equation $f_i'(x_i, \bar{\lambda}_i) = \frac{f_{i\max} - f_{i\min}}{\lambda_{i\max} - \lambda_{i\min}}$. If f_i is concave on Θ_i, then

$$\begin{aligned} &\phi_i\left[f_i - \hat{f}_i + \left(\hat{\lambda}_i - \lambda_i\right) f_{i\max}'\right] \geq \phi_{i\max}\left[f_{i\min} - \hat{f}_i\right. \\ &\left.\left[+ \left(\hat{\lambda}_i - \lambda_{i\min}\right) f_{i\max}'\right]\right. . \end{aligned} \tag{5.34}$$

[3] We know that $\bar{\lambda}_3$ exists from the Mean Value Theorem. In practice, we can determine $\bar{\lambda}_3$ by numerically solving $f_3'(x_3, \bar{\lambda}_3) = \omega_3$.

The proof of Lemma 12 is similar to the one of the Corollary 3 from [128].

5.2.3 Proof of Stability

We use the Lyapunov function candidate

$$V(z) = \frac{J}{2}r_\epsilon^2 + \frac{1}{2}\tilde{\theta}^\intercal \Gamma^{-1}\tilde{\theta} + \frac{1}{2}\sum_{i=1}^{3}\gamma_i^{-1}\tilde{\phi}_i^2 + \sum_{i=1}^{3}\beta_i^{-1}\phi_i \int_0^{\tilde{\lambda}_i} \frac{s}{(\lambda_i + s - \lambda_{i\min})(\lambda_{i\max} - \lambda_i - s)} ds \tag{35}$$

where $z = [r_\epsilon, \tilde{\theta}, \tilde{\phi}_i, \tilde{\lambda}_i]$, $i = 1, 2, 3$. Note that (5.35) is positive definite and radially unbounded with respect to z. Since r_ϵ in (5.15) is continuous for all r, it follows that $\dot{V}$ exists for all r and is given by

$$\dot{V} = r_\epsilon J \dot{r}_\epsilon + \tilde{\theta}^T \Gamma^{-1}\dot{\hat{\theta}} + \sum_{i=1}^{3}\gamma_i^{-1}\tilde{\phi}_i\dot{\hat{\phi}}_i + \sum_{i=1}^{3}\beta_i^{-1}\phi_i \frac{\tilde{\lambda}_i\dot{\hat{\lambda}}_i}{\left(\hat{\lambda}_i - \lambda_{i\min}\right)\left(\lambda_{i\max} - \hat{\lambda}_i\right)}. \tag{5.36}$$

The above derivative will be analyzed for two cases: $|r| \leq \epsilon$ and $|r| > \epsilon$.

Case 1: $|r| \leq \epsilon$

It follows from (5.15) that $r_\epsilon = 0$ and $\dot{r}_\epsilon = 0$. Therefore, the adaptation laws are zero according to (5.21)-(5.23) and $\dot{V} = 0$ from (5.36). Since $|r| \leq \epsilon$, then (5.17) holds.

Case 2: $|r| > \epsilon$

It follows that $\dot{r}_\epsilon = \dot{r}$, so after substituting (5.19)-(5.23) into (5.36), we obtain

$$\dot{V} \leq -k_c r_\epsilon^2 - r_\epsilon \left[\sum_{i=1}^{3}\phi_i\left(f_i - \hat{f}_i + \tilde{\lambda}_i\omega_i\right) + S(\frac{r}{\epsilon})\sum_{i=1}^{3}a_i^*\right] \tag{5.37}$$

where we have used the fact that $rr_\epsilon > r_\epsilon^2$ when $|r| > \epsilon$. We now separate Case 2 into two subcases: $r > \epsilon$ and $r < -\epsilon$.

a) When $r > \epsilon$, we know that $r_\epsilon > 0$ and $S(r/\epsilon) = 1$. Therefore, (5.38) becomes

$$\dot{V} \leq -k_c r_\epsilon^2 - r_\epsilon \sum_{i=1}^{3} L_i \tag{5.38}$$

where

$$L_i = \phi_i\left(f_i - \hat{f}_i + \tilde{\lambda}_i\omega_i\right) + a_i^*. \tag{5.39}$$

We now analyze (5.38) and (5.39) for different concavity/convexity conditions on f_i. When $q \geq 0$

and $\dot{q} < 0$, we know f_1 is convex and f_3 is convex. It then follows from (5.24), (5.26), (5.27), (5.28), and (5.32) that $L_i \geq 0$, $i = 1, 2, 3$ and therefore

$$\dot{V} \leq -k_c r_\epsilon^2. \tag{5.40}$$

A similar process can be followed for the other combinations of the signs of q and $\dot{q}$, leading to (5.40).

b) When $r < -\epsilon$, we have $r_\epsilon < 0$ and $S(r/\epsilon) = -1$. In this case,

$$\dot{V} \leq -k_c r_\epsilon^2 - r_\epsilon \sum_{i=1}^{3} \left[\phi_i \left(f_i - \hat{f}_i + \tilde{\lambda}_i \omega_i \right) - a_i^* \right]. \tag{5.41}$$

Again here, we can invoke Lemma 12 along with the appropriate expressions in (5.26)-(5.31) to arrive at (5.40) for all combinations of the signs of q and $\dot{q}$.

For Case 2, we know from (5.35) and (5.40) that $z(t)$ is bounded for all time. Since $r_\epsilon(t)$ is bounded, we know from (5.15) that $r(t)$ is bounded, and then from (5.14) that $e(t), \dot{e}(t)$ are bounded. We can use (4.3) and its derivative to show that $q(t), \dot{q}(t)$ are bounded. It is not difficult to see from (5.20) and (5.21)-(5.31) that the control input and adaptation laws are bounded for all time. From (5.19), we then know $\dot{r}(t)$ is bounded and therefore $\dot{r}_\epsilon(t)$ is bounded. Now, given (5.40), we can invoke a corollary to Barbalat's lemma [67] to show that $\lim_{t\to\infty} r_\epsilon(t) \to 0$. Finally, we know that (5.17) holds.

5.2.4 Simulation

We simulated (2.1)-(2.4) in closed loop with our adaptive controller (5.20)-(5.31). The model parameters were set to the values in (5.13). The plant initial conditions were set to $q(0) = 0.8$ rad and $\dot{q}(0) = -0.8$ rad/s. The bounds on the parameter estimates were set to

$$b_{2\max} = 0.4 \text{ kg-m}^2\text{/(rad-s)}, \; b_{3\min} = 40 \text{ s/rad}, \; b_{3\max} = 105 \text{ s/rad},$$

$$k_{1\max} = 9.5 \text{ kg-m}^2\text{/(rad-s}^2\text{)}, \; k_{3\max} = 14.92 \text{ kg-m}^2\text{/s}^2, \; k_{2\min} = 1 \text{ 1/rad},$$

$$k_{2\max} = 2.5 \text{ 1/rad}, \; k_{4\min} = 1 \text{ 1/rad}, \; k_{4\max} = 2.5 \text{ 1/rad}.$$

All parameter estimates were initialized to zero except for $\hat{b}_3(0) = 104$ s/rad, $\hat{k}_2(0) = 2.4$ 1/rad,

and $\hat{k}_4(0) = 1.1$ 1/rad.

We chose the reference trajectory as

$$q_d(t) = \frac{7\pi}{24} + \frac{\pi}{8}\sin\left(\pi t - \frac{\pi}{2}\right) \text{ rad.}$$

The control gains were set to $\mu = 3$, $k_c = 4$, and $\epsilon = 0.005$ while the adaptation gains were selected as $\Gamma = \text{diag}\{0.5, 0.8, 0.5\}$, $\gamma_1 = 1.5$, $\gamma_2 = 0.8$, $\gamma_3 = 1$, $\beta_1 = 3.5$, $\beta_2 = 3.5$, and $\beta_3 = 1$.

Figure 5.6 shows the angular position of the lower leg limb along with the tracking error. One can see that the error converges quickly to within the user-defined bound $\pm\epsilon/\mu \approx 0.0017$. The angular velocity data and the torque control input are shown in Figure 5.7, where the control input is observed as a continuous signal.

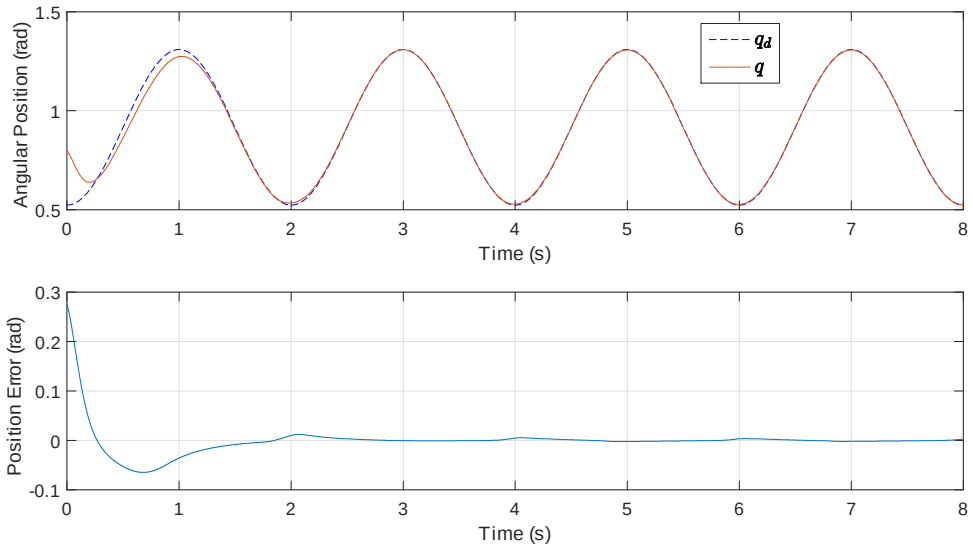

Figure 5.6: Top plot: $q_d(t)$ versus $q(t)$. Bottom plot: tracking error $e(t)$

The parameter estimates are displayed in Figure 5.8-5.10 and show their convergence to steady-state values.

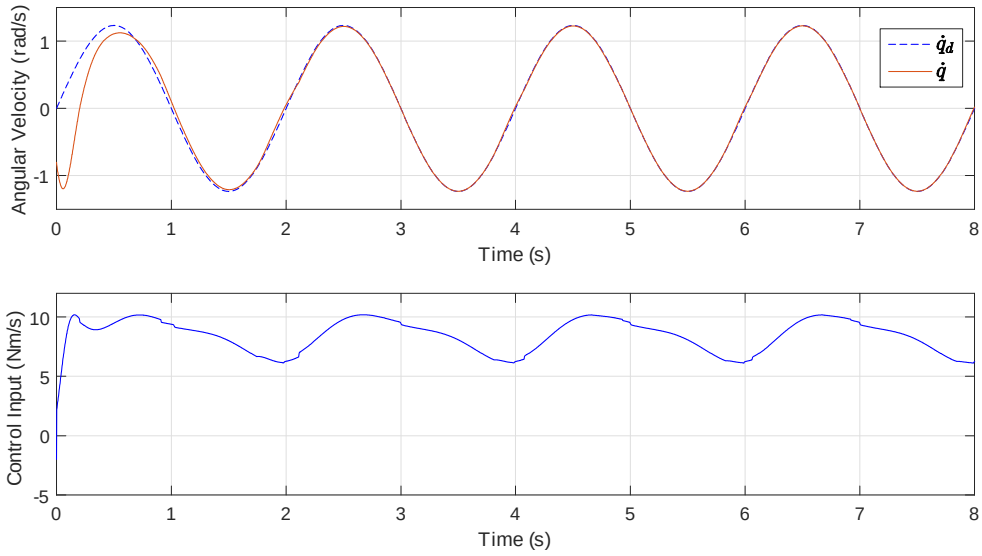

Figure 5.7: Top plot: $\dot{q}_d\,(t)$ versus $\dot{q}\,(t)$. Bottom plot: control input $\tau\,(t)$.

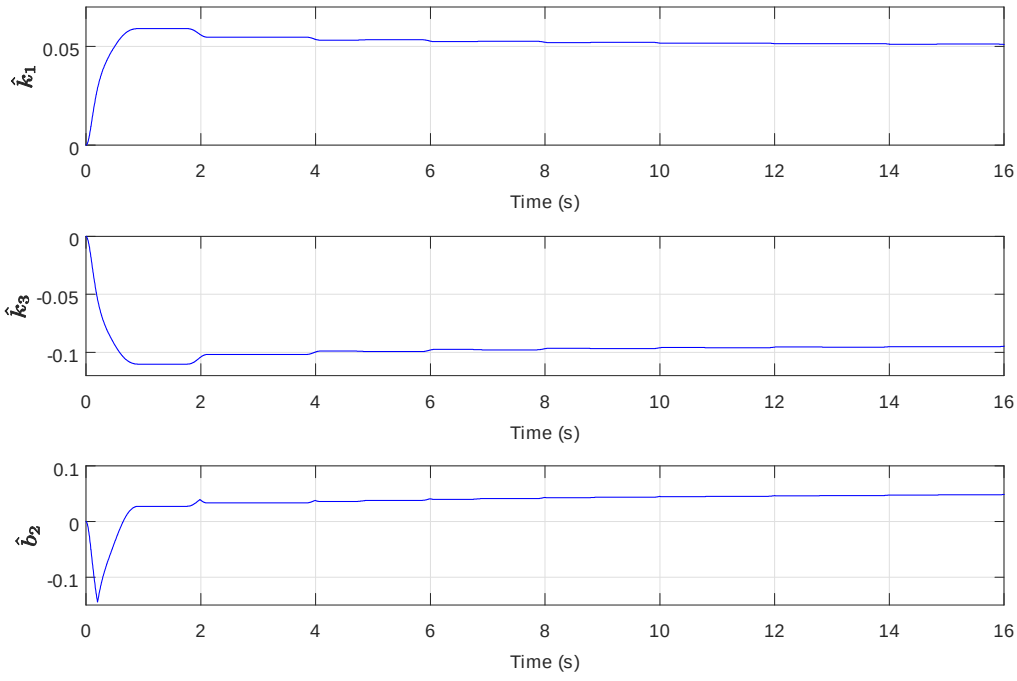

Figure 5.8: Parameter estimate $\hat{\phi}\,(t)$.

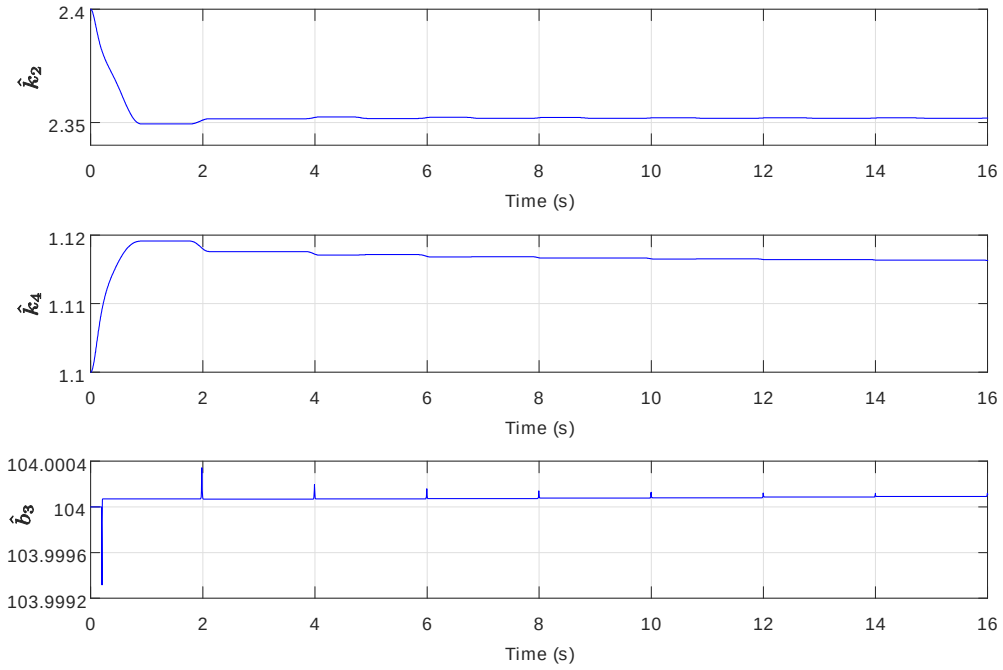

Figure 5.9: Parameter estimate $\hat{\lambda}(t)$.

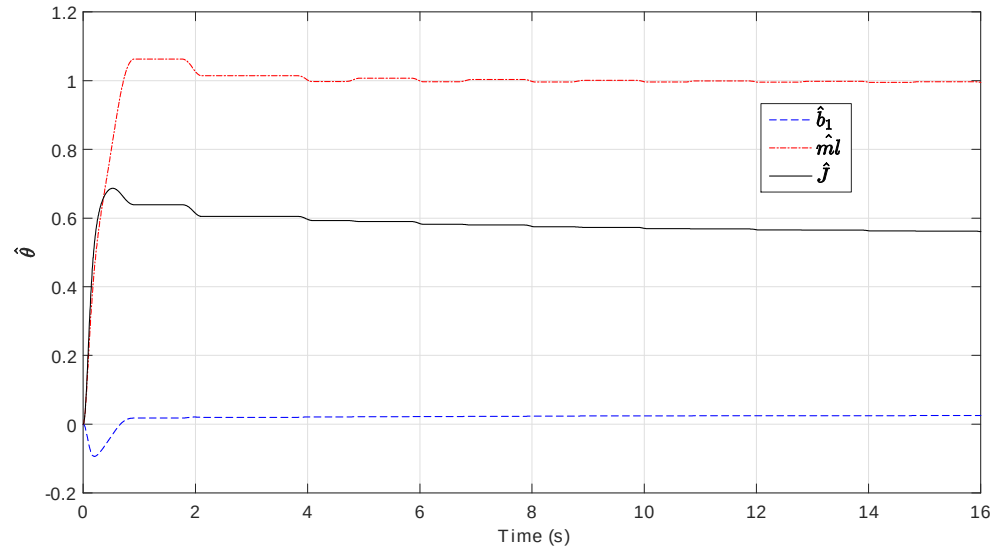

Figure 5.10: Parameter estimate $\hat{\theta}(t)$.

Chapter 6 Robust Adaptive Control

In this chapter, we consider the problem where disturbance torques are present in the passive mechanical dynamics due to functional uncertainties in the elastic moment and/or the presence of time-varying, external loads. To solve this problem, we introduce *robust* versions of the adaptive controllers from Chapter 5. The resulting control laws are continuous and guarantee practical tracking for the shank angular position.

6.1 Problem Statement

We consider here the following passive mechanical dynamic model

$$J\ddot{q} + B(\dot{q}) + K(q) + G(q) + d(q,t) = \tau, \tag{6.1}$$

where $K(q)$, $B(\dot{q})$, and $G(q)$ were defined in (2.2)-(2.4) and $d(q,t) \in \mathbb{R}$ is the disturbance torque representing uncertainties in the elastic effects and/or time-varying external loads.

Remark 1 The model for the elastic moment in (6.1) has been the subject of discussion in the literature. In earlier work [20, 57, 80], the elastic moment was represented by a linear term and two exponential terms:

$$K(q) = a_1 q - a_2 \left[\exp(-a_3 q) - 1\right] + a_4 \left[\exp(a_5 q) - 1\right] \tag{6.2}$$

where $a_i > 0$ for $i = 1, ..., 5$. This model was simplified in [34] by neglecting the first and third terms in (6.2) since their contributions were negligible in the operation range of the system identification experiment ($q \geq \pi/6$). The existence of the non-zero resting knee angle was first reported in [29], resulting in the model shown in (2.2). Since then this model has been widely used in recent control work; see e.g. [98, 107, 111, 112]. Due to the uncertainty in the form of $K(q)$, we include unmodeled elastic effects in $d(q,t)$.

Our control objective is to design a continuous feedback control law $\tau(q, \dot{q}, t)$ to track any

C^2 reference trajectory $q_d(t)$ satisfying $\sup|q_d(t)| < \pi/2$ and $(\dot{q}_d(t), \ddot{q}_d(t)) \in \mathcal{L}_\infty$ under the assumption that the disturbance is upper bounded by

$$|d(q,t)| \leq \delta(q) + d_0, \tag{6.3}$$

where $\delta(q) \geq 0$ is some bounding function and $d_0 > 0$ is constant.

Remark 2 One way of determining $\delta(q)$ is to set it to a function that upper bounds possible elastic model mismatches. For example, $\delta(q) = c_1 \exp(c_2 q)$ with $c_1, c_2 > 0$ bounds the difference between (2.2) and (6.2).

6.2 Lipschitzian Parameterization-Based Control

6.2.1 Control Design

We begin the design by rewriting the system dynamics (6.1) and (2.2)-(2.4) in terms of r defined in (5.14):

$$J\dot{r} = \tau + J(\mu\dot{e} - \ddot{q}_d) - B(\dot{q}) - K(q) - G(q) - d(q,t). \tag{6.4}$$

After segregating the linear parameterizations from the nonlinear ones in (6.4), we obtain

$$J\dot{r} = \tau - W(x,t)\theta + Y(x,\lambda)\phi - d(q,t), \tag{6.5}$$

where $W = [-\mu\dot{e} + \ddot{q}_d, \dot{q}, g\sin(q)]^\top$, $x = [q, \dot{q}]$, $\theta = [J, b_1, ml]$, $\phi = [k_1, k_1 q_0, b_2]$, $\lambda = [k_2, k_2, b_3]$, and

$$Y = [-q\exp(-k_2 q), \exp(-k_2 q), -\tanh(b_3\dot{q})]^\top. \tag{6.6}$$

Let $\psi = \{\psi_i\} \in \mathbb{R}^3$ with

$$\psi_i = (\lambda_i - \lambda_{i\min})\phi_i \tag{6.7}$$

be a new unknown parameter where $\psi_i \in [\psi_{i\min}, \psi_{i\max}] = [0, (\lambda_{i\max} - \lambda_{i\min})\phi_{i\max}]$. We now

define the following positive definite, radially unbounded function $V_L : \mathbb{R} \times \Xi_L \to [0, \infty)$

$$\begin{aligned} V_L &= \frac{1}{2} J r^2 + \sum_{i=1}^{3} \alpha_i^{-1} \int_0^{\tilde{\theta}_i} \frac{s}{(\theta_{i\max} - \theta_i - s)(\theta_i + s - \theta_{i\min})} ds \\ &+ \sum_{i=1}^{3} \beta_i^{-1} \int_0^{\tilde{\phi}_i} \frac{s}{(\phi_{i\max} - \phi_i - s)(\phi_i + s - \phi_{i\min})} ds \\ &+ \sum_{i=1}^{3} \gamma_i^{-1} \int_0^{\tilde{\psi}_i} \frac{s}{(\psi_{i\max} - \psi_i - s)(\psi_i + s - \psi_{i\min})} ds \end{aligned} \tag{6.8}$$

where $\alpha_i, \beta_i, \gamma_i > 0$ are constants and

$$\Xi_L := \left\{ (\tilde{\theta}, \tilde{\phi}, \tilde{\psi}) : (\theta_{\min} - \theta, \theta_{\max} - \theta) \times (\phi_{\min} - \phi, \phi_{\max} - \phi) \times (\psi_{\min} - \psi, \psi_{\max} - \psi) \right\}. \tag{6.9}$$

After taking the time derivative of (6.8) along (6.5), we have

$$\begin{aligned} \dot{V}_L &= r\left[u - W(x,t)\theta + Y(x,\lambda)\phi - d(q,t)\right] + \sum_{i=1}^{3} \alpha_i^{-1} \frac{\tilde{\theta}_i \dot{\hat{\theta}}_i}{\left(\theta_{i\max} - \hat{\theta}_i\right)\left(\hat{\theta}_i - \theta_{i\min}\right)} \\ &+ \sum_{i=1}^{3} \beta_i^{-1} \frac{\tilde{\phi}_i \dot{\hat{\phi}}_i}{\left(\phi_{i\max} - \hat{\phi}_i\right)\left(\hat{\phi}_i - \phi_{i\min}\right)} + \sum_{i=1}^{3} \gamma_i^{-1} \frac{\tilde{\psi}_i \dot{\hat{\psi}}_i}{\left(\psi_{i\max} - \hat{\psi}_i\right)\left(\hat{\psi}_i - \psi_{i\min}\right)} \end{aligned} \tag{6.10}$$

After adding and subtracting the term $rY(x, \lambda_{\min})\phi$ to (6.10) and then applying Lemma 1, we obtain

$$\begin{aligned} \dot{V}_L &\leq r\left[\tau - W(x,t)\theta + Y(x,\lambda_{\min})\phi\right] + |r| L(x)\psi + |r|(\delta(q) + d_0) \\ &+ \tilde{\theta}^\top D^{-1}(\hat{\theta})\alpha^{-1}\dot{\hat{\theta}} + \tilde{\phi}^\top D^{-1}(\hat{\phi})\beta^{-1}\dot{\hat{\phi}} + \tilde{\psi}^\top D^{-1}(\hat{\psi})\gamma^{-1}\dot{\hat{\psi}} \end{aligned} \tag{6.11}$$

where (6.3) was used, $L(x) = [L_1(q), L_2(q), L_3(\dot{q})]^\top$, L_i are Lipschitzian bounding functions given in Appendix A, $\alpha = \text{diag}\{\alpha_i\}$, $\beta = \text{diag}\{\beta_i\}$, $\gamma = \text{diag}\{\gamma_i\}$, and

$$D(\hat{\bullet}) = \text{diag}\left\{(\bullet_{i\max} - \hat{\bullet}_i)(\hat{\bullet}_i - \bullet_{i\min})\right\}. \tag{6.12}$$

Based on (6.11), we propose the following robust adaptive control law

$$\tau = -k_c r + W(x,t)\hat{\theta} - Y(x,\lambda_{\min})\hat{\phi} - \tanh(r\rho_1(x)) L(x)\hat{\psi} - \tanh(r\rho_2(q))(\delta(q) + d_0) \tag{6.13}$$

where $k_c > 0$ is a user-defined control gain,

$$\rho_1(x) = \frac{L(x)\psi_{\max}}{\varepsilon_1} > 0 \tag{6.14}$$

$$\rho_2(q) = \frac{\delta(q) + d_0}{\varepsilon_2} > 0, \tag{6.15}$$

$\varepsilon_i > 0$ are user-defined gains, and the update laws for the parameter estimates are given by [37]

$$\dot{\hat{\theta}} = -\alpha D(\hat{\theta}) W^\top(x,t) r, \quad \hat{\theta}(0) \in (\theta_{\min}, \theta_{\max}) \tag{6.16}$$

$$\dot{\hat{\phi}} = \beta D(\hat{\phi}) Y^\top(x, \lambda_{\min}) r, \quad \hat{\phi}(0) \in (\phi_{\min}, \phi_{\max}) \tag{6.17}$$

$$\dot{\hat{\psi}} = \gamma D(\hat{\psi}) r \tanh(r\rho_1(x)) L^\top(x), \quad \hat{\psi}(0) \in (\psi_{\min}, \psi_{\max}). \tag{6.18}$$

6.2.2 Main Result

The statement of the stability properties of the above robust adaptive controller is given in the following theorem.

Theorem 13 The control algorithm given by (6.13)-(6.15) ensures practical tracking in the sense that

$$\lim_{t\to\infty} |e(t)| \leq \frac{1}{\mu}\sqrt{\frac{c(\varepsilon_1 + \varepsilon_2)}{k_c}},\ c = 0.2758$$

and the boundedness of all other signals for any $(q(0), \dot{q}(0)) \in \mathbb{R}^2$ and $(\hat{\theta}(0), \hat{\phi}(0)\hat{\psi}(0)) \in (\theta_{\min}, \theta_{\max}) \times (\phi_{\min}, \phi_{\max}) \times (\psi_{\min}, \psi_{\max})$.

Proof. Substituting (6.13)-(6.15) into (6.11) yields

$$\begin{aligned}\dot{V}_L \leq\ & -k_c r^2 + |r|(\delta(q) + d_0) - r\tanh(r\rho_2(q))(\delta(q) + d_0) \\ & + |r| L(x)\psi - r\tanh(r\rho_1(x)) L(x)\hat{\psi} + \tilde{\psi}^\intercal r \tanh(r\rho_1(x)) L^\intercal(x).\end{aligned} \tag{6.19}$$

From Lemma 7 and (6.15), we have that

$$\begin{aligned}|r|(\delta(q) + d_0) &\leq \left[r\tanh(r\rho_2(q)) + c\rho_2^{-1}(q)\right](\delta(q) + d_0) \\ &= r\tanh(r\rho_2(q))(\delta(q) + d_0) + c\varepsilon_2.\end{aligned} \tag{6.20}$$

Given that $L(x)\psi \geq 0$, we can use Lemma 7 and (6.14) to claim that

$$\begin{aligned} |r|\, L(x)\psi &\leq \left[r\tanh\left(r\rho_1(x)\right) + c\rho_1^{-1}(x)\right] L(x)\psi \\ &\leq r\tanh\left(r\rho_1(x)\right) L(x)\psi + c\rho_1^{-1}(x) L(x)\psi_{\max} \\ &= r\tanh\left(r\rho_1(x)\right) L(x)\psi + c\varepsilon_1 \end{aligned} \tag{6.21}$$

when $\rho_1(x) > 0$. Therefore,

$$|r|\, L(x)\psi - r\tanh\left(r\rho_1(x)\right) L(x)\hat{\psi} + \tilde{\psi}^{\mathsf{T}} r\tanh\left(r\rho_1(x)\right) L^{\mathsf{T}}(x) \leq c\varepsilon_1 \tag{6.22}$$

when $\rho_1(x) > 0$. Now, when $\rho_1(x) = 0$, we know from (6.14) that $L(x) = 0$, so the left-hand side of (6.22) is zero. Applying these results to (6.19) yields

$$\dot{V}_L \leq -k_c r^2 + c\left(\varepsilon_1 + \varepsilon_2\right). \tag{6.23}$$

Since the projection algorithm in (6.15) ensures $(\hat{\theta}(t), \hat{\phi}(t), \hat{\psi}(t)) \in \mathcal{L}_\infty$, we know $(\tilde{\theta}(t), \tilde{\phi}(t), \tilde{\psi}(t)) \in \mathcal{L}_\infty$ by the definition of the parameter estimate and estimate error. From (6.8) and (6.23), we can show that $r(t) \in \mathcal{L}_\infty$ by analyzing the following two cases: (i) $|r(t)| \leq \sqrt{c\left(\varepsilon_1 + \varepsilon_2\right)/k_c}$ and (ii) $|r(t)| > \sqrt{c\left(\varepsilon_1 + \varepsilon_2\right)/k_c}$. Case (i) directly gives that $r(t)$ is bounded. For Case (ii), we know that $\dot{V}_L < 0$ and hence $V_L(t) \in \mathcal{L}_\infty$ and $r(t)$ is ultimately bounded with effective bound given by $\sqrt{c\left(\varepsilon_1 + \varepsilon_2\right)/k_c}$. Combining both cases yields $\lim_{t\to\infty} |r(t)| \leq \sqrt{c\left(\varepsilon_1 + \varepsilon_2\right)/k_c}$ for any $r(0)$. Therefore, we have from (5.17) that $\lim_{t\to\infty} |e(t)| \leq \mu^{-1}\sqrt{c\left(\varepsilon_1 + \varepsilon_2\right)/k_c}$ for any $e(0)$.

Given that $(r(t), e(t)) \in \mathcal{L}_\infty$, we have that $\dot{e}(t) \in \mathcal{L}_\infty$ from (5.14). Because $(q_d(t), \dot{q}_d(t), \ddot{q}_d(t)) \in \mathcal{L}_\infty$ by design, then $(q(t), \dot{q}(t)) \in \mathcal{L}_\infty$ from (4.3). We can now conclude that all functions on the right-hand side of (6.13) are bounded and thus $\tau(t) \in \mathcal{L}_\infty$. Since $d(q,t) \in \mathcal{L}_\infty$ from (6.3), we can use (6.1) to state that $\ddot{q}(t) \in \mathcal{L}_\infty$. Since no restrictions were placed on q and $\dot{q}$ during the above analysis, the stability result holds globally for q and $\dot{q}$. ■

Remark 3 The bound $\sqrt{c\left(\varepsilon_1 + \varepsilon_2\right)/k_c}$ in the above proof is referred to as an *effective* bound because it is not exact. That is, when $|r(t)| > \sqrt{c\left(\varepsilon_1 + \varepsilon_2\right)/k_c}$, the trajectory of $|r(t)|$ is

pulled back towards $\sqrt{c\left(\varepsilon_1+\varepsilon_2\right)/k_c}$ by the fact that $\dot{V}_L < 0$, and a balance occurs at $|r\left(t\right)| \approx \sqrt{c\left(\varepsilon_1+\varepsilon_2\right)/k_c}$.

6.3 Convex/Concave Parameterization-Based Control

6.3.1 Control Design

This control design will be based on the concavity or convexity of the elements of $Y\left(x,\lambda\right)$ defined in (6.6). Specifically, notice that if $\Theta_i := [\lambda_{i\min}, \lambda_{i\max}]$, then

- Y_1 is concave on Θ_1 for $q \geq 0$ and convex for $q < 0$;
- Y_2 is convex on Θ_2 for all q;
- Y_3 is convex on Θ_3 for $\dot{q} \geq 0$ and concave for $\dot{q} < 0$.

Based on (6.5) and the above concavity or convexity characteristics, we propose the following robust adaptive controller

$$\tau = -k_c r + W(x,t)\hat{\theta} - Y(x,\hat{\lambda})\hat{\phi} - S\left(\frac{r}{\epsilon}\right)\sum_{i=1}^{3} a_i^* - \tanh\left(r_\epsilon \rho_2\left(q\right)\right)\left(\delta\left(q\right)+d_0\right) \tag{6.24}$$

where r_ϵ was defined in (5.15),

$$\dot{\hat{\theta}} = -\alpha D(\hat{\theta}) W^{\intercal}(x,t) r_\varepsilon, \quad \hat{\theta}(0) \in (\theta_{\min}, \theta_{\max}) \tag{6.25}$$

$$\dot{\hat{\phi}} = \beta D(\hat{\phi}) Y^{\intercal}(x,\hat{\lambda}) r_\varepsilon, \quad \hat{\phi}(0) \in (\phi_{\min}, \phi_{\max}) \tag{6.26}$$

$$\dot{\hat{\lambda}} = \sigma D(\hat{\lambda}) U^{\intercal}(x,\lambda_{\min}) r_\varepsilon, \quad \hat{\lambda}(0) \in (\lambda_{\min}, \lambda_{\max}), \tag{6.27}$$

$\sigma = \text{diag}\{\sigma_i\} \in \mathbb{R}^{3\times 3}$ is positive definite,

$$U = [Y_1'(q,\lambda_{1\min}), Y_2'(q,\lambda_{2\min}), Y_3'(\dot{q},\lambda_{3\min})]^{\intercal}, \tag{6.28}$$

$Y_i'(\cdot,\lambda_i) = \partial Y_i/\partial\lambda_i$, and $\rho_2\left(q\right)$ was defined in (6.15). The a_i^* functions in (6.24) are defined as follows. If $r \geq 0$:

$$a_1^* = \begin{cases} \phi_{1\max}\left[Y_{1\min} - \hat{Y}_1 + \left(\hat{\lambda}_1 - \lambda_{1\min}\right)U_1\right], \text{ if } q \geq 0 \\ \phi_{1\max}\left[Y_{1\max} - \hat{Y}_1 + \left(\hat{\lambda}_1 - \lambda_{1\max}\right)U_1\right], \text{ if } q < 0, \end{cases} \tag{6.29}$$

$$a_2^* = \phi_{2\max}\left[Y_{2\max} - \hat{Y}_2 + \left(\hat{\lambda}_2 - \lambda_{2\max}\right)U_2\right], \tag{6.30}$$

$$a_3^* = \begin{cases} \phi_{3\max}\left[Y_{3\max} - \hat{Y}_3 + \left(\hat{\lambda}_3 - \lambda_{3\max}\right) U_3\right], \text{ if } \dot{q} \geq 0 \\ \phi_{3\max}\left[Y_{3\min} - \hat{Y}_3 + \left(\hat{\lambda}_3 - \lambda_{3\min}\right) U_3\right], \text{ if } \dot{q} < 0; \end{cases} \tag{6.31}$$

if $r < 0$:

$$a_1^* = \begin{cases} -\phi_{1\max}\left[Y_{1\max} - \hat{Y}_1 + \left(\hat{\lambda}_1 - \lambda_{1\max}\right) U_1\right], \text{ if } q \geq 0 \\ -\phi_{1\max}\left[Y_{1\min} - \hat{Y}_1 + \left(\hat{\lambda}_1 - \lambda_{1\min}\right) U_1\right], \text{ if } q < 0, \end{cases} \tag{6.32}$$

$$a_2^* = -\phi_{2\max}\left[Y_{2\min} - \hat{Y}_2 + \left(\hat{\lambda}_2 - \lambda_{2\min}\right) U_2\right], \tag{6.33}$$

$$a_3^* = \begin{cases} -\phi_{3\max}\left[Y_{3\min} - \hat{Y}_3 + \left(\hat{\lambda}_3 - \lambda_{3\min}\right) U_3\right], \text{ if } \dot{q} \geq 0 \\ -\phi_{3\max}\left[Y_{3\max} - \hat{Y}_3 + \left(\hat{\lambda}_3 - \lambda_{3\max}\right) U_3\right], \text{ if } \dot{q} < 0, \end{cases} \tag{6.34}$$

where, for simplicity of notation, $Y_{i\min} = Y_i(\cdot, \lambda_{i\min})$, $Y_{i\max} = Y_i(\cdot, \lambda_{i\max})$, and $\hat{Y}_i = Y_i(\cdot, \hat{\lambda}_i)$.

Remark 4 Despite the switching between (6.29)-(6.31) and (6.32)-(6.34), the continuity of control law (6.24) is guaranteed by the saturation function $S(r/\epsilon)$ multiplying a_i^*. That is, for each i, $\lim_{r\to 0^-} S(r/\epsilon)\, a_i^* = \lim_{r\to 0^+} S(r/\epsilon)\, a_i^* = 0$.

Remark 5 The use of (6.28)-(6.34) was inspired by the min-max optimization strategy proposed in [77]. However, we use specific forms for U and a_i^* instead of the generalized ones in [77] that were introduced for the purpose of minimizing the amplitude of the control term $\sum_{i=1}^{3} a_i^*$. Since optimization is not our main control objective, our designs in (6.28)-(6.34) simplify the overall control law. Also, different with the adaptive approach in Section 5.2, we simplify the design of tuning function a_i^* by removing the process of numerically solving the parameter $\bar{\lambda}_3$ from some nonlinear function, which is beneficial for the control implementations by alleviating the burden of calculation.

6.3.2 Main Result

Theorem 14 The control algorithm given by (6.24)-(6.34) ensures practical tracking in the sense of

$$\lim_{t\to\infty} |e(t)| \leq \frac{1}{\mu}\left(\epsilon + \sqrt{\frac{c\varepsilon_1}{k_c}}\right),\ c = 0.2758 \tag{6.35}$$

and the boundedness of all other signals for any $(q(0), \dot{q}(0)) \in \mathbb{R}^2$ and $(\hat{\theta}(0), \hat{\phi}(0)\hat{\lambda}(0)) \in (\theta_{\min}, \theta_{\max})\times (\phi_{\min}, \phi_{\max}) \times (\lambda_{\min}, \lambda_{\max})$.

Proof. Consider the Lyapunov function candidate $V_C : \mathbb{R} \times \Xi_C \to [0, \infty)$

$$\begin{aligned} V_C &= \frac{1}{2}Jr_\epsilon^2 + \sum_{i=1}^{3}\alpha_i^{-1}\int_0^{\tilde{\theta}_i}\frac{s}{(\theta_{i\max}-\theta_i-s)(\theta_i+s-\theta_{i\min})}ds \\ &+ \sum_{i=1}^{3}\beta_i^{-1}\int_0^{\tilde{\phi}_i}\frac{s}{(\phi_{i\max}-\phi_i-s)(\phi_i+s-\phi_{i\min})}ds \\ &+ \sum_{i=1}^{3}\sigma_i^{-1}\phi_i\int_0^{\tilde{\lambda}_i}\frac{s}{(\lambda_{i\max}-\lambda_i-s)(\lambda_i+s-\lambda_{i\min})}ds \end{aligned} \tag{6.36}$$

where

$$\Xi_C := \left\{(\tilde{\theta}, \tilde{\phi}, \tilde{\lambda}) : (\theta_{\min}-\theta, \theta_{\max}-\theta) \times (\phi_{\min}-\phi, \phi_{\max}-\phi) \times (\lambda_{\min}-\lambda, \lambda_{\max}-\lambda)\right\}. \tag{6.37}$$

Since r_ϵ in (5.15) is continuous for all r, it follows that $\dot{V}_C$ exists for all r [11] and is given by

$$\dot{V}_C = r_\epsilon J\dot{r}_\epsilon + \tilde{\theta}^\top D^{-1}(\hat{\theta})\alpha^{-1}\dot{\hat{\theta}} + \tilde{\phi}^\top D^{-1}(\hat{\phi})\beta^{-1}\dot{\hat{\phi}} + \phi^\top \text{diag}\left(\tilde{\lambda}\right) D^{-1}(\hat{\lambda})\sigma^{-1}\dot{\hat{\lambda}} \tag{6.38}$$

where D was defined in (6.12) and $\text{diag}(\tilde{\lambda}) := \text{diag}\{\tilde{\lambda}_i\}$. The above derivative will be analyzed for two cases: $|r| \leq \epsilon$ and $|r| > \epsilon$.

Case 1: $|r| \leq \epsilon$

It follows from (5.15) that $r_\epsilon = 0$ and $\dot{r}_\epsilon = 0$. Therefore, the adaptation laws are zero according to (6.24) and $\dot{V}_C = 0$ from (6.38). Since $|r| \leq \epsilon$, then (5.17) holds for which (6.35) is a sufficient condition. Since $(\hat{\theta}(t), \hat{\phi}(t), \hat{\psi}(t)) \in \mathcal{L}_\infty$ by the projection in (6.24) and $r(t), e(t) \in \mathcal{L}_\infty$, we can follow the arguments from the proof of Theorem 1 to conclude the boundedness of all signals

inclusive of the control (6.24)-(6.34).

Case 2: $|r| > \epsilon$

In this case, $\dot{r}_\epsilon = \dot{r}$, so after substituting (6.5) and (6.24) into $r_\epsilon J\dot{r}_\epsilon$, we obtain

$$\begin{aligned} r_\epsilon J\dot{r}_\epsilon &\leq -k_c r_\epsilon^2 + r_\epsilon \left[W(x,t)\tilde{\theta} - d\left(q,t\right) - \tanh\left(r_\epsilon \rho_2\left(q\right)\right)\left(\delta\left(q\right) + d_0\right)\right] \\ &\quad + r_\epsilon \left(Y\left(x,\lambda\right)\phi - Y(x,\hat{\lambda})\hat{\phi} - S(\frac{r}{\epsilon})\sum_{i=1}^{3} a_i^*\right) \end{aligned} \tag{6.39}$$

where we have used the fact that $rr_\epsilon > r_\epsilon^2$ when $|r| > \epsilon$. Adding and subtracting $r_\epsilon Y(x,\hat{\lambda})\phi$ to (6.39) yields

$$\begin{aligned} r_\epsilon J\dot{r}_\epsilon &\leq -k_c r_\epsilon^2 + r_\epsilon \left[W(x,t)\tilde{\theta} - Y(x,\hat{\lambda})\tilde{\phi} - d\left(q,t\right) - \tanh\left(r_\epsilon \rho_2\left(q\right)\right)\left(\delta\left(q\right) + d_0\right)\right] \\ &\quad + r_\epsilon \left(\left[Y(x,\lambda) - Y(x,\hat{\lambda})\right]\phi - S(\frac{r}{\epsilon})\sum_{i=1}^{3} a_i^*\right) \end{aligned} \tag{6.40}$$

Now, substituting (6.40), (6.24), and (6.3) into (6.38) gives

$$\dot{V}_C \leq -k_c r_\epsilon^2 + r_\epsilon \sum_{i=1}^{3} H_i + |r_\epsilon|\left(\delta\left(q\right) + d_0\right) - r_\varepsilon \tanh\left(r_\varepsilon \rho_2\left(q\right)\right)\left(\delta\left(q\right) + d_0\right) \tag{6.41}$$

where

$$H_i = \phi_i \left[Y_i(x,\lambda_i) - Y_i(x,\hat{\lambda}_i) + \tilde{\lambda}_i U_i\right] - S(\frac{r}{\epsilon})a_i^*. \tag{6.42}$$

Applying Lemma 1 and (6.15) to (6.41) gives

$$\dot{V}_C \leq -k_c r_\epsilon^2 + c\varepsilon_2 + r_\varepsilon \sum_{i=1}^{3} H_i. \tag{6.43}$$

We now separate Case 2 into two subcases: $r > \epsilon$ and $r < -\epsilon$.

a) When $r > \epsilon$, we know that $r_\epsilon > 0$ and $S(r/\epsilon) = 1$. We can show that $H_i \leq 0$, $i = 1, 2, 3$ always. For brevity, we only demonstrate this for H_1 for the case where $q \geq 0$. A similar process can be followed for other combinations of the signs of q and $\dot{q}$ for all H_i. When $q \geq 0$, a_1^* is given by (6.29) and Y_1 is concave. Therefore, from (3.8a) and the fact that $\hat{\lambda}_1(t) \in (\lambda_{i\min}, \lambda_{i\max})$, we

have $Y_{1\min} - \hat{Y}_1 + \left(\hat{\lambda}_1 - \lambda_{1\min}\right) U_1 \geq 0$ and

$$\begin{aligned} H_1 &= \phi_1 \left[Y_1 - \hat{Y}_1 + \left(\hat{\lambda}_1 - \lambda_1\right) U_1 \right] - \phi_{1\max} \left[Y_{1\min} - \hat{Y}_1 + \left(\hat{\lambda}_1 - \lambda_{1\min}\right) U_1 \right] \\ &\leq \phi_1 \left[Y_1 - \hat{Y}_1 + \left(\hat{\lambda}_1 - \lambda_1\right) U_1 - Y_{1\min} + \hat{Y}_1 - \left(\hat{\lambda}_1 - \lambda_{1\min}\right) U_1 \right] \\ &= \phi_1 \left[Y_1 - Y_{1\min} + \left(\lambda_{1\min} - \lambda_2\right) Y'_{1\min} \right] \leq 0 \end{aligned} \tag{6.44}$$

where (6.28) was used and $Y'_{1\min} = Y'_1(q, \lambda_{1\min})$. Since $H_i \leq 0$, $i = 1, 2, 3$, it follows from (6.43) that

$$\dot{V}_C \leq -k_c r_\epsilon^2 + c\varepsilon_2. \tag{6.45}$$

b) When $r < -\epsilon$, we have $r_\epsilon < 0$ and $S(r/\epsilon) = -1$. Similar to Case a, we can invoke Corollary 3 along with the appropriate expressions in (6.29)-(6.34) to show that $H_i \geq 0$, $i = 1, 2, 3$ (6.45) for all combinations of the signs of q and $\dot{q}$. After applying this result to (6.43), we arrive at (6.45).

For Case 2, we can follow the arguments used in the proof of Theorem 13 to show that $(\tilde{\theta}(t), \tilde{\phi}(t), \tilde{\lambda}(t)) \in \mathcal{L}_\infty$ and $\lim_{t\to\infty} |r_\epsilon(t)| \leq \sqrt{c\varepsilon_2/k_c}$. It then follows from (5.15) that $\lim_{t\to\infty} |r(t)| \leq \sqrt{c\varepsilon_2/k_c} + \epsilon$ and from (5.17) that $\lim_{t\to\infty} |e(t)| \leq \mu^{-1}\left(\sqrt{c\varepsilon_2/k_c} + \epsilon\right)$. Now, we can use the signal chasing arguments from the proof of Theorem 13 to show the boundedness of the remaining signals including the control (6.24)-(6.34).

Finally, since the combined analyses of Cases 1 and 2 placed no restrictions on q and $\dot{q}$, the stability result holds for all $q(0)$ and $\dot{q}(0)$. ■

6.4 Simulation

6.4.1 Description

The performance of the robust adaptive controllers was tested via computer simulations conducted in Simulink with ode solver `ode45`. The parameters in (6.1) were set to

$$\begin{gathered} J = 0.39 \text{ kg-m}^2\text{/rad}, \; b_1 = 0.3 \text{ kg-m}^2\text{/(rad-s)}, \; b_2 = 0.1 \text{ kg-m}^2\text{/(rad-s)}, \\ b_3 = 45 \text{ s/rad}, \; k_1 = 3.657 \text{ kg-m}^2\text{/(rad-s}^2\text{)}, \; k_2 = 1.68 \text{ 1/rad}, \\ q_0 = \pi/15 \text{ rad}, \; ml = 1.025 \text{ kg-m}. \end{gathered} \tag{6.46}$$

The compact sets for the parameters were chosen as follows

$$\begin{aligned}
[J_{\min}, J_{\max}] &= [0.292, 0.400],\ [b_{1\,\min}, b_{1\,\max}] = [0.270, 0.377],\ [b_{2\,\min}, b_{2\,\max}] = [0.09, 0.15], \\
[b_{3\,\min}, b_{3\,\max}] &= [45, 75],\ [k_{1\,\min}, k_{1\,\max}] = [1.990, 4.679],\ [k_{2\,\min}, k_{2\,\max}] = [1.317, 2.204], \\
[q_{0\,\min}, q_{0\,\max}] &= [0.087, 0.262],\ [ml_{\min}, ml_{\max}] = [0.790, 1.204].
\end{aligned}$$

The above values were based on the experiments reported in [29, 107]. All parameter estimates were initialized to $\hat{\bullet}(0) = \bullet_{\min} + 0.01$. The initial conditions for the states were set to $q(0) = \pi/15$ rad and $\dot{q}(0) = 0$ rad/s.

For comparison purposes, we also simulated the dynamic robust control proposed in [99, 124], which was applied to the shank dynamics in [110] under the name "RISE" control. This control is typically used to compensate for sufficiently smooth functional uncertainties; specifically, it assumes the terms J, $B(\dot{q})$, $K(q)$, $G(q)$, and $d(q,t)$ in (6.1) are uncertain $\mathcal{C}^2$ functions. The dynamic robust control law has a relatively simple structure given by [110]

$$u(t) = (k_1 + 1) r(t) - (k_1 + 1) r(0) + \int_0^t \left[(k_1 + 1) k_2 r(\tau) + k_3 \text{sgn}(r(\tau)) \right] d\tau, \tag{6.47}$$

where r was defined in (5.14) with $\mu > 1/2$, $k_1, k_3 > 0$ are sufficiently large control gains dependent on the initial conditions and upper bounds on the functional uncertainties, respectively, and $k_2 > 1$.

Three sets of simulations were conducted using different reference trajectories and/or disturbances to capture different system operating conditions.

Simulation 1: The reference trajectory was set to

$$q_d(t) = \frac{\pi}{18} + \frac{7\pi}{24}\left(1 - \exp\left(-0.8t^3\right)\right) + \frac{\pi}{8}\left(1 - \exp\left(-0.4t^3\right)\right) \sin \omega(t) t \text{ rad} \tag{6.48}$$

where $\omega(t) = 0.6\pi + 0.5\pi/\cosh(0.6(t-13))$ rad/s is the time-varying frequency. Note that $q_d(0) = \pi/18$ and $\dot{q}_d(0) = \ddot{q}_d(0) = 0$. This trajectory, which is shown in Figure 6.1a, mimics a walking gait whose period varies rapidly from 1.8 s to 3.5 s.

The disturbance was chosen as

$$d\left(q,t\right)=0.3\exp\left(0.2q\right)+0.1q \tag{6.49}$$

to capture unmodeled elastic effects. This disturbance was bounded as in (6.3) with

$$\delta(q)=3.5\exp\left(0.2\left|q\right|\right)+4. \tag{6.50}$$

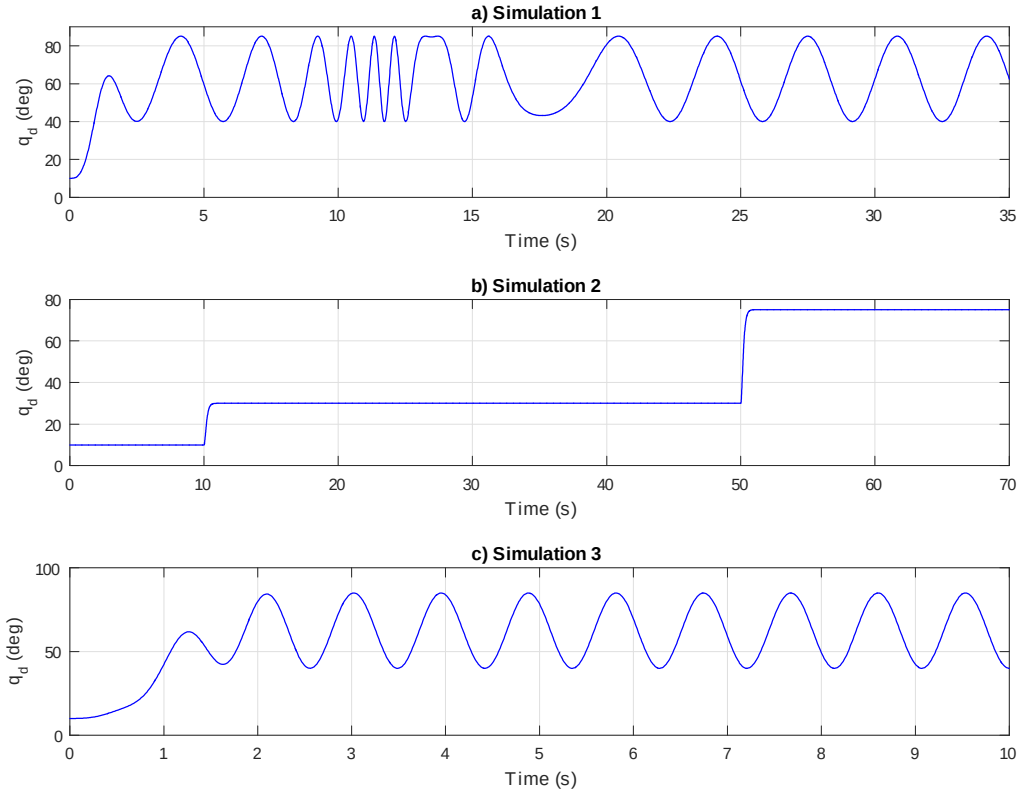

Figure 6.1: Reference trajectory $q_d(t)$ used in each simulation.

Simulation 2: Here, the reference trajectory was set to a sequence of two smooth step commands generated by the dynamical system

$$\begin{aligned}\dot{x}&=\begin{bmatrix}0&1&0\\0&0&1\\-6000&-1300&-80\end{bmatrix}x+\begin{bmatrix}0\\0\\1\end{bmatrix}w\\ y&=x,\end{aligned} \tag{6.51}$$

where $x = [q_d, \dot{q}_d, \ddot{q}_d]^\top$ and

$$w = \begin{cases} 1000\pi/3, & 0 \leq t < 10 \text{ s} \\ 1000\pi, & 10 \leq t < 50 \text{ s} \\ 2500\pi, & t \geq 50 \text{ s}, \end{cases}$$

with initial condition $x(0) = [\pi/18, 0, 0]^\top$. The plot of $q_d(t)$ is shown in Figure 6.1b. This trajectory simulates a typical motion conducted during rehabilitation sessions. The same disturbance in (6.49) was used in this simulation.

Simulation 3: In this case, the reference trajectory was given by (6.48), but with a constant frequency of $\omega = 2.15\pi$ rad/s (see Figure 6.1c). This represents a walking gait with period of 0.9 s, and therefore faster than the one in Simulation 1. The disturbance was selected as

$$d\left(q, t\right) = 0.3 \exp\left(0.2q\right) + 0.1q + d_l\left(t\right), \tag{6.52}$$

where $d_l\left(t\right)$ is the discontinuous signal

$$d_l\left(t\right) = \begin{cases} 0, & 0 \leq t < 10 \text{ s} \\ 7.2 \text{ Nm}, & 10 \leq t < 15 \text{ s} \\ 0, & 15 \leq t < 20 \text{ s} \\ -3.6 \text{ Nm}, & 20 \leq t < 25 \text{ s} \\ 0, & t \geq 25 \text{ s} \end{cases} \tag{6.53}$$

that simulates unintentional muscle contractions and/or the addition of loads. The same bounding function (6.50) was used in this simulation.

In all simulations, the following gains were used. Lipschitzian parameterization-based (LPB) control:

$$\begin{aligned} k_c &= 2,\ \mu = 2.7,\ \varepsilon_1 = 0.04,\ \varepsilon_2 = 0.75,\ \alpha = \text{diag}\{80, 170, 35\},\ \beta = \text{diag}\{140, 90, 100\}, \\ \gamma &= \text{diag}\{170, 450, 80000\}; \end{aligned}$$

convex/concave parameterization-based (CCPB) control:

$$k_c = 2,\ \mu = 2.7,\ \varepsilon_2 = 0.75,\ \epsilon = 0.003,\ \alpha = \text{diag}\{80, 170, 35\},\ \beta = \text{diag}\{140, 90, 100\},$$

$$\sigma = \text{diag}\{80, 250, 8800\};$$

and dynamic robust (DR) control:

$$k_1 = 1,\ \mu = 2.7,\ k_2 = 2,\ k_3 = 40.$$

Note that the gains that are common across the control laws were kept at the same value to enable proper comparison. For example, since the first term on the right-hand side of (6.13) and (6.24) is the same as the one in (6.47) with $k_c = k_1 + 1$, we set $k_1 = 1$.

In order to quantify the performance of each controller, we calculated the root mean square (RMS) of the tracking error (e_{rms}) and control input (u_{rms}) as defined by

$$\bullet_{\text{rms}} = \sqrt{\frac{1}{t_f}\int_0^{t_f} \bullet^2(t)dt} \tag{6.54}$$

where t_f is the final simulation time.

6.4.2 Results and Discussion

The results for the three simulations described above are presented next. Figures 6.2-6.11 show the tracking errors, control inputs, and parameter estimates for the LPB, CCPB, and DR controls for Simulation 1. The same variables are shown in Figures 6.3-6.14 and Figures 6.4-6.17 for Simulations 2 and 3, respectively. For comparison purposes, e_{rms} and u_{rms} for each controller for each simulation are given in Table 6.1. The final time for calculating (6.54) for each simulation was as follows: Simulation 1: $t_f = 35$ s; Simulation 2: $t_f = 70$ s; Simulation 3: $t_f = 40$ s.

The results show that the LPB and CCPB controllers outperformed the DR control in the sense that they produced significantly smaller e_{rms} values with very similar control energy (i.e., u_{rms} values) across the three simulations. We believe that this better performance has the following causes. First, the robust adaptive controllers incorporate more model information than the DR controller, which is essentially model-independent and attempts to dominate the uncertainties through high-

gain feedback. Second, the inability of the DR controller to track or reject high-frequency signals very well comes from the fact that it assumes the signals are sufficiently smooth. In particular, notice the large spikes in the tracking error of the DR controller in Figures 6.2, 6.3, 6.4, which coincide with the higher frequency period of $q_d(t)$ in Figure 6.1a, the steps in $q_d(t)$ in Figure 6.1b, and the discontinuities in $d_l\,(t)$ in Figure 6.5, respectively. These spikes can be troublesome in practice since the knee joint is not capable of moving beyond approximately $\pm\pi/2$ rad.

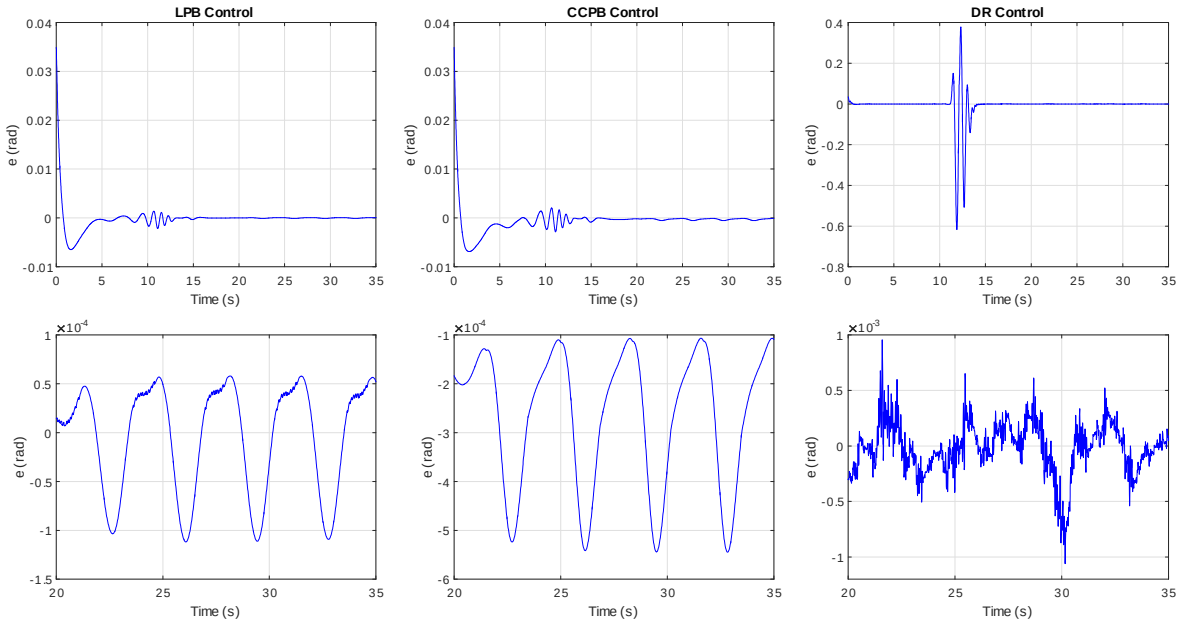

Figure 6.2: Simulation 1: Tracking error $e(t)$.

The control input of the DR controller also has higher frequency content than those of the robust adaptive controllers as can be seen from Figures 6.6, 6.7, and 6.8. The high frequency arises from the term $\int_0^t k_3 \text{sign}(r\,(\tau))\,d\tau$ in (6.47). This is of concern since torque-level control laws have to be embedded into low-level control loops, potentially magnifying their high-frequency content.

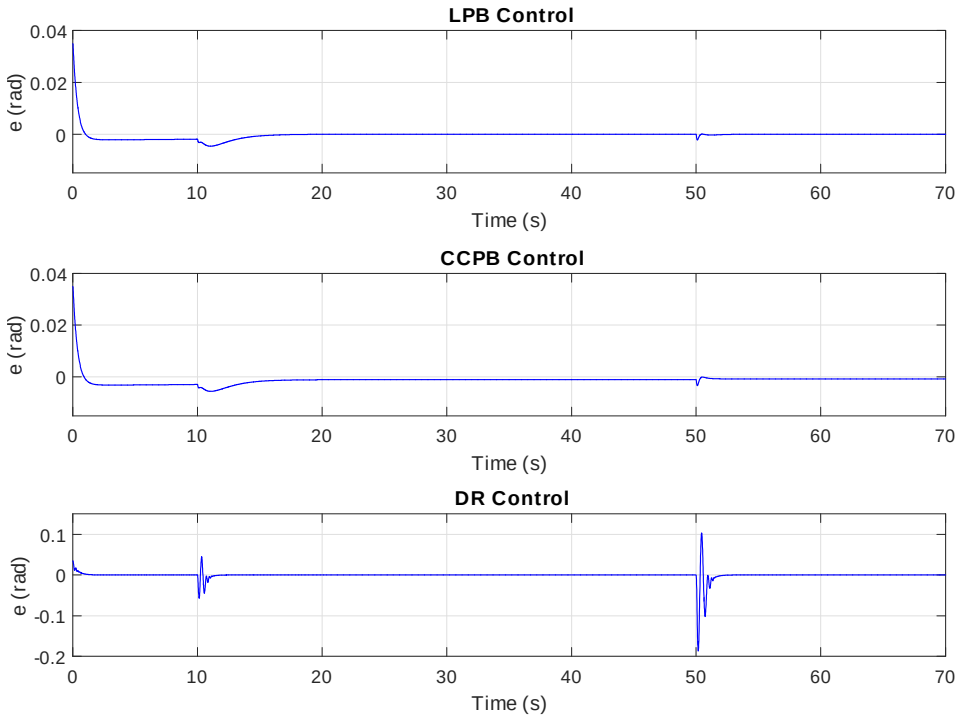

Figure 6.3: Simulation 2: Tracking error $e(t)$.

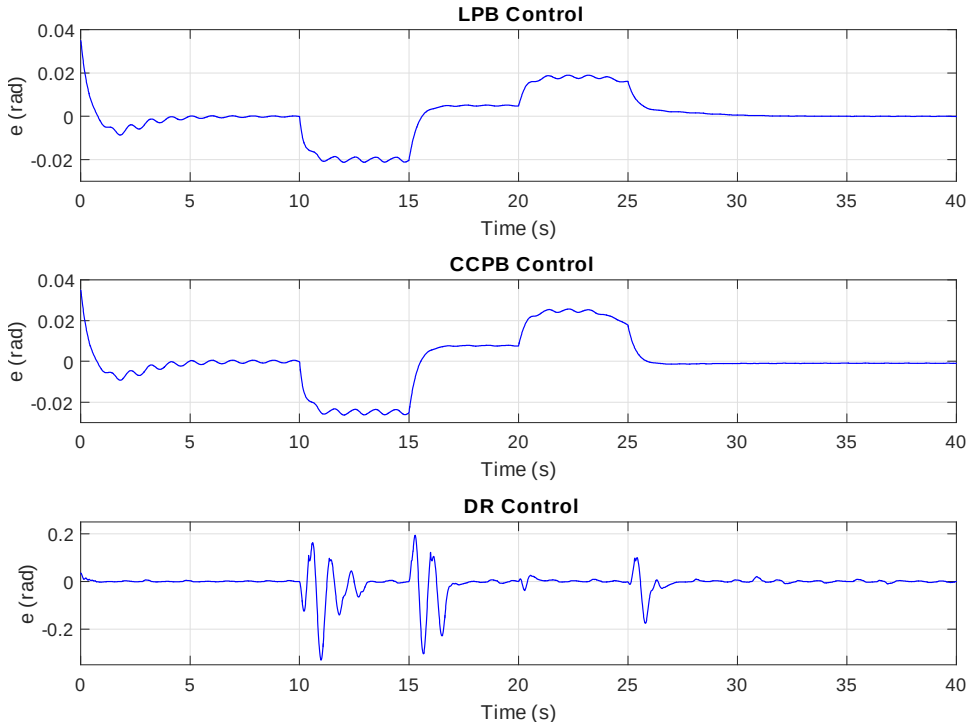

Figure 6.4: Simulation 3: Tracking error $e(t)$.

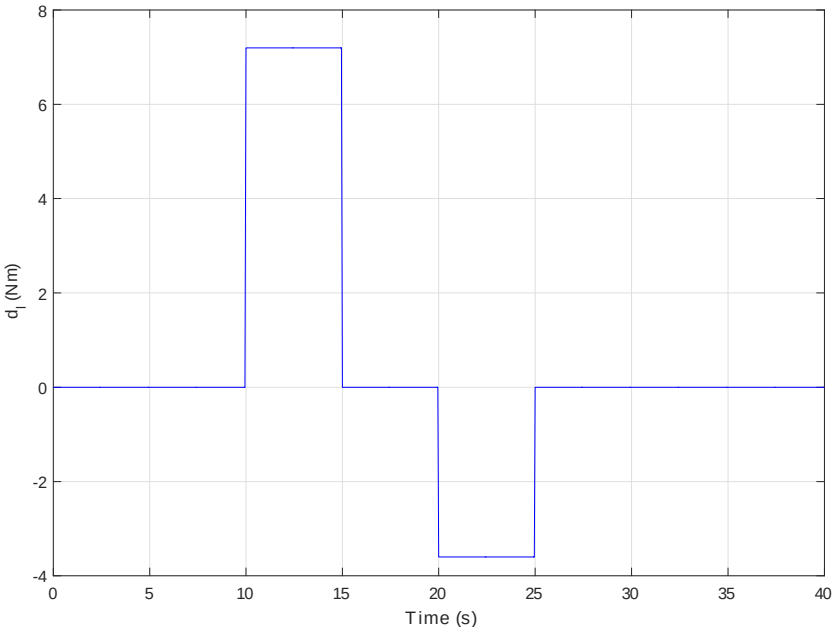

Figure 6.5: Simulation 3: Disturbance term $d_l(t)$.

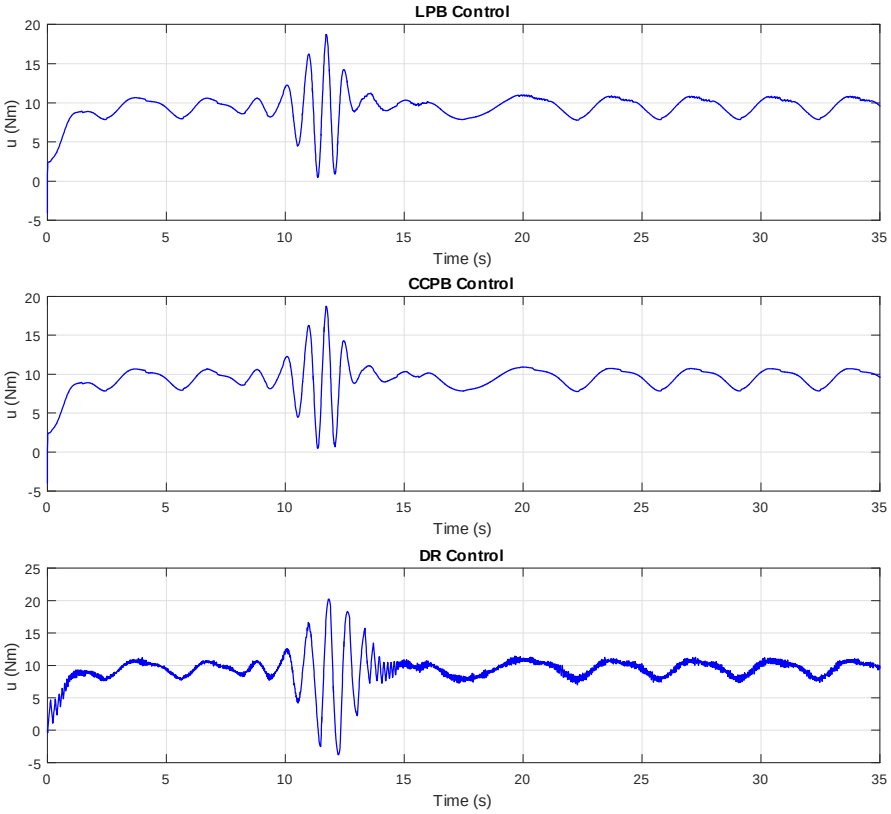

Figure 6.6: Simulation 1: Control input $\tau(t)$.

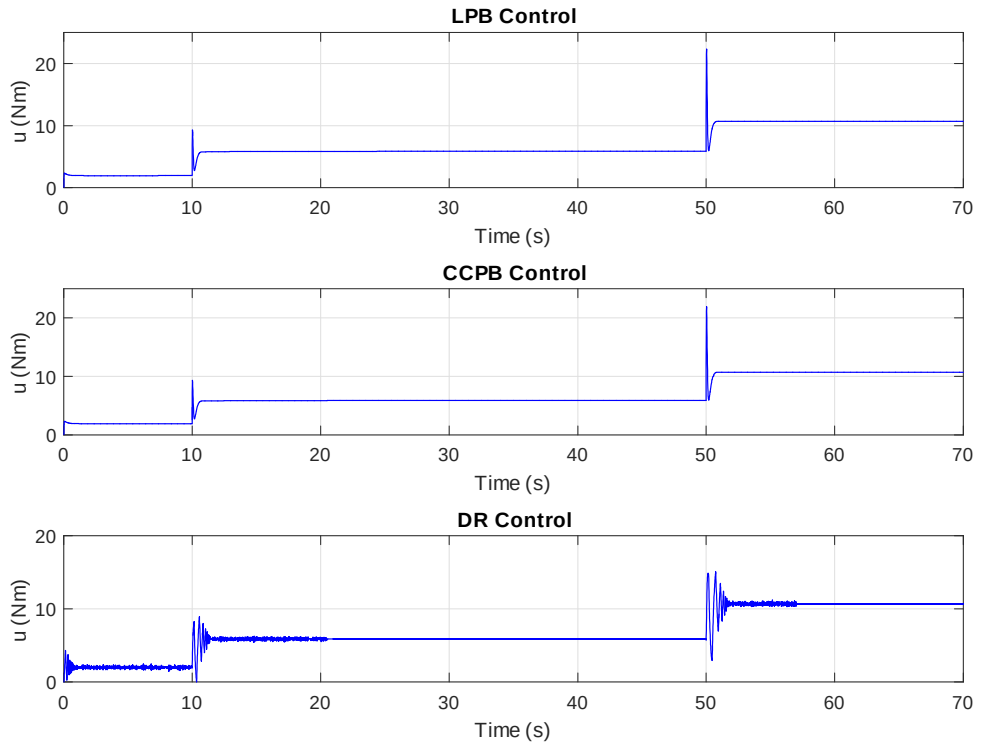

Figure 6.7: Simulation 2: Control input $\tau(t)$.

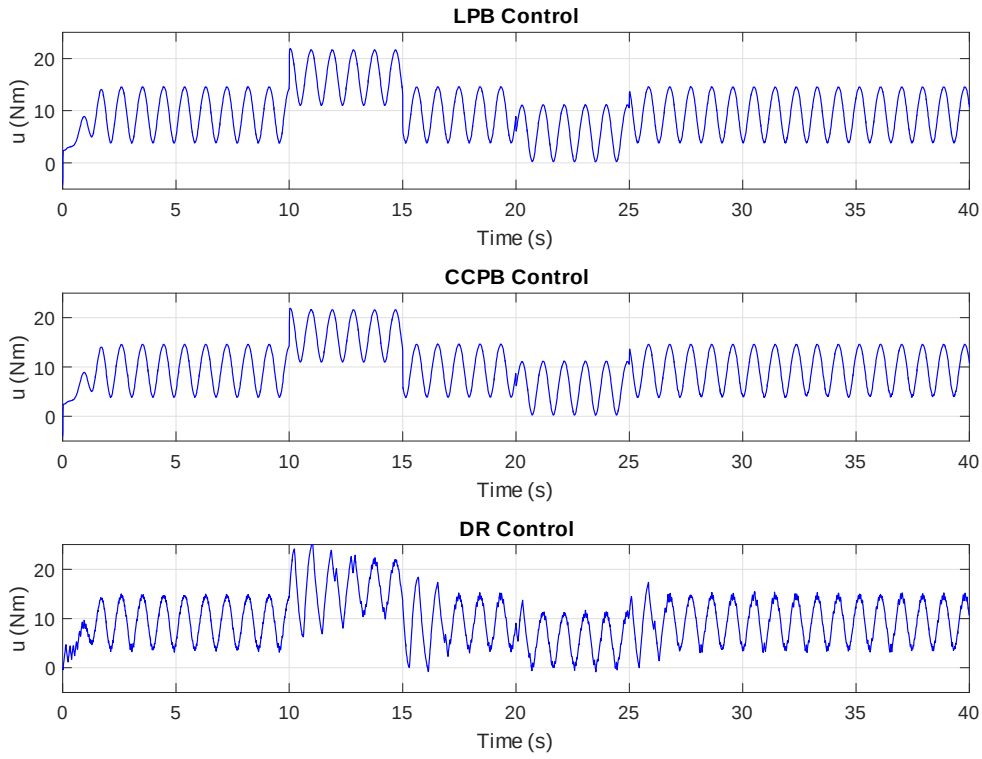

Figure 6.8: Simulation 3: Control input $\tau(t)$.

Table 6.1: Comparison of RMS Values

Simulation	Control	e_{rms} (rad)	u_{rms} (Nm)
1	LPB	0.0027	9.615
	CCPB	0.0029	9.592
	DR	0.0711	9.635
2	LPB	0.0020	7.269
	CCPB	0.0024	7.263
	DR	0.0113	7.272
3	LPB	0.0098	10.946
	CCPB	0.0124	10.950
	DR	0.0482	10.985

Between the two robust adaptive controllers, the LPB controller performed slightly better than the CCPB control, although the improvement was not significant (see Table 6.1). The parameter estimates $\hat{\theta}(t)$ and $\hat{\phi}(t)$ had similar profiles for both controllers with the difference being due to their adaptation laws being different for each control (see (6.15) and (6.24)).

The simulations reported here are not meant to be an exhaustive and definitive study of the performance of the proposed robust adaptive controllers, nor do they imply that these controllers are necessarily "better" than the DR controller (or any other controller, for that matter) when applied to the human shank musculoskeletal system. Such questions are impossible to address in general since the answer is application dependent. Rather, the simulations are meant to demonstrate with reasonable confidence that the robust adaptive controllers are a viable solution for the torque-level control of the human shank musculoskeletal system and can provide good performance for various operating conditions.

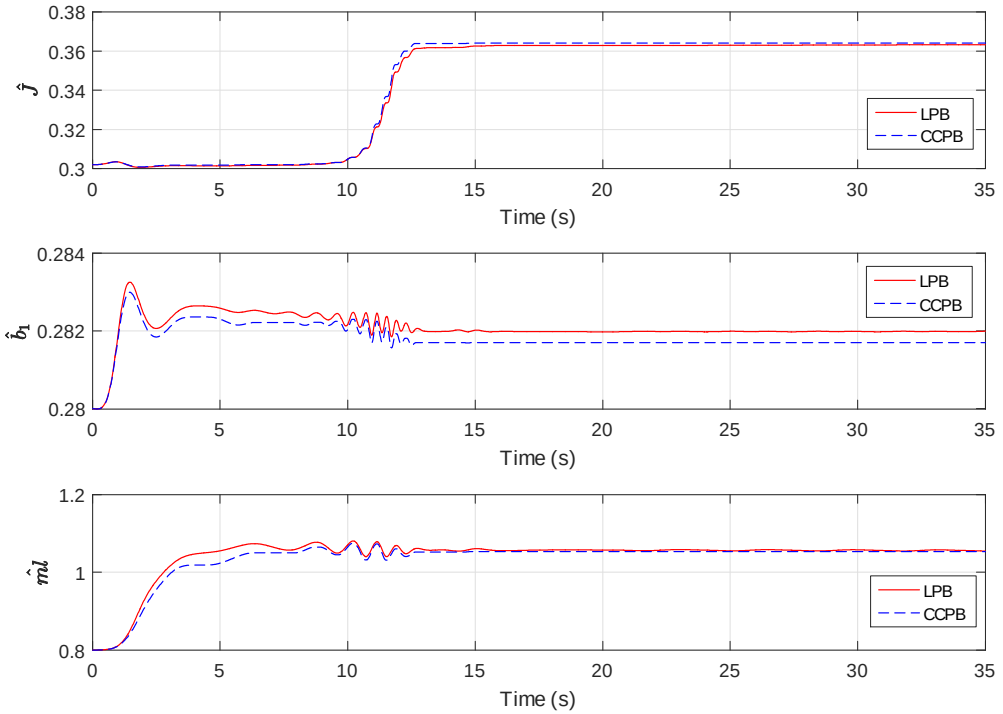

Figure 6.9: Simulation 1: Parameter estimates $\hat{\theta}(t)$.

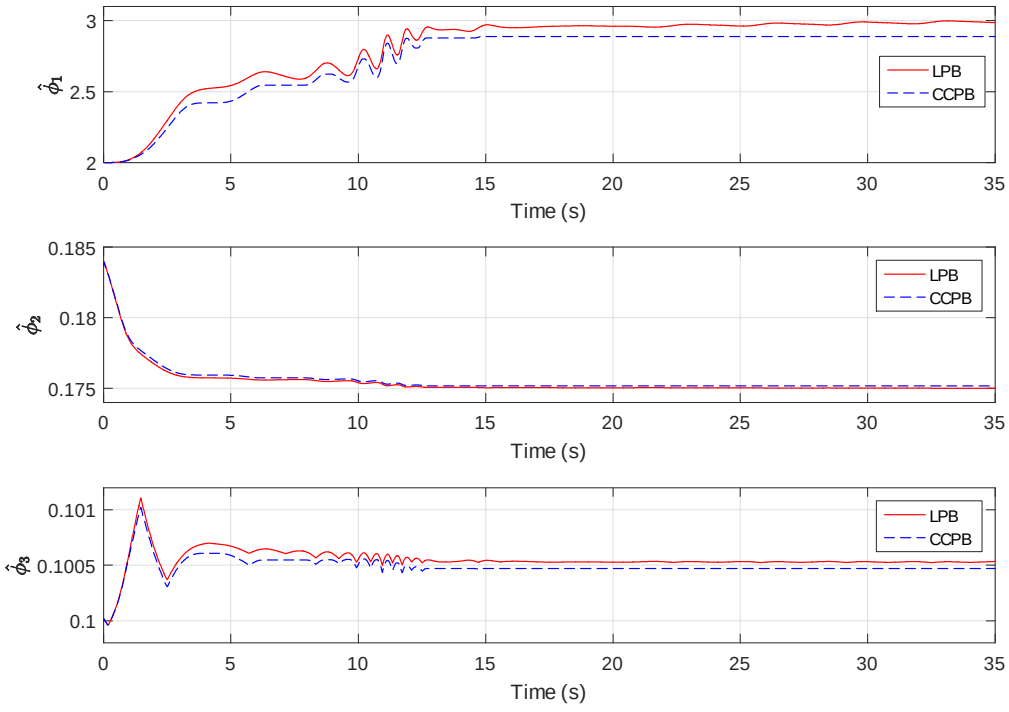

Figure 6.10: Simulation 1: Parameter estimates $\hat{\phi}(t)$.

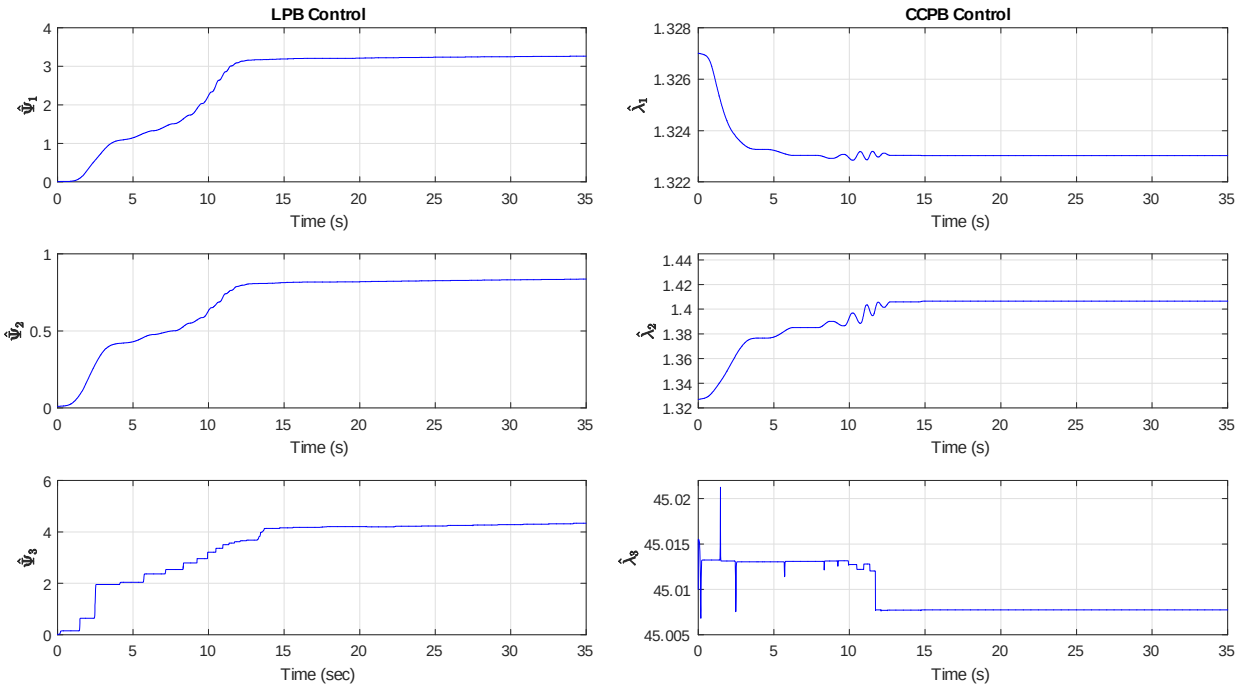

Figure 6.11: Simulation 1: Parameter estimates $\hat{\Psi}(t)$ for LPB control (left column) and parameter estimates $\hat{\lambda}(t)$ for CCPB control (right column).

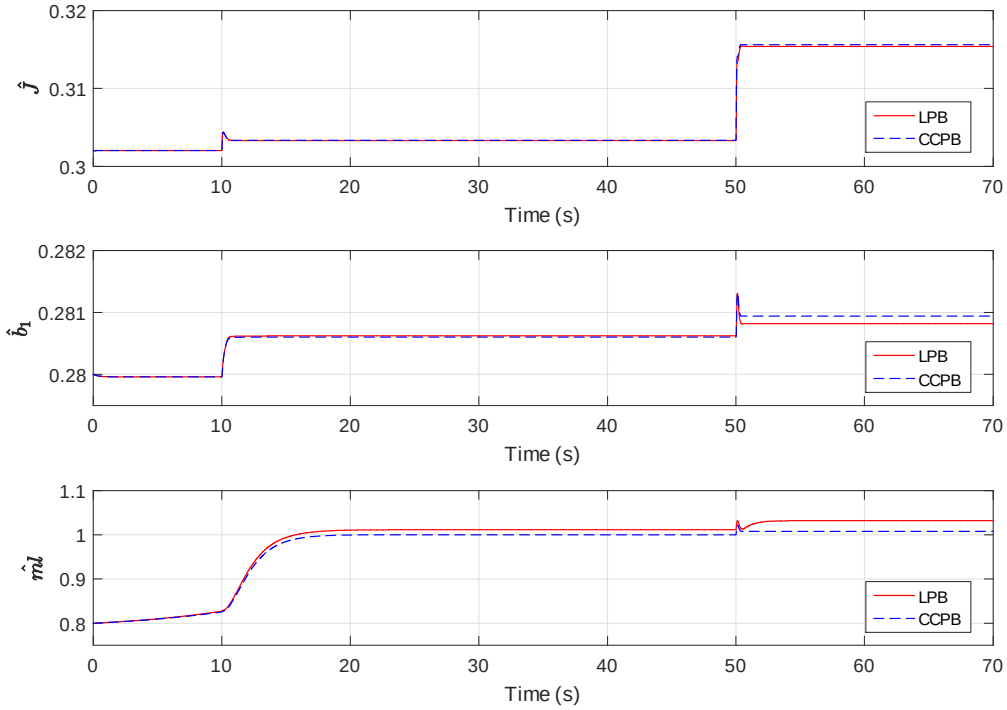

Figure 6.12: Simulation 2: Parameter estimates $\hat{\theta}(t)$.

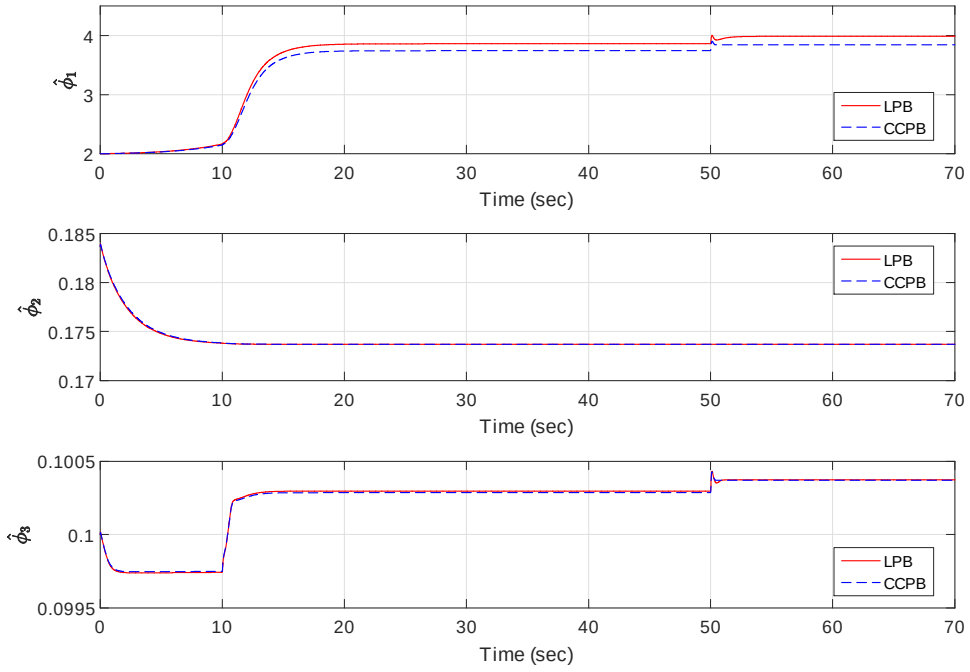

Figure 6.13: Simulation 2: Parameter estimates $\hat{\phi}(t)$.

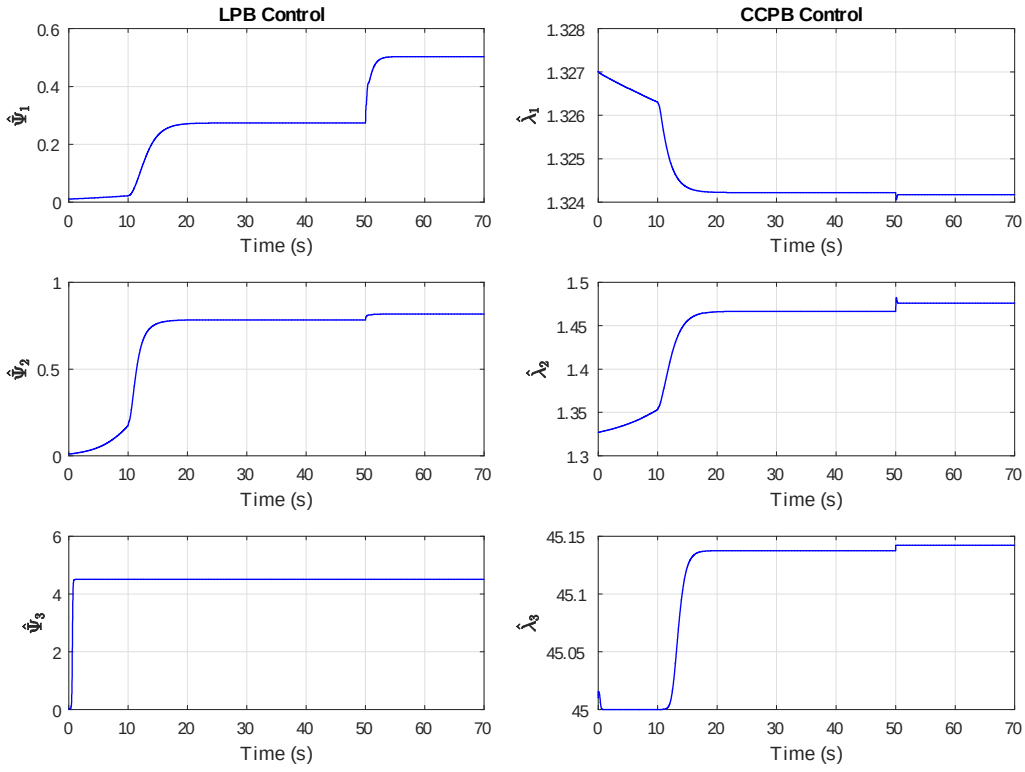

Figure 6.14: Simulation 2: Parameter estimates $\hat{\Psi}(t)$ for LPB control (left column) and parameter estimates $\hat{\lambda}(t)$ for CCPB control (right column).

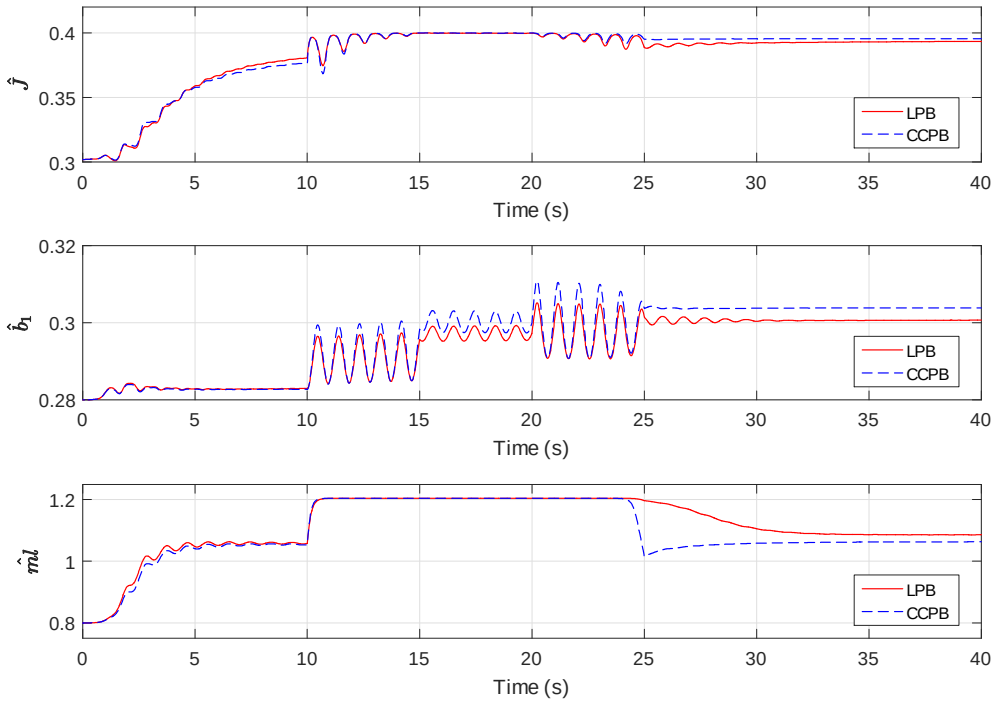

Figure 6.15: Simulation 3: Parameter estimates $\hat{\theta}(t)$.

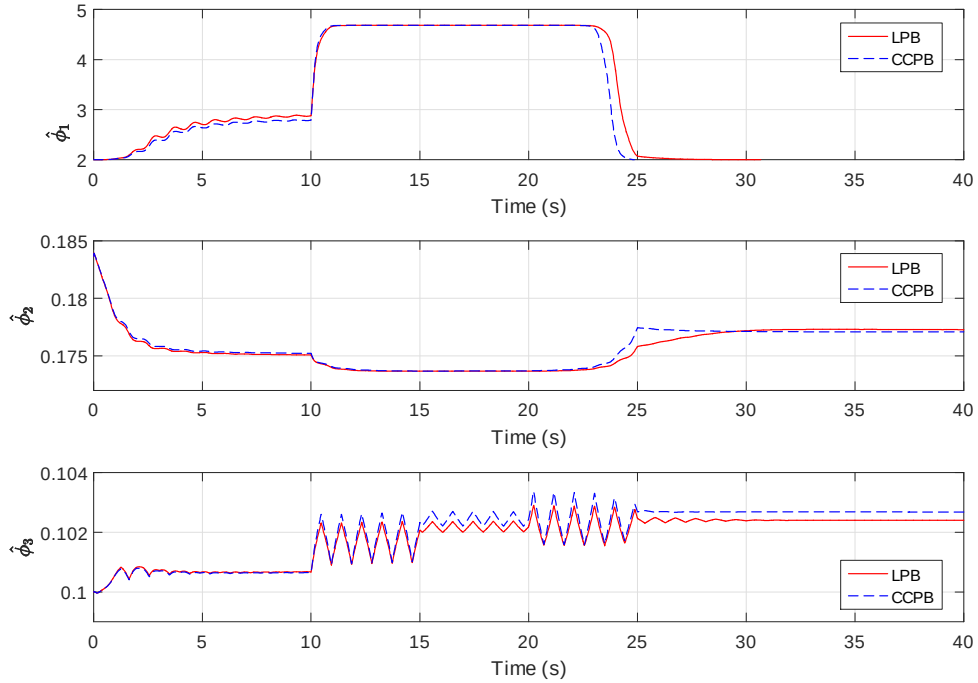

Figure 6.16: Simulation 3: Parameter estimates $\hat{\phi}(t)$.

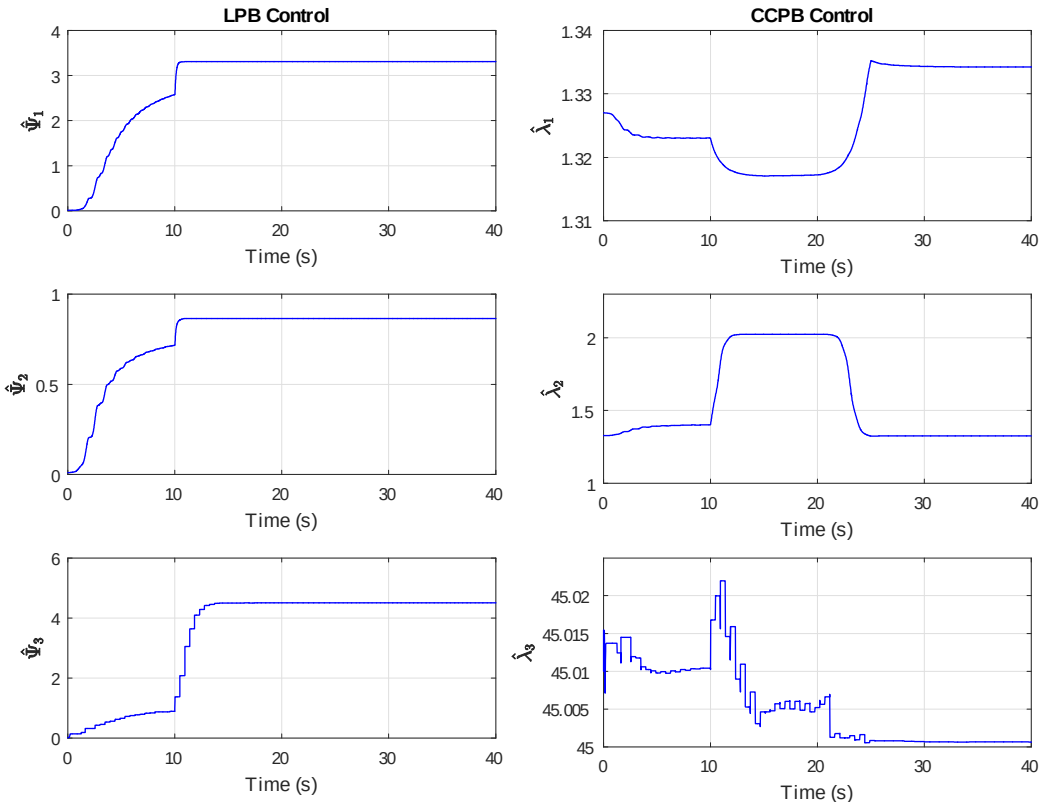

Figure 6.17: Simulation 3: Parameter estimates $\hat{\Psi}(t)$ for LPB control (left column) and parameter estimates $\hat{\lambda}(t)$ for CCPB control (right column).

Chapter 7 Neural Network-Based Control

In this chapter, we add the muscle contractile mechanics to the NMES model considered for control. The muscle contractile term relates the joint torque to the voltage applied to the electrodes; hence, our control input in this chapter is at the *voltage level* as opposed to the torque-level input of the previous chapters. Since the voltage-torque relationship is highly uncertain, the control problem in this chapter can be cast as one where the *control coefficient is unknown*. To deal with this uncertainty, we will use a NN-based control strategy. Two control strategies will be formulated: one for the case where the voltage input is not amplitude-limited and the other where it is subject to saturation.

7.1 Problem Statement

To consider more model uncertainties for the passive mechanical dynamics, we introduce a torque-level disturbance term $d(q, \dot{q}, t)$ such that the model in (6.1) is updated by

$$J\ddot{q} + B(\dot{q}) + K(q) + G(q) + d(q, \dot{q}, t) = \tau, \tag{7.1}$$

where $K(q)$, $B(\dot{q})$, and $G(q)$ were defined in (2.2)-(2.4) and the disturbance $d(q, \dot{q}, t) \in \mathbb{R}$ represents all unmodeled dynamics, e.g., elastic and damping moments, muscle fatigue, response delays, spasms, and/or time-varying external loads, and $d(q, \dot{q}, t)$ is bounded if $(q, \dot{q}) \in \mathcal{L}_\infty$ and the time-varying external loads are bounded. The active torque τ generated by electrode stimulation of the quadriceps muscles is the product of muscle contractile mechanics described by

$$\tau = F_m \varsigma(q) \eta(q, \dot{q}) u \tag{7.2}$$

where $\varsigma(q)$ is the moment arm defined in (2.7), the constant $F_m > 0$ is the maximum isometric force developed by electrical stimulation, $\eta(q, \dot{q}) := \eta_l(q) \eta_v(q, \dot{q})$ with $\eta_l(q)$ and $\eta_v(q, \dot{q})$ given by (2.10) and (2.11), respectively, and $u \in \mathbb{R}$ represents the voltage input that triggers the stimulus signals of the electrodes.

The dynamics in (7.1) can be rewritten as

$$\begin{aligned} \dot{x}_1 &= x_2 \\ J\dot{x}_2 &= f(x,t) + \Omega(x)\, u \end{aligned} \tag{7.3}$$

where $x = [x_1, x_2]^\top := [q, \dot{q}]^\top$,

$$f(x,t) = -K(x_1) - B(x_2) - G(x_1) - d(x,t), \tag{7.4}$$

$$\Omega(x) = F_m \varsigma(x_1)\, \eta(x). \tag{7.5}$$

We consider that the functions $f(x,t)$ and $\Omega(x)$ in (7.3) are unknown. Our control objective is to design $u(x,t)$ to practically track any bounded C^2 reference trajectory $x_{1d}(t)$ satisfying $\sup|x_{1d}(t)| < \pi/2$ and $(\dot{x}_{1d}(t), \ddot{x}_{1d}(t)) \in \mathcal{L}_\infty$ despite the functional uncertainties present in (7.3).

Since $\varsigma(x_1)$ and $\eta(x)$ are both positive and bounded for all $x \in (-\pi/2, \pi/2) \times \mathbb{R}$ from (2.7), (2.10), (2.11), and (2.12), we know that the control coefficient $\Omega(x)$ satisfies

$$g_0 \leq \Omega(x) \leq g_1, \tag{7.6}$$

where g_0 and g_1 are unknown positive constants. Moreover, the function $\Omega(x)$ is continuously differentiable with bounded first derivative with respect to x. In [38, 134], the upper bound on $\Omega(x)$ was assumed to be known. Though one can claim that an upper bound can always be found by picking it to be large enough, this practice may lead to unecessary, higher control efforts.

To facilitate constructing the controller, we make the following assumption about the unknown nonlinearity $f(x,t)$:

Assumption 1 The function $f(x,t)$ is continuous with respect to x and t.

This assumption relaxes the assumption in [112] that $d(x,t)$ be differentiable with respect to t. Here, we only require its continuity with respect to t.

7.2 Control Formulation

7.2.1 Design without Input Saturation

Using the tracking error defined in (4.3), we follow the backstepping approach presented in Section 4.2.

Step 1:

We first define z_1 as in (4.5) and write its dynamics as

$$\dot{z}_1 = x_2 - \dot{x}_{1d} = z_2 + \alpha - \dot{x}_{1d}. \tag{7.7}$$

where α is the virtual control and

$$z_2 = x_2 - \alpha. \tag{7.8}$$

Based on (7.7), we design the virtual control as

$$\alpha\left(z_1, t\right) = -k_1 z_1 + \dot{x}_{1d} \tag{7.9}$$

where $k_1 > 0$ is a control gain, which gives the closed-loop system

$$\dot{z}_1 = -k_1 z_1 z_2 - k_1 z_1. \tag{7.10}$$

Now, given the positive-definite and radially unbounded function

$$V_1 = \frac{1}{2} z_1^2, \tag{7.11}$$

its derivative along (7.10) yields

$$\dot{V}_1 = -K_1 z_1^2 + z_1 z_2. \tag{7.12}$$

Step 2:

The dynamics of z_2 is given by

$$\begin{aligned} J\dot{z}_2 &= J\dot{x}_2 - J\dot{\alpha} \\ &= f(x,t) + \Omega\left(x\right) u\left(t\right) - J\dot{\alpha}. \end{aligned} \tag{7.13}$$

where (7.3) was used and

$$\dot{\alpha} = -K_1 z_2 + K_1^2 z_1 + \ddot{x}_{1d}. \tag{7.14}$$

We now define the positive-definite and radially unbounded function

$$V_2\left(z_1, z_2\right) = \frac{J}{g_1}\int_0^{z_2} \tanh\left(s\right)\beta(z_1 + x_{1d}, s + \alpha)ds \tag{7.15}$$

where

$$\beta\left(x_1, x_2\right) = \frac{g_1}{\Omega\left(x\right)}, \tag{7.16}$$

and (4.5) and (7.8) were used. Based on (7.6), we have

$$1 \leq \beta\left(x_1, x_2\right) \leq \frac{g_1}{g_0} \tag{7.17}$$

where $\beta\left(x_1, x_2\right)$ is continuously differentiable with respect to x. Therefore,

$$V_2 \leq \frac{J}{g_0}\int_0^{z_2} \tanh\left(s\right) ds = \frac{J}{g_0}\ln\left(\cosh\left(z_2\right)\right), \tag{7.18}$$

and

$$V_2 \geq \frac{J}{g_1}\ln\left(\cosh\left(z_2\right)\right). \tag{7.19}$$

Remark 6 The function in (7.15) is inspired by the one proposed in [134, 38]. In this work, we modified the function in [134, 38] by using $\tanh\left(s\right)$ in replace of s. This was motivated by the desire to attenuate the transient amplitude of the control input signal. That is, for large initial conditions, we observed that the control signal in (7.29) has significantly smaller transients than the control in [134, 38].

After taking the time derivative of (7.15), we obtain

$$\dot{V}_2 = \frac{\partial V_2}{\partial z_1}\dot{z}_1 + \frac{\partial V_2}{\partial z_2}\dot{z}_2 + \frac{\partial V_2}{\partial t}, \tag{7.20}$$

where

$$\frac{\partial V_2}{\partial z_1}\dot{z}_1 = \frac{J}{g_1}\int_0^{z_2} \tanh\left(s\right)\left(\frac{\partial\beta\left(x_1, s+\alpha\right)}{\partial x_1}\frac{\partial x_1}{\partial z_1}\dot{z}_1 + \frac{\partial\beta\left(x_1, s+\alpha\right)}{\partial\alpha}\frac{\partial\alpha}{\partial z_1}\dot{z}_1\right)ds, \tag{7.21}$$

$$\frac{\partial V_2}{\partial z_2}\dot{z}_2 = \frac{J\dot{z}_2}{g_1}\tanh\left(z_2\right)\beta\left(x_1, x_2\right),$$

$$\frac{\partial V_2}{\partial t} = \frac{J}{g_1}\int_0^{z_2} \tanh\left(s\right)\left(\frac{\partial\beta\left(x_1, s+\alpha\right)}{\partial x_1}\frac{\partial x_1}{\partial x_{1d}}\dot{x}_{1d} + \frac{\partial\beta\left(x_1, s+\alpha\right)}{\partial\alpha}\frac{\partial\alpha}{\partial t}\right)ds, \tag{7.22}$$

$$\frac{\partial x_1}{\partial z_1} = \frac{\partial x_1}{\partial x_{1d}} = 1, \text{ and } \frac{\partial \beta\left(x_1, s+\alpha\right)}{\partial \alpha} = \frac{\partial \beta\left(x_1, s+\alpha\right)}{\partial s}. \tag{7.23}$$

From (7.20)-(7.23), we get

$$\begin{aligned}
\dot{V}_2 &= \frac{J}{g_1}\left(\dot{z}_1 + \dot{x}_{1d}\right)\int_0^{z_2} \tanh\left(s\right)\frac{\partial \beta\left(x_1, s+\alpha\right)}{\partial x_1} ds \\
&\quad + \frac{J}{g_1}\left(\frac{\partial \alpha}{\partial z_1}\dot{z}_1 + \frac{\partial \alpha}{\partial t}\right)\int_0^{z_2} \tanh\left(s\right)\frac{\partial \beta\left(x_1, s+\alpha\right)}{\partial s} ds \\
&\quad + \frac{1}{g_1}\tanh\left(z_2\right)\beta\left(x_1, x_2\right)\left[f\left(x,t\right) + \Omega\left(x\right)u - J\dot{\alpha}\right] \\
&= \frac{J}{g_1}\left[\dot{x}_1\int_0^{z_2} \tanh\left(s\right)\frac{\partial \beta\left(x_1, s+\alpha\right)}{\partial x_1} ds\right. \\
&\quad \left. + \dot{\alpha}\left(\tanh\left(z_2\right)\beta\left(x_1, x_2\right) - \int_0^{z_2} \beta\left(x_1, x_2\right)\text{sech}^2\left(s\right) ds\right)\right] \\
&\quad + \frac{1}{g_1}\tanh\left(z_2\right)\beta\left(x_1, x_2\right) f\left(x,t\right) + \tanh\left(z_2\right)u - \frac{J}{g_1}\tanh\left(z_2\right)\beta\left(x_1, x_2\right)\dot{\alpha} \\
&= \tanh\left(z_2\right)\left(h\left(y\right) + u\right),
\end{aligned} \tag{7.24}$$

where $y = \left[x_1, x_2, x_{1d}, \dot{x}_{1d}, \ddot{x}_{1d}, z_2\right]^\top$ and

$$\begin{aligned}
h\left(y\right) &= \frac{J}{g_1\tanh\left(z_2\right)}\left[\dot{x}_1\int_0^{z_2} \tanh\left(s\right)\frac{\partial \beta\left(x_1, s+\alpha\right)}{\partial x_1} ds - \dot{\alpha}\int_0^{z_2} \beta\left(x_1, s+\alpha\right)\text{sech}^2\left(s\right) ds\right] \\
&\quad + \frac{1}{g_1}\beta\left(x_1, x_2\right) f\left(x,t\right).
\end{aligned} \tag{7.25}$$

Remark 7 In spite of $\tanh\left(z_2\right)$ appearing in the denominator of (7.25), the first two terms of $h\left(y\right)$ are still bounded as $z_2 \to 0$ due to the boundedness of the first derivative of $\Omega\left(x\right)$ with respect to x**.** That is, applying L'Hopital's rule yields

$$\begin{aligned}
&\lim_{z_2\to 0}\frac{\dot{x}_1}{\tanh\left(z_2\right)}\int_0^{z_2} \tanh\left(s\right)\frac{\partial \beta\left(x_1, s+\alpha\right)}{\partial x_1} ds = \lim_{z_2\to 0}\frac{\partial\left[\dot{x}_1\int_0^{z_2} \tanh\left(s\right)\frac{\partial \beta\left(x_1, s+\alpha\right)}{\partial x_1} ds\right]/\partial z_2}{\partial \tanh\left(z_2\right)/\partial z_2} \\
&= \lim_{z_2\to 0}\frac{\int_0^{z_2} \tanh\left(s\right)\frac{\partial \beta\left(x_1, s+\alpha\right)}{\partial x_1} ds + \dot{x}_1\tanh\left(z_2\right)\frac{\partial \beta\left(x_1, x_2\right)}{\partial x_1}}{\text{sech}^2\left(z_2\right)} \\
&= 0,
\end{aligned} \tag{7.26}$$

and

$$\begin{aligned}
&\lim_{z_2\to 0}\frac{\dot{\alpha}}{\tanh(z_2)}\int_0^{z_2}\beta(x_1,s+\alpha)\,\text{sech}^2(s)\,ds=\lim_{z_2\to 0}\frac{\partial\left[\dot{\alpha}\int_0^{z_2}\beta(x_1,s+\alpha)\,\text{sech}^2(s)\,ds\right]/\partial z_2}{\partial\tanh(z_2)/\partial z_2}\\
&=\lim_{z_2\to 0}\frac{-K_1\int_0^{z_2}\beta(x_1,s+\alpha)\,\text{sech}^2(s)\,ds+\dot{\alpha}\beta(x_1,x_2)\,\text{sech}^2(z_2)}{\text{sech}^2(z_2)}\\
&=(-K_1+K_1^2z_1+\ddot{x}_{1d})\,\beta(x_1,\alpha)\,.
\end{aligned}\tag{7.27}$$

where the last line of (7.27) used (7.14).

Since $f(x,t)$ is continuous and $\beta(x_1,x_2)$ continuously differentiable with respect to x and t, we know that (7.25) is continuous with respect to y. Thus, we can invoke Theorem **??** to state that for $y\in\Theta$ where Θ is a compact set,

$$h(y)=W^\top S\left(V^\top\bar{y}\right)+\delta(y)\tag{7.28}$$

where $\bar{y}=[y^\top,1]^\top\in\mathbb{R}^7$ and W,V are the *unknown*, ideal weights. Based on (7.24) and (7.28), we design the control law as

$$u=-k(t)\tanh(z_2)-\hat{W}^\top S\left(\hat{V}^\top\bar{y}\right)-\frac{z_1z_2+K_2\ln(\cosh(z_2))}{\tanh(z_2)},\tag{7.29}$$

where

$$k(t)=\frac{1}{\varepsilon}\left(\left\|\bar{y}\hat{W}^\top\hat{S}'\right\|_F^2+\left\|\hat{S}'\hat{V}^\top\bar{y}\right\|^2+1\right),\tag{7.30}$$

$\varepsilon>0$ is a control gain, and $\hat{W}(t)\in\mathbb{R}^L$ and $\hat{V}(t)\in\mathbb{R}^{7\times L}$ are estimates of the weights W and V, respectively. Note that the last term in (7.29) remains bounded as $z_2\to 0$ due to the facts that $\lim_{z_2\to 0}[z_2/\tanh(z_2)]=1$ and $\lim_{z_2\to 0}[\ln(\cosh(z_2))/\tanh(z_2)]=0$.

Our main result is included in the following theorem:

Theorem 15 For any initial condition $x(0)\in(-\pi/2,\pi/2)\times\mathbb{R}$ of the uncertain muscle-joint dynamic system (7.3), the NN-based control (7.29) and (7.30) ensures that z_1 is ultimately uniformly bounded and all other signals are bounded if the weight estimates are updated by

$$\dot{\hat{W}}=\Gamma_w\left[\tanh(z_2)\left(\hat{S}-\hat{S}'\hat{V}^\top\bar{y}\right)-\gamma_w\hat{W}\right],\tag{7.31}$$

$$\dot{\hat{V}} = \Gamma_v \left[\tanh(z_2)\, \bar{y} \hat{W}^\top \hat{S}' - \gamma_v \hat{V} \right] \tag{7.32}$$

where $\Gamma_w = \Gamma_w^\top > 0$, $\Gamma_v = \Gamma_v^\top > 0$, and γ, γ_w, $\gamma_v > 0$ are adaptation gains.

Proof. We define the following Lyapunov function candidate

$$\mathcal{V} = V_1 + V_2 + \tilde{W}^\top \Gamma_w^{-1} \tilde{W} + \text{tr}\{\tilde{V}^\top \Gamma_v^{-1} \tilde{V}\} \tag{7.33}$$

Using (7.12) and (7.24), we can obtain the following relation by taking a derivative of (7.33)

$$\dot{\mathcal{V}} = -K_1 z_1^2 + z_1 z_2 + \tanh(z_2)\,(h(y) + u) + \tilde{W}^\top \Gamma_w^{-1} \dot{\hat{W}} + tr\left\{ \tilde{V}^\top \Gamma_v^{-1} \dot{\hat{V}} \right\}. \tag{7.34}$$

Substituting (7.29), (7.31)-(7.32) into (7.34) and applying Lemma 5 yield

$$\begin{aligned}
\dot{\mathcal{V}} &= -K_1 z_1^2 - K_2 \ln(\cosh(z_2)) + \tilde{W}^\top \left[\Gamma_w^{-1} \dot{\hat{W}} - \tanh(z_2) \left(\hat{S} - \hat{S}' \hat{V}^\top \bar{y} \right) \right] \\
&\quad + \text{tr}\left\{ \tilde{V}^\top \left(\Gamma_v^{-1} \dot{\hat{V}} - \tanh(z_2)\, \bar{y} \hat{W}^\top \hat{S}' \right) \right\} + \tanh(z_2)\,(-d_u + \delta) - k(t) \tanh^2(z_2) \\
&\leq -K_1 z_1^2 - K_2 \ln(\cosh(z_2)) - \gamma_w \tilde{W}^\top \hat{W} - \gamma_v tr\left\{ \tilde{V}^\top \hat{V} \right\} - k(t) \tanh^2(z_2) \\
&\quad + |\tanh(z_2)| \left(\|V\|_F \left\| \bar{y} \hat{W}^\top \hat{S}' \right\|_F + \|W\| \left\| \hat{S}' \hat{V}^\top \bar{y} \right\| + |W|_1 + \delta \right).
\end{aligned} \tag{7.35}$$

The first equality in (7.35) holds because $\hat{W}^\top \hat{S}' \tilde{V}^\top \bar{y} \in \mathbb{R}$, and $\hat{W}^\top \hat{S}' \tilde{V}^\top \bar{y} = \text{tr}\left\{ \hat{W}^\top \hat{S}' \tilde{V}^\top \bar{y} \right\} = \text{tr}\left\{ \tilde{V}^\top \bar{y} \hat{W}^\top \hat{S}' \right\}$. After applying the following Young's inequalities

$$\begin{aligned}
-\frac{1}{\varepsilon} \left\| \bar{y} \hat{W}^\top \hat{S}' \right\|_F^2 \tanh^2(z_2) + \|V\|_F \left\| \bar{y} \hat{W}^\top \hat{S}' \right\|_F |\tanh(z_2)| &\leq \frac{\varepsilon}{4} \|V\|_F^2, \\
-\frac{1}{\varepsilon} \left\| \hat{S}' \hat{V}^\top \bar{y} \right\|^2 \tanh^2(z_2) + \|W\| \left\| \hat{S}' \hat{V}^\top \bar{y} \right\| |\tanh(z_2)| &\leq \frac{\varepsilon}{4} \|W\|^2, \\
-\frac{1}{\varepsilon} \tanh^2(z_2) + (|W|_1 + \delta) |\tanh(z_2)| &\leq \frac{\varepsilon}{4} (|W|_1 + \delta_0)^2, \\
-\tilde{W}^\top W &\leq \frac{1}{2} \left(\tilde{W}^\top \tilde{W} + W^\top W \right),
\end{aligned}$$

substituting (7.30) into (7.35) and utilizing Lemma 8 give

$$\begin{aligned}\dot{\mathcal{V}} &\leq -K_1 z_1^2 - K_2 \ln(\cosh(z_2)) - \gamma_w \tilde{W}^\top \hat{W} - \gamma_v tr\left\{\tilde{V}^\top \hat{V}\right\} \\ &\quad + \frac{\varepsilon}{4}\left[\|V\|_F^2 + \|W\|^2 + (|W|_1 + \delta)^2\right] \\ &\leq -K_1 z_1^2 - K_2 \ln(\cosh(z_2)) - \frac{\gamma_w}{2}\tilde{W}^\top \tilde{W} - \frac{\gamma_v}{2}\text{tr}\left\{\tilde{V}^\top \tilde{V}\right\} \\ &\quad + \left(\frac{\varepsilon}{4} + \frac{\gamma_w}{2}\right)\|V\|_F^2 + \left(\frac{\varepsilon}{4} + \frac{\gamma_v}{2}\right)\|W\|^2 + \frac{\varepsilon}{4}(|W|_1 + \delta_0)^2. \end{aligned} \tag{7.36}$$

Recalling the relation (7.18) and picking $\gamma_w = \lambda_{\min}(\Gamma_w^{-1})$ and $\gamma_v = \lambda_{\min}(\Gamma_v^{-1})$, we obtain

$$\dot{\mathcal{V}} \leq -c_1 \mathcal{V} + c_2, \tag{7.37}$$

where $c_1 = \min\left\{2K_1, \frac{g_0}{J}K_2, \gamma\right\}$ and $c_2 = \left(\frac{\varepsilon}{4} + \frac{\gamma_w}{2}\right)\|V\|_F^2 + \left(\frac{\varepsilon}{4} + \frac{\gamma_v}{2}\right)\|W\|^2 + \frac{\varepsilon}{4}(|W|_1 + \delta_0)^2$. ■

Since the inequality (7.37) gives

$$\mathcal{V}(t) \leq e^{-c_1 t}\mathcal{V}(0) + \frac{c_2}{c_1}\left(1 - e^{-c_1 t}\right),$$

recalling the relation (7.19) hence yields

$$\begin{aligned}&\frac{1}{2}z_1^2 + \frac{J}{g_1}\ln(\cosh(z_2)) + \frac{1}{2}\left(\tilde{W}^\top \Gamma_w^{-1}\tilde{W} + tr\{\tilde{V}^\top \Gamma_v^{-1}\tilde{V}\}\right) \\ \leq\ & \mathcal{V}(t) \leq e^{-c_1 t}\mathcal{V}(0) + \frac{c_2}{c_1}\left(1 - e^{-c_1 t}\right). \end{aligned} \tag{7.38}$$

Therefore, considering the knee joint constraint for the angular position output, for any initial condition $V(0) = V\left(z_1(0), z_2(0), \tilde{W}(0), tr\left\{\tilde{V}(0)\right\}\right)$ such that $z_1(0) \in (-\pi, \pi)$, the signals $z_1(t)$, $z_2(t)$, $\tilde{W}(t)$, $\text{tr}\left\{\tilde{V}(t)\right\}$ are bounded and there is a compact set Θ_1 such that the vector $Z(t) = \left[z_1, z_2, \tilde{W}^\top, \text{tr}\left\{\tilde{V}(t)\right\}\right]^\top$ uniformly remains in

$$\begin{aligned}\Theta_1 &= \{Z(t) |\, z_1^2 + \frac{2J}{g_1}\ln(\cosh(z_2)) + \tilde{W}^\top \Gamma_w^{-1}\tilde{W} + \text{tr}\{\tilde{V}^\top \Gamma_v^{-1}\tilde{V}\} \\ &\leq 2e^{-c_1 t}\mathcal{V}(0) + 2c_2/c_1\left(1 - e^{-c_1 t}\right)\} \end{aligned} \tag{7.39}$$

for all $t > 0$ with the constants c_1 and c_2. More specifically, for $t \to \infty$, $Z(t)$ can be ultimately bounded in a compact set

$$\Theta_2 = \left\{Z(\infty) |\, z_1^2 + \frac{2J}{g_1}\ln(\cosh(z_2)) + \tilde{W}^\top \Gamma_w^{-1}\tilde{W} + \text{tr}\{\tilde{V}^\top \Gamma_v^{-1}\tilde{V}\} \leq 2c_2/c_1\right\}, \tag{7.40}$$

and for high gains K_1, K_2, γ and a small gain ε, the ultimate boundedness $2c_2/c_1$ can be arbitrarily

small.

Due to the boundedness of $Z(t)$ and desired trajectory $(x_{1d}, \dot{x}_{1d}, \ddot{x}_{1d})$, we know that $x_1(t) \in \mathcal{L}_\infty$ from (4.3) and (4.5), $\alpha \in \mathcal{L}_\infty$ from (7.9), $x_2(t) \in \mathcal{L}_\infty$ from (7.8), $\left(\hat{W}(t), \hat{V}(t)\right) \in \mathcal{L}_\infty$ from the definition of the parameter estimate and estimate error, and the NN input vector $y(t) \in \mathcal{L}_\infty$. On the other hand, because $\hat{V}(t) \in \mathcal{L}_\infty$, $\left(\hat{S}, \hat{S}'\right) \in \mathcal{L}_\infty$ and hence, $\left(\dot{\hat{W}}(t), \dot{\hat{V}}(t)\right) \in \mathcal{L}_\infty$ from (7.31)-(7.32), and $k(t) \in \mathcal{L}_\infty$ from (7.30). Therefore, we know $u(t) \in \mathcal{L}_\infty$ by (7.29). Since $(x_1, x_2) \in \mathcal{L}_\infty$, the disturbance $d(x,t) \in \mathcal{L}_\infty$. Finally, we have $\dot{x}_2(t) \in \mathcal{L}_\infty$.

7.2.2 Design with Input Saturation

In Section 7.2.1, an adaptive NN controller (7.29) is constructed to handle the unknown control coefficient without the singularity problem, ensuring a globally uniformly ultimately bounded position tracking of the shank. However, like most literatures in NMES control, e.g., [17, 111, 112, 120], it fails to account for the input constraints inherently existing in the physical equipment. In fact, the voltage input (7.29) has to be limited in its proper operation range in case of undesired tracking performance. We simply set the following input constraint

$$u \in [0, u_m], \tag{7.41}$$

where $u_m > 0$ is the maximum voltage value that can be provided by the stimulator. To this end, (7.29) along with any other controllers in [17, 111, 112, 120] is obviously not able to satisfy (7.41).

Remark 8 In practice, stimulation is typically applied in the form of discrete pulses delivered from the electrodes. The continuous voltage/current signal computed by the designed controller is delivered to the stimulator to modify the amplitude/pulse width of the stimulus pulses. Although some commercial electrical stimulators among the market produce biphasic (positive and negative phases) stimulus pulse trains by the same amplitude, it does not require that the control input is commanded negative. In fact, a controller commands positive voltage signals only to active the muscle contraction since negative voltage values may imply muscle push, which is not true for the

reality. [4]

To handle the input saturation problem of the voltage signal, the NN control with Nussbaum-type gains is applied in this section. To assist the control design, an auxiliary control input signal $v \in \mathbb{R}$ is introduced by the following relation

$$u = \frac{1}{2} u_m \left(\tanh \left(v \right) + 1 \right). \tag{7.42}$$

Note that the stimulus voltage signal $u\left(t\right)$ is monotonic with respect to the auxiliary control $v\left(t\right)$, and for all $v \in \mathbb{R}$, $u \in \left(0, u_m\right)$ is ensured. In the rest of this paper, our task is to design the auxiliary control input v. Once v is determined, the voltage signal u could be calculated by (7.42).

Remark 9 In many previous literatures, e.g., [74, 75, 122, 137, 138], the input saturation problem is deliberately described by a saturation function that is required to be approximated by a hyperbolic tangent function and an additional bounded disturbance term for sake of control design. Different with these results, (7.42) simply redefines the pattern of the input saturation by abandoning the saturation function. Such a change mainly brings two advantages: 1) Regardless of the incapability of reaching the constraint limits, i.e., $u = 0$ and $u = u_m$, (7.42) bypasses the approximation process and therefore simplifies the analysis; 2) Due to the monotonicity of hyperbolic tangent functions, (7.42) is invertible and any $u \in \left(0, u_m\right)$ can be uniquely mapped by v. That is, any $v\left(t\right)$ calculated by the controller can be used to produce a value for $u\left(t\right)$. For a simple saturation function $u = sat\left(v\right)$ instead, any $\left|v\left(t\right)\right| > 1$ returns 1 or -1, and the variation of the states reflected on $v\left(t\right)$ fails to reach that of $u\left(t\right)$, which, to the authors, can be viewed as an information waste. Also note that $v\left(t\right)$ in (7.42) does not require any physical implementations. Therefore, a large magnitude of $v\left(t\right)$ is feasible to reach $u\left(t\right)$ values close to the input constraints. Finally, to the best knowledge of the authors', this simple idea has not been explicitly stated in any previous

[4] We thank Mr. Victor Duenas and Dr. Warren Dixon for explaining why only the non-negative voltage input is observed during the experiments in [17, 111, 112].

literatures, and the authors believe it can be a useful tool to simplify the input saturation problem.

The basic idea to handle the input saturation problem above is to remove the nonlinearity of v by utilizing mean-value theorem [137]. According to the mean-value theorem, the smooth function $\tanh(v)$ could be rewritten as

$$\tanh(v) = \tanh(v_0) + \frac{\partial \tanh}{\partial v}(v)\Big|_{v=v^*}(v - v_0) = \tanh(v_0) + g(v^*)(v - v_0), \tag{7.43}$$

where $v_0 = 0$ for simplicity, $v^* = \mu v + (1-\mu) v_0$ with $\mu \in (0,1)$, and $g(v^*) = \frac{\partial \tanh}{\partial v}(v)\big|_{v=v^*}$. Despite that v^* is an unknown time-varying variable determined by $v(t)$, and hence the function $g(v^*)$ is also time-varying and unknown, the boundedness of $g(v^*)$ is available and clear: $g(v^*) \in (0,1]$ for all $v^* \in \mathbb{R}$. By substituting (7.42)-(7.43) into (7.3), the system dynamics is rewritten as

$$\begin{aligned} \dot{x}_1 &= x_2 \\ J\dot{x}_2 &= f_u(x,t) + \Omega_u(x) g(v^*) v(t) \end{aligned}, \tag{7.44}$$

where $f_u(x,t) = f(x,t) + \frac{1}{2}u_m\Omega(x)$, and $\Omega_u(x) = \frac{1}{2}u_m\Omega(x)$. Since $\Omega(x) \in [g_0, g_1]$ for $x \in \mathbb{R}^2$ by (7.6), we know that $\Omega_u(x) \in [g_{u0}, g_{u1}]$ with $g_{ui} = \frac{1}{2}u_m g_i$ for $i = 0, 1$. Also, g_{u0} and g_{u1} are unknown. The control design is based on a similar backstepping method as follows.

Step 1:

We follow "Step 1" of the control design procedure in Section 7.2.1 by using the same definition of $e(t)$, $z_1(t)$ and $z_2(t)$ in (4.3), (4.5) and (7.8), respectively, and designing the same virtual control signal $\alpha(z_1, t)$ in (7.9) with a constant control gain $K_{N1} > 0$ and picking the same positive-definite function V_1 in (7.11).

Step 2:

Using the nonlinear function $\beta(x_1, x_2)$ defined in (7.16) and the following positive-definite and radially unbounded function

$$V_{u2} = \frac{g_1}{g_{u1}} V_2 \tag{7.45}$$

with $V_2(z_1, z_2, t)$ in (7.15), we are capable of obtaining the following relations similar to (7.18)-

(7.24):

$$\frac{J}{g_{u1}}\ln\left(\cosh\left(z_2\right)\right) \leq V_{u2} \leq \frac{J}{g_{u0}}\ln\left(\cosh\left(z_2\right)\right), \tag{7.46}$$

$$\dot{V}_{u2} = \tanh\left(z_2\right)\left[h_u\left(y\right) + g\left(v^*\right)v\right], \tag{7.47}$$

where $y = \left[x_1, x_2, x_{1d}, \dot{x}_{1d}, \ddot{x}_{1d}, z_2\right]^\top$, and

$$h_u\left(y\right) = \frac{g_1}{g_{u1}}h\left(y\right) \tag{7.48}$$

where $h\left(y\right)$ is defined in (7.25). Similar to $h\left(y\right)$, the nonlinear function h_u is also continuously differentiable with respect to $y\left(t\right)$ and can be approximated by the neural network in (3.9) with the NN wights $W_N \in \mathbb{R}^L$ and $V_N \in \mathbb{R}^{(m+1)\times L}$ and the functional approximation error $\delta_N\left(y\right)$ such that $\left|\delta_N\left(y\right)\right| \leq \delta_{N0}$.

The auxiliary control input is constructed as follows by utilizing the Nussbaum-type function

$$v = N\left(\zeta\right)\varpi \tag{7.49}$$

$$\dot{\zeta} = K_{N3}\tanh\left(z_2\right)\varpi,\ \zeta\left(0\right) = 0 \tag{7.50}$$

$$\varpi = k_N\left(t\right)\tanh\left(z_2\right) + \hat{W}_N^\top S\left(\hat{V}_N^\top\bar{y}\right) + \frac{z_1 z_2 + K_{N2}\ln\left(\cosh\left(z_2\right)\right)}{\tanh\left(z_2\right)}, \tag{7.51}$$

where $K_{N2}, K_{N3} > 0$ are control gains, $N\left(\zeta\right) = \zeta^2\cos\left(\omega\zeta\right)$ with $\omega > 0$ being a tunable frequency, and $k_N\left(t\right)$ is a similar time-varying gain designed in (7.30)

$$k_N\left(t\right) = \frac{1}{\varepsilon_N}\left(\left\|\bar{y}\hat{W}_N^\top\hat{S}_N'\right\|_F^2 + \left\|\hat{S}_N'\hat{V}_N^\top\bar{y}\right\|^2 + 1\right) \tag{7.52}$$

with a constant control gain $\varepsilon_N > 0$. Substituting the control (7.49)-(7.51) into (7.47) consequently gives

$$\begin{aligned}\dot{V}_{u2} &= \tanh\left(z_2\right)h_u\left(y\right) + \frac{1}{K_{N3}}\left[g\left(v^*\right)N\left(\zeta\right) + 1\right]\dot{\zeta} - \frac{1}{K_{N3}}\dot{\zeta} \\ &= \tanh\left(z_2\right)\left[h_u\left(y\right) - \varpi\right] + \frac{1}{K_{N3}}\left[g\left(v^*\right)N\left(\zeta\right) + 1\right]\dot{\zeta}.\end{aligned} \tag{7.53}$$

Our main result is stated by the following theorem.

Theorem 16 For all initial conditions $x_1(0) \in \left(-\frac{\pi}{2}, \frac{\pi}{2}\right)$ and $x_2(0) \in \mathbb{R}$ of the uncertain muscle-joint dynamic system (7.44), a neural network-based control (7.49)-(7.51) and (7.42) are capable of ensuring an ultimately uniformly bounded tracking of any desired trajectory $x_{1d}(t)$ such that $\sup_{t>0}|x_{1d}(t)| \leq \frac{\pi}{2}$, $(\dot{x}_{1d}(t), \ddot{x}_{1d}(t)) \in \mathcal{L}_\infty$ and all signals in (7.3) bounded if the NN weights are updated by

$$\dot{\hat{W}}_N = \Gamma_{wN}\left[\tanh(z_2)\left(\hat{S}_N - \hat{S}'_N\hat{V}_N^\top\bar{y}\right) - \gamma_{wN}\hat{W}_N\right], \tag{7.54}$$

$$\dot{\hat{V}}_N = \Gamma_{vN}\left[\tanh(z_2)\,\bar{y}\hat{W}_N^\top\hat{S}'_N - \gamma_{vN}\hat{V}_N\right] \tag{7.55}$$

where $\Gamma_{wN} = \Gamma_{wN}^\top > 0$, $\Gamma_{vN} = \Gamma_{vN}^\top > 0$, $\gamma_{wN} > 0$ and $\gamma_{vN} > 0$ are adaptation gains.

Proof. We define the Lyapunov function candidate

$$\mathcal{V} = V_1 + V_{u2} + \frac{1}{2\gamma_N}\left(\tilde{W}_N^\top\Gamma_{wN}^{-1}\tilde{W}_N + tr\{\tilde{V}_N^\top\Gamma_{vN}^{-1}\tilde{V}_N\}\right). \tag{7.56}$$

Following the stability proof in Section 7.2.1 and picking the corresponding adaptation gains $\gamma_{wN} = \lambda_{\min}\left(\Gamma_{wN}^{-1}\right)$ and $\gamma_{vN} = \lambda_{\min}\left(\Gamma_{vN}^{-1}\right)$, we simply obtain

$$\dot{\mathcal{V}} \leq -c_1\mathcal{V} + \frac{1}{K_{N3}}\left[g(v^*)N(\zeta) + 1\right]\dot{\zeta} + c_2, \tag{7.57}$$

where $c_1 = \min\left\{2K_{N1}, \frac{g_{u0}}{J}K_{N2}, \gamma_N\right\}$ and $c_2 = \left(\frac{\varepsilon_N}{4} + \frac{\gamma_{wN}}{2}\right)\|V_N\|_F^2 + \left(\frac{\varepsilon_N}{4} + \frac{\gamma_{vN}}{2}\right)\|W_N\|^2 + \frac{\varepsilon_N}{4}\left(|W_N|_1 + \delta_{N0}\right)^2$. Integrating (7.57) on $[0,t]$, $\forall t \in [0,t_f)$ yields

$$\begin{aligned}\mathcal{V}(t) &\leq \mathcal{V}(0)e^{-c_1t} + e^{-c_1t}\int_0^t \frac{1}{K_{N3}}\left[g(v^*)N(\zeta)+1\right]\dot{\zeta}e^{c_1\tau}d\tau \\ &\quad + \frac{c_2}{c_1}\left(1 - e^{-c_1t}\right) \\ &\leq c_0 + e^{-c_1t}\int_0^t \frac{1}{K_{N3}}\left[g(v^*)N(\zeta)+1\right]\dot{\zeta}e^{c_1\tau}d\tau,\end{aligned} \tag{7.58}$$

where $c_0 = \mathcal{V}(0) + c_2/c_1$. Applying Lemma 6, we can conclude that $\zeta(t)$, $\int_0^t g(v^*)N(\zeta)\dot{\zeta}d\tau$ and $\mathcal{V}(t)$ must be bounded on $[0,t_f)$. According to Property 2 in [106], if the solution of the closed-loop system is bounded, then $t_f = +\infty$. Consequently, $\mathcal{V}(t) \in \mathcal{L}_\infty$ for all $t > 0$. Recalling the

relation (7.46), we claim that the following relation holds

$$\begin{aligned} & \frac{1}{2}z_1^2 + \frac{J}{g_{u1}}\ln\left(\cosh\left(z_2\right)\right) + \frac{1}{2}\left(\tilde{W}_N^\top \Gamma_{wN}^{-1}\tilde{W}_N + tr\{\tilde{V}_N^\top \Gamma_{vN}^{-1}\tilde{V}_N\}\right) \\ \leq \;& \mathcal{V}\left(t\right) \leq \mathcal{V}\left(0\right)e^{-c_1 t} + \frac{c_2}{c_1}\left(1 - e^{-c_1 t}\right) + \frac{M}{K_{N3}} \end{aligned} \tag{7.59}$$

for some positive constant $M = \sup_{t>0}\left|\int_0^t \left[g\left(v^*\right)N\left(\zeta\right)+1\right]\dot{\zeta}e^{c_1(\tau-t)}d\tau\right|$. Therefore, we can conclude that for any initial condition $\mathcal{V}\left(0\right) = \mathcal{V}\left(z_1\left(0\right), z_2\left(0\right), \tilde{W}\left(0\right), tr\left\{\tilde{V}\left(0\right)\right\}\right)$ such that $z_1\left(0\right) \in \left(-\pi, \pi\right)$, the vector $Z\left(t\right) = \left[z_1, z_2, \tilde{W}^\top, tr\left\{\tilde{V}\left(t\right)\right\}\right]^\top$ is uniformly ultimately bounded in a compact set

$$\begin{aligned} \Theta_1 &= \{Z\left(t\right)| \, z_1^2 + \frac{2J}{g_{u1}}\ln\left(\cosh\left(z_2\right)\right) + \tilde{W}_N^\top \Gamma_{wN}^{-1}\tilde{W}_N + tr\{\tilde{V}_N^\top \Gamma_{vN}^{-1}\tilde{V}_N\} \\ &\leq 2\mathcal{V}\left(0\right)e^{-c_1 t} + 2c_2/c_1\left(1 - e^{-c_1 t}\right) + \frac{M}{K_{N3}}\} \end{aligned} \tag{7.60}$$

for all $t > 0$. More specifically, for $t \to \infty$, $Z\left(t\right)$ can be ultimately bounded in a compact set

$$\begin{aligned} \Theta_2 &= \{Z\left(\infty\right)| \, z_1^2 + \frac{2J}{g_{u1}}\ln\left(\cosh\left(z_2\right)\right) + \tilde{W}_N^\top \Gamma_{wN}^{-1}\tilde{W}_N + tr\{\tilde{V}_N^\top \Gamma_{vN}^{-1}\tilde{V}_N\} \\ &\leq 2c_2/c_1 + \frac{M}{K_{N3}}\}, \end{aligned} \tag{7.61}$$

and for high gains K_{N1}, K_{N2}, K_{N3}, γ_N and a small gain ε_N, the ultimate boundedness $2c_2/c_1 + M/K_{N3}$ can be arbitrarily small. ■

The boundedness of $x_i\left(t\right)$, $\alpha\left(z_1, t\right)$, $\hat{W}_N\left(t\right)$, $\hat{V}_N\left(t\right)$, $\hat{S}_N$, $\hat{S}_N'$, $\dot{\hat{W}}_N\left(t\right)$, $\dot{\hat{V}}_N\left(t\right)$, $\tau_d\left(x_1, x_2, t\right)$ and $k_N\left(t\right)$ can be concluded following the boundedness analysis in Section 7.2.1. Therefore, $\varpi \in \mathcal{L}_\infty$ from (7.51) and hence, $\dot{\zeta}\left(t\right) \in \mathcal{L}_\infty$ from (7.50). Since $\zeta\left(t\right) \in \mathcal{L}_\infty$ from Lemma 6, the Nussbaum type function $N\left(\zeta\right) \in \mathcal{L}_\infty$ holds, and consequently, the auxiliary control signal $v\left(t\right) \in \mathcal{L}_\infty$ from (7.49). Due to the boundedness of voltage input $u\left(t\right)$, we finally have $\dot{x}_2\left(t\right) \in \mathcal{L}_\infty$.

7.3 Simulation

7.3.1 Description

The performance of both adaptive NN control designs were illustrated in Simulink with ode solver `ode45`. All plant parameters in the passive mechanical subsystem (7.1) were defined by (6.46). The parameters in the muscle contractile subsystem (7.2) and (2.10)-(2.11) were from the

experimental results in [102]

$$\begin{aligned} n_1 &= 0.058,\ n_2 = 2,\ n_3 = 0.0284,\ F_m = 200 \text{ N}, \\ m_1 &= 0.54,\ m_2 = 5.69,\ m_3 = 0.51,\ m_4 = 0.745, \\ l_{opt} &= 0.086,\ C = 0.11,\ \epsilon = 0.4,\ v_m = 0.51. \end{aligned}$$

The desired trajectory was set as

$$q_d(t) = \frac{\pi}{18} + \frac{7\pi}{24}\left(1 - \exp\left(-0.8t^3\right)\right) + \frac{\pi}{8}\left(1 - \exp\left(-0.4t^3\right)\right)\sin\omega(t)t \text{ rad} \tag{7.62}$$

with a constant frequency of $\omega = 2.15\pi$ rad/s. The shape of $q_d(t)$ is shown in Figure 7.1.

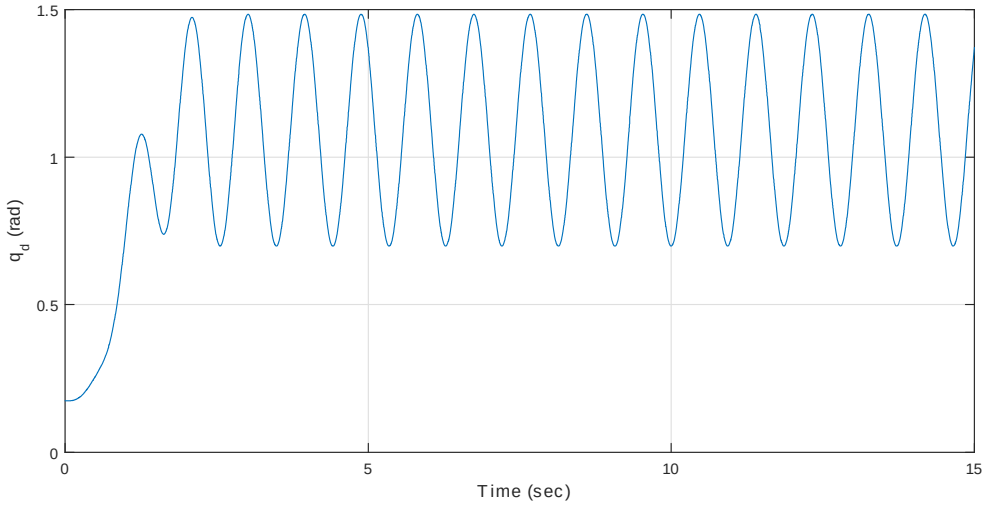

Figure 7.1: Desired trajectory $q_d(t)$

The disturbance term was described by

$$d(x,t) = d_e(x_1) + d_d(x_2) - d_f(t), \tag{7.63}$$

where $d_e(x_1) = 0.3\exp(0.2x_1) + 0.1x_1$ represents unmodeled elastic moment, $d_d(x_2) = 0.05\tanh(45x_2)$ approximates the error moment between (2.3) and the damping moment component caused by Coulomb friction, and $d_f(t)$ satisfying

$$\dot{d_f} = -0.6d_f + S(0.04(t-25)) + 0.125,\ d_f(0) = 0 \tag{7.64}$$

where the function $S(\cdot)$ is defined in (5.16), simulates the dynamics of muscle fatigue, spasms and/or a time-varying external load.

Remark 10 The muscle fatigue phenomenon is mimicked and included by the 1-st order differential equation (7.64). This approximation stems from the fatigue characteristics, i.e., it increases, if not strictly, during successive muscle contraction until it reaches the maximum. In fact, the muscle fatigue dynamics can approximately be a nonlinear 1-st order differential equation of fatigue state and the stimulus signal, consisting of fatigue and recovery components [101, 102]. We just use the linear equation (7.64) for sake of simplicity, and we also assume that the muscle is fully rested when $t = 0$.

Two sets of simulations were conducted for the adaptive NN control (ANNb) and the adaptive NN control with Nussbaum-type gain (ANN-N). The neural networks used in two controllers contained 20 hidden nodes, i.e., $L = 20$ and the parameter in the activation function (3.10) was set to $\sigma = 3$. The adaptation gains in both neural networks were picked as the same values: $\gamma_w = \gamma_{wN} = 0.1$, $\gamma_v = \gamma_{vN} = 0.05$,

Simulation 1: For comparison purposes, we simulated the adaptive NN controller proposed in [38, 134] (ANNa) to demonstrate the initial condition sensitivity problem in terms of control input spikes, where a set of "good" initial states (close to the stable equilibrium), $x_1(0) = \pi/15$ rad, $x_2(0) = 0$ rad/s, and a set of "bad" initial states (far from the stable equilibrium), $x_1(0) = -\pi/10$ rad, $x_2(0) = -1.5$ rad/s were used. For both sets of initial conditions, the initial weights $\hat{W}(0) = \mathbf{0}^{20\times 1}$, $\hat{V}(0) = \mathbf{0}^{7\times 20}$, the control gains and adaptation gains for both ANNa and ANNb control were set to

$$\begin{aligned} K_1 &= 7.5,\ K_2 = 1.5,\ \varepsilon = 0.05,\ \gamma_w = 0.1,\ \gamma_v = 0.05, \\ \Gamma_w &= I_{20\times 20},\ \Gamma_v = 5I_{7\times 7}. \end{aligned}$$

Simulation 2: The performance of ANNb and ANN-N controls was compared. The initial conditions for both controls were set to $x_1(0) = -\pi/10$ rad and $x_2(0) = 1.5$ rad/s, the initial weights $\hat{W}_N(0) = \mathbf{0}^{20\times 1}$, $\hat{V}_N(0) = \mathbf{0}^{7\times 20}$, and the control gains and adaptation gains for ANNb

were set the same as those in Simulation 1, and all the gains and physical constraints for ANN-N were set to

$$\begin{aligned} K_{1N} &= 7.5,\ K_{2N} = 1.5,\ K_{3N} = 0.27,\ \varepsilon_N = 0.05,\ \gamma_{wN} = 0.1, \\ \gamma_{vN} &= 0.05,\ \Gamma_{wN} = I_{20\times 20},\ \Gamma_{vN} = 5I_{7\times 7}. \end{aligned}$$

To test the ANN-N control, we also set the physical constrain for the input as $u_m = 35$ V.

7.3.2 Results and Discussion

The results for the two simulations described above are presented next. For Simulation 1, the initial condition sensitivity problem is presented in Figure 7.2, where the top plots show the initial input values of ANNa and ANNb controllers under the "good" initial states, i.e., $x_1(0) = \pi/15$ rad and $x_2(0) = 0$ rad/s, and the bottom plots show the initial input values of the controllers under the "bad" initial states $x_1(0) = -\pi/10$ rad and $x_2(0) = -1.5$ rad/s. Indeed, for the initial states close to the equilibrium point, both controllers gave a similar initial value ($u(0) \approx -6$); for the initial states far from the equilibrium point, however, the ANNa controller from [38, 134] yielded a significantly larger spike ($u(0) \approx 110$) than the one ($u(0) \approx 28$) produced by the ANNb controller. This fact indicates that due to the saturation property of the hyperbolic tangent function, the modified integral-type Lyapunov function for the ANNb control design is capable of effectively suppressing the initial input spike caused by the initial conditions. This is obviously beneficial to the protection and maintenance of the controller and the actuators.

The comparison of the ANNb and ANN-N control is presented in Simulation 2 under the same schedule of the control gains. The performance of the tracking error $e(t)$ and the control input $u(t)$ are shown in Figure 7.3-7.4, respectively. From the Figure 7.3, the convergence of $e(t)$ is faster and the steady state boundedness is smaller for the ANNb control; In Figure 7.4, the steady state boundedness of $u(t)$ is significantly smaller for ANNb control and hence, the ANNb control shows a promising potential from the perspective of energy consuming. However, since some

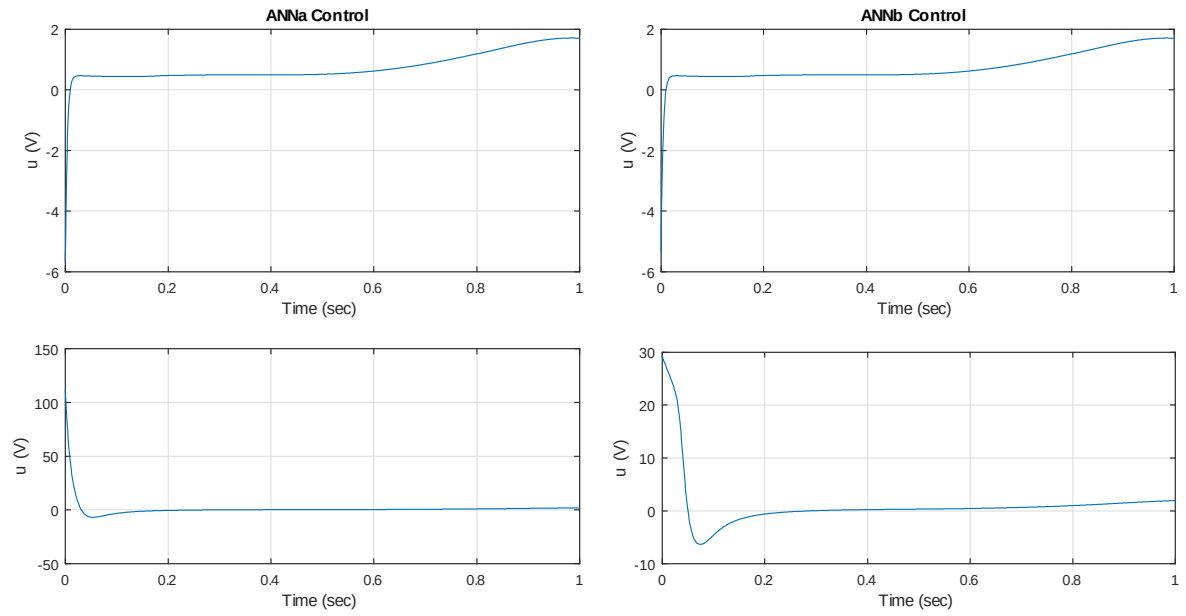

Figure 7.2: Simulation 1: The control input $u(t)$ under "good" and "bad" initial conditions.

negative values are involved for the transient performance and the input constraint is violated, the ANNb controller is probably not safe for implementations. Instead, the ANN-N control shows a larger input amplitude during the steady state though, the input signal is guaranteed to stay inside the valid physical constraints, i.e., $u\left(t\right) \in \left(0, u_m\right)$ for all $t \geq 0$.

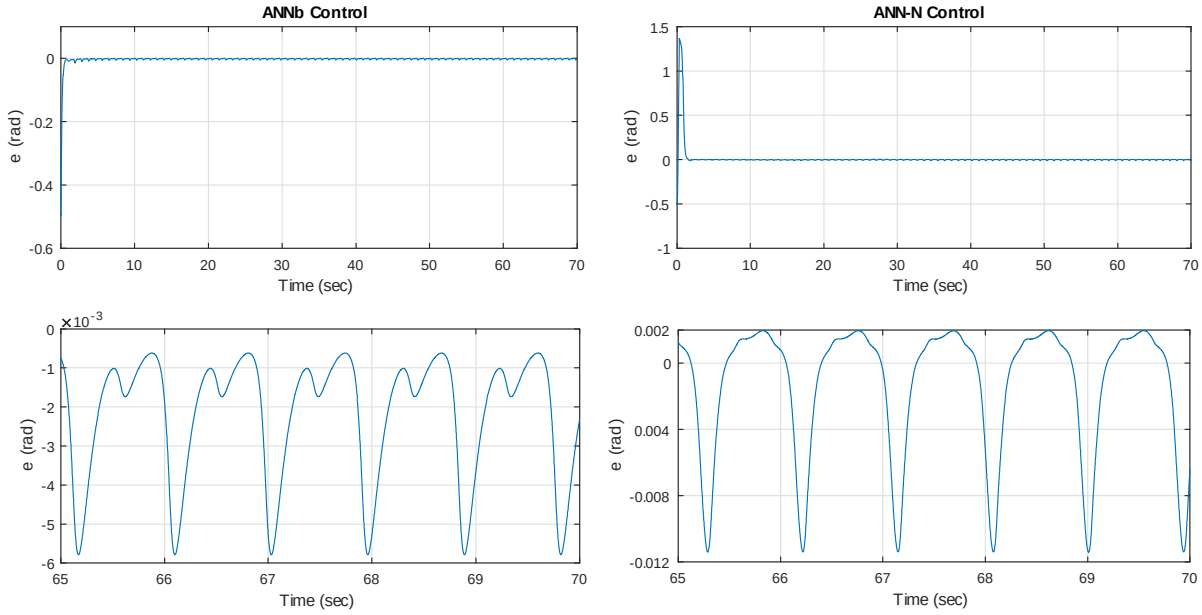

Figure 7.3: Simulation 2: Tracking error $e\left(t\right)$.

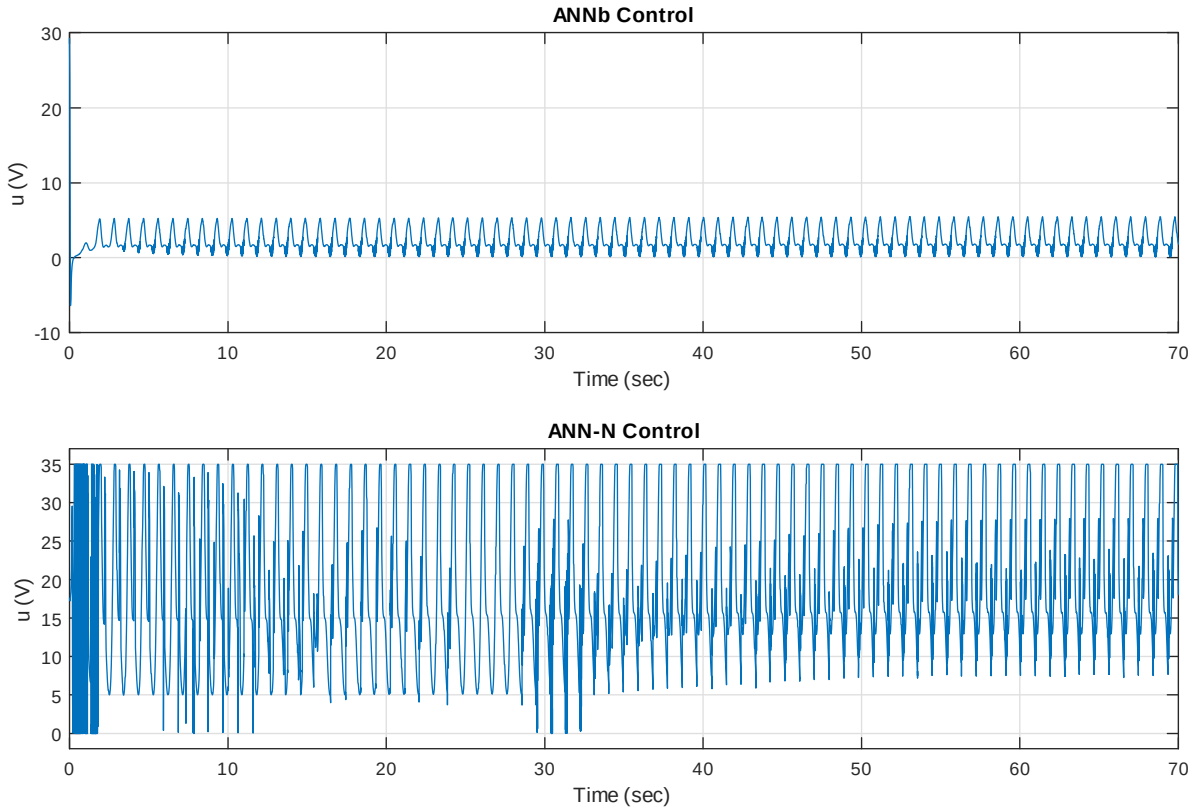

Figure 7.4: Simulation 2: Control input $u(t)$.

For the ANN-N control, the performance of the auxiliary controller $v(t)$ and the adaptive variable $\zeta(t)$ can be found in Figure 7.5-7.6. In Figure 7.7, the disturbance $d(x,t)$ is presented.

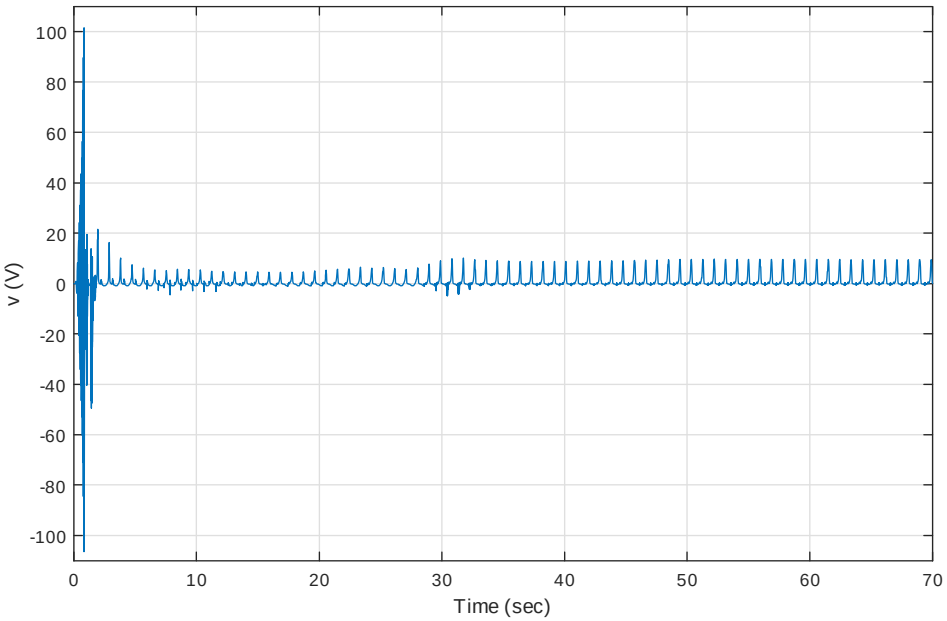

Figure 7.5: Simulation 2: Auxiliary control input $v\left(t\right)$.

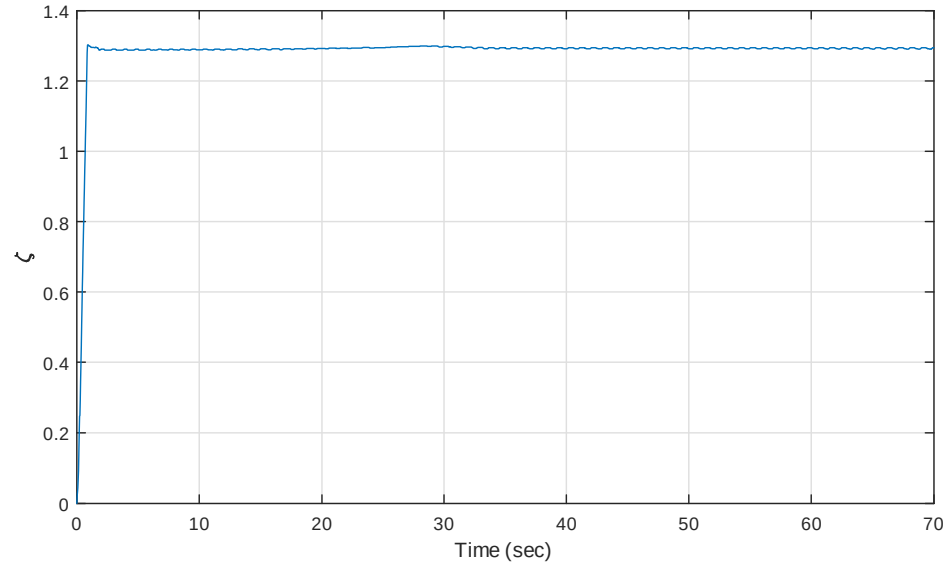

Figure 7.6: Simulation 2: adaptive variable $\zeta\left(t\right)$.

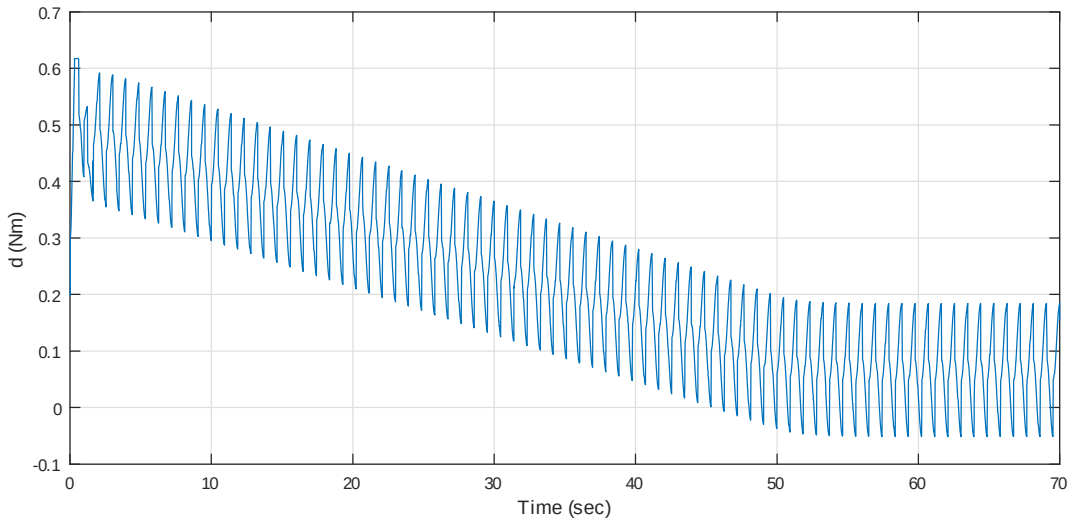

Figure 7.7: Simulation 2: Disturbance $d\left(x,t\right)$.

Chapter 8 Partial-State Feedback Control

In this chapter, we augment the NMES model from Chapter 7 with the muscle activation dynamics proposed in [29]. Under the assumption that the state of the activation dynamics is unmeasurable, we present two *partial-state* feedback control strategies for stabilizing the resulting, third-order NMES model. The first design uses a model-based observer to estimate the unknown state. In the second design, we assume parametric uncertainty is present in the activation dynamics, which precludes the use of the model-based observer. Instead, we design a filter-based estimator inspired by the work in [67]. Both partial-state feedback controller are shown to guarantee asymptotic position tracking.

To the best of our knowledge there are only a few results in the literature that addressed the state estimation problem for the activation dynamics. In [17, 120], the activation state was indirectly estimated by lumping the mechanical passive dynamics and the muscle activation dynamics into a third-order differential equation and then desiging a NN-based observer for the unmeasurable shank acceleration. In [109], an activation state observer was formulated but the estimation error was not included in the stability analysis.

8.1 Model Description

The NMES model utilized in this chapter is described by

$$\dot{x}_1 = x_2 \tag{8.1}$$

$$J\dot{x}_2 = h(x) + x_3 \tag{8.2}$$

$$\dot{x}_3 = -ax_3 + bu \tag{8.3}$$

where the states $x = [x_1, x_2]^\top = [q, \dot{q}]^\top$ are measurable, $h(x)$ was defined in (4.2), $x_3 \in \mathbb{R}$ is the active torque applied on the knee joint, which is unmeasurable during non-isometric muscle contraction, $u \in \mathbb{R}$ denotes the control input signal in the form of the stimulus pulse width, and J, a, and b are positive constant parameters.

Remark 11 The model (8.1) was proposed in [29] where the equations (8.1)-(8.2) represent the passive mechanical dynamics that we are familiar with in Chapter 4-5, and (8.3) reflects the relationship between the electrical stimulus and joint torque. In [29], the experimental data show that the simple linear relation (8.3) is valid for step and ramp stimulation patterns of the pulse width. It is reported that the constant a depends on the stimulus pattern (ramp or step) while the gain b is directly dependent on stimulation frequency. To design an output feedback controller, we first attempt to adopt (8.1) rather than the full-order model introduced in Chapter 2 since the model (8.1) is simpler and more convenient for analysis.

To rationalize the control design in the rest of the chapter, we make the following assumptions:

Assumption 2 *Model (8.3) is regarded as an optimal model of the electrical stimulus-joint torque relation only under ramp-like or step-like stimulus patterns.*

8.2 Observer-Based Design

8.2.1 Problem Statement

We first consider the NMES model in (8.1) totally certain, i.e., all the constant parameters and nonlinear functions are known. Our control objective, similar to the ones in Chapter 4-7, is to design the control input $u(t)$ to ensure the tracking of any desired trajectory $x_{1d}(t)$ such that $\sup_{t>0} |x_{1d}(t)| \leq \frac{\pi}{2}$ and $(\dot{x}_{1d}(t), \ddot{x}_{1d}(t)) \in \mathcal{L}_\infty$ under the constraint that only x is measurable.

8.2.2 Control Design

Our tracking objective is quantified, again, by the tracking error (4.3). To facilitate the control design, we also use the filtered tracking error defined by (5.14). The dynamics of $r(t)$ is then derived from (8.1) to be

$$\begin{aligned} J\dot{r} &= h(x) + x_3 - J(\ddot{x}_d - \mu\dot{e}) \\ &= f(x,t) + x_3 \end{aligned} \tag{8.4}$$

where $f(x,t) := h(x) - J(\ddot{x}_d - \mu\dot{e})$. We now apply the backstepping approach to construct the controller.

Step 1:

We define

$$z_1 = r \tag{8.5}$$

and have

$$J\dot{z}_1 = f(x,t) + x_3. \tag{8.6}$$

By introducing the virtual control α and a new state

$$z_2 = \hat{x}_3 - \alpha \tag{8.7}$$

where $\hat{x}_3$ is the estimate of unmeasurable state x_3, we can rewrite (8.6) as follows by adding and subtracting $\hat{x}_3 + \alpha$ to the right-hand side

$$J\dot{z}_1 = f(x,t) - \tilde{x}_3 + z_2 + \alpha, \tag{8.8}$$

where

$$\tilde{x}_3 = \hat{x}_3 - x_3 \tag{8.9}$$

is the state estimation error. The virtual control is therefore designed as

$$\alpha = -f(x,t) - K_1 z_1, \tag{8.10}$$

where $K_1 > 0$ is a control gain. Substituting (8.10) into (8.8) gives

$$J\dot{z}_1 = -K_1 z_1 + z_2 - \tilde{x}_3. \tag{8.11}$$

Remark 12 Distinct from the regular backstepping approach applied on systems with full-state feedback, the one presented here also backsteps on $\hat{x}_3$ to obtain a cross-term in the Lyapunov derivative. This cross-term will be cancelled (instead of dominated) by the *correction term* introduced in the observer design later. Therefore, the design of the observer is *interlaced* with that of the controller.

We next define the positive-definite, radially unbounded function

$$V_1 = \frac{1}{2} J z_1^2. \tag{8.12}$$

The time derivative of (8.12) along (8.11) gives

$$\dot{V}_1 = -K_1 z_1^2 + z_1 z_2 - z_1 \tilde{x}_3. \tag{8.13}$$

Step 2:

We use the following nonlinear observer

$$\dot{\hat{x}}_3 = -a\hat{x}_3 + bu + \phi, \tag{8.14}$$

where ϕ is a tuning function to be designed. It follows that the dynamics of z_2 and $\tilde{x}_3$ are given by

$$\begin{aligned} \dot{z}_2 &= \dot{\hat{x}}_3 - \dot{\alpha} \\ &= -a\hat{x}_3 + bu + \phi - \frac{\partial \alpha}{\partial x_1} x_2 - \frac{1}{J} \frac{\partial \alpha}{\partial x_2} \left(h\left(x\right) + \hat{x}_3 + \tilde{x}_3 \right) - \frac{\partial \alpha}{\partial t} \end{aligned} \tag{8.15}$$

and

$$\begin{aligned} \dot{\tilde{x}}_3 &= \dot{\hat{x}}_3 - \dot{x}_3 \\ &= -a\tilde{x}_3 + \phi. \end{aligned} \tag{8.16}$$

Based on (8.13) and (8.15), we design the following control law

$$u = \frac{1}{b} \left(a\hat{x}_3 + P - K_2 z_2 - z_1 - \phi \right), \tag{8.17}$$

where

$$P = \frac{\partial \alpha}{\partial x_1} x_2 + \frac{1}{J} \frac{\partial \alpha}{\partial x_2} \left(h\left(x\right) + \hat{x}_3 \right) + \frac{\partial \alpha}{\partial t}, \tag{8.18}$$

$K_2 > 0$ is a control gain, and

$$\phi = z_1 + \frac{1}{J} z_2 \frac{\partial \alpha}{\partial x_2}. \tag{8.19}$$

Substituting (8.17) into (8.15) yields

$$\dot{z}_2 = -K_2 z_2 - z_1 - \frac{1}{J} \tilde{x}_3 \frac{\partial \alpha}{\partial x_2}. \tag{8.20}$$

The following theorem gives our main result.

Theorem 17 The observer-controller given by (8.14), (8.17), and (8.19) ensures asymptotic po-

sition tracking and the boundedness of all other system signals.

Proof. We define the Lyapunov function candidate

$$V = \frac{1}{2}z_2^2 + \frac{1}{2}\tilde{x}_3^2 + V_1, \tag{8.21}$$

and the following relation can be achieved by using (8.20), (8.16) and (8.13)

$$\begin{aligned} \dot{V} &= z_2\left(-K_2 z_2 - z_1 - \frac{1}{J}\tilde{x}_3\frac{\partial\alpha}{\partial x_2}\right) + \tilde{x}_3\left(-a\tilde{x}_3 + \phi\right) - K_1 z_1^2 + z_1 z_2 - z_1\tilde{x}_3 \\ &= -K_1 z_1^2 - K_2 z_2^2 - a\tilde{x}_3^2 + \tilde{x}_3\left(-\frac{1}{J}z_2\frac{\partial\alpha}{\partial x_2} + \phi - z_1\right). \end{aligned} \tag{8.22}$$

After substituting (8.19) into (8.22), we obtain that

$$\dot{V} = -K_1 z_1^2 - K_2 z_2^2 - a\tilde{x}_3^2. \tag{8.23}$$

From (8.12), (8.21), and (8.23), we know that $(z_1, z_2, \tilde{x}_3) = 0$ is exponentially stable. Since $\lim_{t\to\infty} z_1(t) = 0$, we can claim that $(e(t), \dot{e}(t)) \to 0$ as $t \to \infty$ from (5.14). Based on the fact that $(x_d(t), \dot{x}_d(t), \ddot{x}_d(t)) \in \mathcal{L}_\infty$, we know that $(x_1(t), x_2(t)) \in \mathcal{L}_\infty$ by (4.3). Thus, $h(x,t) \in \mathcal{L}_\infty$, and $(\alpha(t), \dot{\alpha}(t), \phi(t)) \in \mathcal{L}_\infty$ due to (8.10) and (2.2)-(2.4). Since $\alpha(t) \in \mathcal{L}_\infty$ and $\lim_{t\to\infty} z_2(t) = 0$, it is clear that $\hat{x}_3(t) \in \mathcal{L}_\infty$ from (8.7), which is therefore followed by the fact that $u(t) \in \mathcal{L}_\infty$ by (8.17). Because $\lim_{t\to\infty}\tilde{x}_3(t) = 0$, we then have that $x_3(t) \in \mathcal{L}_\infty$. Finally, we know that $(\dot{x}_2(t), \dot{x}_3(t)) \in \mathcal{L}_\infty$ from (8.1). ■

Remark 13 It should be noted from (8.16) that the exponential decay of $\tilde{x}_3(t)$ to zero is determined by the system parameter a. In order words, observer (8.14) has an open-loop-like nature. In contrast, the acceleration observer in [17, 120] is a closed-loop one since the stabilization of the estimation error dynamics is controlled by a user-defined gain.

8.3 Filter-Based Design

8.3.1 Problem Statement

With the fundamental idea form Section 8.2, we gradually relax the strict assumption of model

uncertainties in this section. Here, for the purpose of reducing the model identification process, we consider the parameter a is unknown while all other parameters and nonlinear functions are still certain in (8.1). Similar to that in Section 8.2.1, our control objective is to construct an adaptive controller $u(t)$ to achieve asymptotic tracking of some desired trajectory $x_d(t)$ discussed in Section 8.2.1 and ensure all system signals bounded.

We use the tracking error and the filtered tracking error defined in (4.3) and (5.14), respectively, for the rest of the control design. Note that the difficulty of the design arises due to the coupling of the unknown parameter a and unmeasurable state $x_3(t)$, and a direct nonlinear observer design in Section 8.2.2 fails since the uncertainty cannot be dominated or cancelled in the Lyapunov function derivative. Instead, we turn to a filter design inspired by [67].

8.3.2 Filter Design

We first transform (8.1) to the class of parametric output-feedback systems by defining a new unmeasurable state

$$\zeta = x_3 + aJz_1. \tag{8.24}$$

Consequently, the transformed system is

$$J\dot{z}_1 = f(x,t) + \zeta - aJz_1 \tag{8.25}$$

$$\dot{\zeta} = af(x,t) + bu \tag{8.26}$$

where (8.25) is from (8.4), and (8.26) uses (8.3) and (8.25). We next define a state vector $w = [z_1, \zeta]^\top$ and a constant matrix

$$A = \begin{bmatrix} -\frac{k_1}{J} & \frac{1}{J} \\ -k_2 & 0 \end{bmatrix}$$

where $k_i > 0$, $i = 1, 2$ are the control gains chosen to ensure that A is Hurwitz, and hence the system (8.24) can be rewritten as

$$\dot{w} = Aw + \varphi_1(x,t) + a\varphi_2(x,t) + kz_1 + \beta u, \tag{8.27}$$

where

$$\varphi_1 = \frac{1}{J}\begin{bmatrix} f(x,t) \\ 0 \end{bmatrix},\ \varphi_2 = \begin{bmatrix} -z_1 \\ f(x,t) \end{bmatrix},\ \beta = \begin{bmatrix} 0 \\ b \end{bmatrix},\ k = \begin{bmatrix} \frac{k_1}{J} \\ k_2 \end{bmatrix}.$$

Two filters are used to estimate w by

$$\hat{w} = \xi_0 + a\xi_1 \tag{8.28}$$

where $\xi_0(t) = [\xi_{01}, \xi_{02}]^\top$ and $\xi_1(t) = [\xi_{11}, \xi_{12}]^\top$ are the filter outputs. Since $w = \hat{w} - \tilde{w}$, we have

$$z_1 = \xi_{01} + a\xi_{11} - \tilde{w}_1 \tag{8.29}$$

$$\zeta = \xi_{02} + a\xi_{12} - \tilde{w}_2 \tag{8.30}$$

The filters are designed by

$$\dot{\xi}_0 = A\xi_0 + \varphi_1 + kz_1 + \beta u + \phi,\ \xi_0(0) = \mathbf{0}, \tag{8.31}$$

$$\dot{\xi}_1 = A\xi_1 + \varphi_2,\ \xi_1(0) = \mathbf{0}, \tag{8.32}$$

where $\phi = [\phi_1, \phi_2]^\top$ is a tuning function yet to be designed. Using (8.27), (8.28) and (8.31)-(8.32), we know that

$$\begin{aligned} \dot{\tilde{w}} &= \dot{\xi}_0 + a\dot{\xi}_1 - \dot{w} \\ &= A\xi_0 + \varphi_1 + kz_1 + \beta u + \phi + a(A\xi_1 + \varphi_2) \\ &\quad - [Aw + \varphi_1(x,t) + a\varphi_2(x,t) + kz_1 + \beta u] \\ &= A(\xi_0 + a\xi_1 - w) + \phi \\ &= A\tilde{w} + \phi. \end{aligned} \tag{8.33}$$

8.3.3 Control Design

We follow the backstepping approach to construct the adaptive partial-state feedback control as follows.

Step 1:

By backstepping the filter output ξ_{02} from (8.30) and defining

$$z_2 = \xi_{02} - \alpha, \tag{8.34}$$

where $\alpha\left(x, \xi_{12}, \hat{a}, t\right)$ is the virtual control to be designed, we can rewrite the dynamics of z_1 in (8.24) by

$$J\dot{z}_1 = f\left(x,t\right) + z_2 + a\left(\xi_{12} - Jz_1\right) - \tilde{w}_2 + \alpha.$$

The virtual control is hence designed by

$$\alpha\left(x, \xi_{12}, \hat{a}, t\right) = -f\left(x,t\right) - \hat{a}\left(\xi_{12} - Jz_1\right) - K_1 z_1, \tag{8.35}$$

and the dynamics of z_1 yields

$$J\dot{z}_1 = -K_1 z_1 + z_2 - \tilde{a}\left(\xi_{12} - Jz_1\right) - \tilde{w}_2. \tag{8.36}$$

We now Define a positive definite and radially unbounded function

$$V_1\left(z_1, \tilde{a}\right) = \frac{1}{2}Jz_1^2 + \frac{1}{2\gamma}\tilde{a}^2 \tag{8.37}$$

with $\gamma > 0$ a control gain. Taking the derivative of (8.37) along (8.36) gives

$$\dot{V}_1 = -K_1 z_1^2 + z_1 z_2 - z_1\tilde{w}_2 + \tilde{a}\left(\frac{1}{\gamma}\dot{\hat{a}} - z_1\left(\xi_{12} - Jz_1\right)\right). \tag{8.38}$$

Step 2:

The dynamics of z_2 can be obtained by (8.28), (8.31)-(8.32) and (8.34)

$$\begin{aligned}\dot{z}_2 &= -k_2\xi_{01} + k_2 z_1 + bu + \phi_2 - \frac{\partial\alpha}{\partial x_1}x_2 - \frac{\partial\alpha}{\partial t} \\ &\quad -\frac{1}{J}\frac{\partial\alpha}{\partial x_2}\left[h\left(x\right) + \xi_{02} + a\left(\xi_{12} - Jz_1\right) - \tilde{w}_2\right] \\ &\quad -\frac{\partial\alpha}{\partial\xi_{12}}\left(-k_2\xi_{11} + f\left(x,t\right)\right) - \frac{\partial\alpha}{\partial\hat{a}}\dot{\hat{a}}.\end{aligned} \tag{8.39}$$

Now, we design the control input

$$u = \frac{1}{b}\left[k_2\left(\xi_{01} - z_1\right) - \phi_2 + M - K_2 z_2 - z_1 + \Phi\right] \tag{8.40}$$

where $K_2 > 0$ is a control gain, Φ is a tuning function to be designed, and

$$M = \frac{\partial\alpha}{\partial x_1}x_2 + \frac{\partial\alpha}{\partial t} + \frac{\partial\alpha}{\partial\xi_{12}}\left(-k_2\xi_{11} + f\left(x,t\right)\right) + \frac{1}{J}\frac{\partial\alpha}{\partial x_2}\left[h\left(x\right) + \xi_{02} + \hat{a}\left(\xi_{12} - Jz_1\right)\right]. \tag{8.41}$$

Substituting (8.40) and (8.41) back into (8.39), we have

$$\dot{z}_2 = -K_2 z_2 - z_1 + \frac{1}{J}\frac{\partial \alpha}{\partial x_2}\left[\tilde{a}\left(\xi_{12} - Jz_1\right) + \tilde{w}_2\right] + \Phi - \frac{\partial \alpha}{\partial \hat{a}}\dot{\hat{a}}. \tag{8.42}$$

We next define the Lyapunov function candidate

$$V = V_1 + \frac{1}{2}z_2^2 + \frac{1}{\rho}\tilde{w}^\top P \tilde{w}, \tag{8.43}$$

where $\rho > 0$ is a control gain, $P = P^\top \succ 0$ satisfies $PA + A^\top P = -I$. Taking the derivative of (8.43) along (8.33) and (8.42) and using (8.38) yield

$$\begin{aligned}
\dot{V} &= -K_1 z_1^2 + z_1 z_2 - z_1 \tilde{w}_2 + \tilde{a}\left(\frac{1}{\gamma}\dot{\hat{a}} - z_1\left(\xi_{12} - Jz_1\right)\right) \\
&\quad -K_2 z_2^2 - z_1 z_2 + \frac{1}{J}z_2\frac{\partial \alpha}{\partial x_2}\tilde{a}\left(\xi_{12} - Jz_1\right) + \frac{1}{J}z_2\frac{\partial \alpha}{\partial x_2}\tilde{w}_2 \\
&\quad +z_2\left(\Phi - \frac{\partial \alpha}{\partial \hat{a}}\dot{\hat{a}}\right) + \frac{1}{\rho}\left[\left(\tilde{w}^\top A^\top + \phi^\top\right)P\tilde{w} + \tilde{w}P\left(A\tilde{w} + \phi\right)\right] \\
&= -\sum_{i=1}^{2} K_i z_i^2 + \tilde{a}\left[\frac{1}{\gamma}\dot{\hat{a}} + \left(\xi_{12} - Jz_1\right)\left(\frac{1}{J}z_2\frac{\partial \alpha}{\partial x_2} - z_1\right)\right] \\
&\quad +z_2\left(\Phi - \frac{\partial \alpha}{\partial \hat{a}}\dot{\hat{a}}\right) + \tilde{w}_2\left(\frac{1}{J}z_2\frac{\partial \alpha}{\partial x_2} - z_1\right) - \frac{1}{\rho}\tilde{w}^\top\tilde{w} \\
&\quad +\frac{2}{\rho}\phi^\top P\tilde{w}.
\end{aligned} \tag{8.44}$$

We state our main result by the following theorem:

Theorem 18 The designed filters (8.31)-(8.32), the controller (8.40) along with the tuning functions

$$\Phi = -\gamma\frac{\partial \alpha}{\partial \hat{a}}\left(\xi_{12} - Jz_1\right)\left(\frac{1}{J}z_2\frac{\partial \alpha}{\partial x_2} - z_1\right), \tag{8.45}$$

$$\phi = \frac{\rho}{2}P^{-1}\omega \tag{8.46}$$

with $\omega = [\omega_1, \omega_2]^\top = \left[0, z_1 - \frac{1}{J}z_2\frac{\partial \alpha}{\partial x_2}\right]^\top$ and the update law

$$\dot{\hat{a}} = -\gamma\left(\xi_{12} - Jz_1\right)\left(\frac{1}{J}z_2\frac{\partial \alpha}{\partial x_2} - z_1\right) \tag{8.47}$$

are capable of ensuring asymptotic tracking and all system signals bounded.

Proof. The stability can be explored by simply substituting (8.46)-(8.47) into (8.44). Recalling

the fact that $(P^{-1})^{\top} = P^{-1}$, we have

$$\begin{aligned}
\dot{V} &= -\sum_{i=1}^{2} K_i z_i^2 + \left(\tilde{a} - \gamma z_2 \frac{\partial \alpha}{\partial \hat{a}}\right)\left[\frac{1}{\gamma}\dot{\hat{a}} + (\xi_{12} - Jz_1)\left(\frac{1}{J} z_2 \frac{\partial \alpha}{\partial x_2} - z_1\right)\right] \\
&\quad -\frac{1}{\rho}\tilde{w}^{\top}\tilde{w} + \tilde{w}_2\left(\frac{1}{J} z_2 \frac{\partial \alpha}{\partial x_2} - z_1\right) + \omega^{\top}\left(P^{-1}\right)^{\top} P\tilde{w} \\
&= -\sum_{i=1}^{2} K_i z_i^2 - \frac{1}{\rho}\tilde{w}^{\top}\tilde{w} + \tilde{w}_2\left(\frac{1}{J} z_2 \frac{\partial \alpha}{\partial x_2} - z_1 + \omega_2\right) \\
&= -\sum_{i=1}^{2} K_i z_i^2 - \frac{1}{\rho}\tilde{w}^{\top}\tilde{w} \leq 0. \qquad (8.48)
\end{aligned}$$

Due to (8.43) and (8.48), we conclude that the function V is a Lyapunov function, and $V(t) \in \mathcal{L}_{\infty}$. Therefore, $(z_i(t), \tilde{w}_i(t), \tilde{a}(t)) \in \mathcal{L}_{\infty}$ for $i = 1, 2$, and $(z_i(t), \tilde{w}_i(t)) \in \mathcal{L}_2$. Since $z_1(t) \in \mathcal{L}_{\infty}$ and $(x_d(t), \dot{x}_d(t)) \in \mathcal{L}_{\infty}$, we know that $(x_1(t), x_2(t)) \in \mathcal{L}_{\infty}$ from (5.14), and hence, $(f(x,t), h(x)) \in \mathcal{L}_{\infty}$, and additionally, $(\varphi_1(t), \varphi_2(t)) \in \mathcal{L}_{\infty}$. Since $\varphi_2(t) \in \mathcal{L}_{\infty}$, it is clear that $\left(\xi_1(t), \dot{\xi}_1(t)\right) \in \mathcal{L}_{\infty}$ from (8.32), which means $(\xi_{11}(t), \xi_{12}(t)) \in \mathcal{L}_{\infty}$. Also, since $\tilde{a}(t) \in \mathcal{L}_{\infty}$, we know that $\hat{a}(t) \in \mathcal{L}_{\infty}$ from the definition of the parameter estimate and estimate error, and we further claim that $(\alpha(t), \dot{z}_1(t)) \in \mathcal{L}_{\infty}$ from (8.35) and (8.36), respectively. Because $(z_2(t), \alpha(t)) \in \mathcal{L}_{\infty}$, we know $\xi_{02} \in \mathcal{L}_{\infty}$ from (8.34), and furthermore, the fact that $(z_1, \xi_{11}, \xi_{12}, \tilde{w}_i) \in \mathcal{L}_{\infty}$ yields $(\xi_{01}(t), \zeta(t)) \in \mathcal{L}_{\infty}$ from (8.28). Therefore, $\xi_0 \in \mathcal{L}_{\infty}$ and we know $x_3 \in \mathcal{L}_{\infty}$ from (8.24). Due to the property of certain nonlinear functions $f(x)$ and $h(x,t)$, we know that $\left(\frac{\partial \alpha}{\partial x_i}(t), \frac{\partial \alpha}{\partial t}(t)\right) \in \mathcal{L}_{\infty}$ for $i = 1, 2$, and since $\frac{\partial \alpha}{\partial \xi_{12}} = -\hat{a}$ and $\frac{\partial \alpha}{\partial \hat{a}} = -\xi_{12} + Jz_1$, it is clear that $\left(\frac{\partial \alpha}{\partial \xi_{12}}, \frac{\partial \alpha}{\partial \hat{a}}\right) \in \mathcal{L}_{\infty}$. Therefore, $(\phi(t), \Phi(t), \hat{a}(t)) \in \mathcal{L}_{\infty}$ from (8.46)-(8.47). Based on the facts above, we can consequently conclude that $u \in \mathcal{L}_{\infty}$ from (8.40)-(8.41), $\dot{z}_2(t) \in \mathcal{L}_{\infty}$ from (8.42), $\dot{\xi}_0(t) \in \mathcal{L}_{\infty}$ from (8.31) and $\dot{\tilde{w}}(t) \in \mathcal{L}_{\infty}$ from (8.33). Now since $(z_i(t), \tilde{w}_i(t)) \in \mathcal{L}_{\infty} \cup \mathcal{L}_2$, and $\left(\dot{z}_i(t), \dot{\tilde{w}}_i(t)\right) \in \mathcal{L}_{\infty}$ for $i = 1, 2$, we can apply Barbalat's Lemma and obtain that $\dot{z}_i$ and $\dot{\tilde{w}}_i$are uniformly continuous and

$$\lim_{t \to \infty} z_i(t) = 0, \ \lim_{t \to \infty} \tilde{w}_i(t) = 0.$$

Finally, we also have that $\dot{x}_2(t), \dot{x}_3(t) \in \mathcal{L}_{\infty}$. ■

8.3.4 Simulation

The performance of the filter-based adaptive output feedback controller was illustrated by the following computer simulation. The plant parameters in (8.1) were set by (6.46), and

$$a = 1/1.1 \text{ s}^{-1},\ b = 0.04/1.1 \text{ Nm/(s-}\mu\text{s)}.$$

Note that the parameters a and b were estimated from [29]. The initial states were set to $x_1(0) = \pi/15$ rad, $x_2(0) = 0$ rad/s, and $x_3(0) = 0$ Nm.

The simulations was conducted using a step-like reference trajectory that was set to a sequence of two smooth step commands generated by the dynamical system

$$\dot{x}_r = \begin{bmatrix} 0 & 1 & 0 & 0 \\ 0 & 0 & 1 & 0 \\ 0 & 0 & 0 & 1 \\ -625 & -500 & -150 & -20 \end{bmatrix} x_r + \begin{bmatrix} 0 \\ 0 \\ 0 \\ 1 \end{bmatrix} u_r \tag{8.49}$$

$$y_r = x_r, \tag{8.50}$$

where $x_r = [x_d, \dot{x}_d, \ddot{x}_d, \dddot{x}_d]^\top$ and

$$u_r = \begin{cases} 625\pi/18, & 0 \le t < 10 \text{ s} \\ 625\pi/6, & 10 \le t < 50 \text{ s} \\ 3125\pi/12, & t \ge 50 \text{ s}, \end{cases}$$

with initial condition $x_r(0) = [\pi/18, 0, 0, 0]^\top$. The plot of $x_d(t)$ is shown in Figure 8.1. This trajectory simulates a typical motion conducted during rehabilitation sessions.

The following gains were used in the simulation

$$k_1 = 3,\ k_2 = 5.5,\ K_1 = 1.5,\ K_2 = 5.5,$$

$$\mu = 2,\ \rho = 1,\ \gamma = 0.6,\ P = \begin{bmatrix} 1 & 0 \\ 0 & 2 \end{bmatrix}.$$

The results for the simulation described above is presented next. The performance of the tracking error $e(t)$ and the control input $u(t)$ are shown in Figure 8.2-8.3, respectively. From Figure

8.2, the tracking error of the smooth step command shows an asymptotical convergence. In Figure 8.3, the pulse width input signal approximately demonstrates the shape of the corresponding reference trajectory, which, as predicted, does not violate Assumption 2.

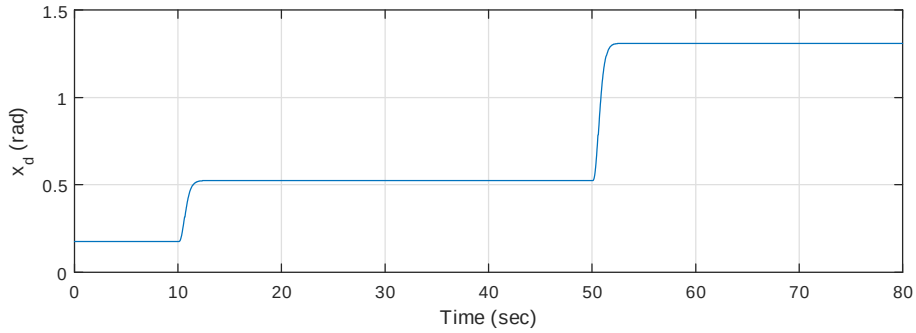

Figure 8.1: The step-like reference trajectory $q_d(t)$.

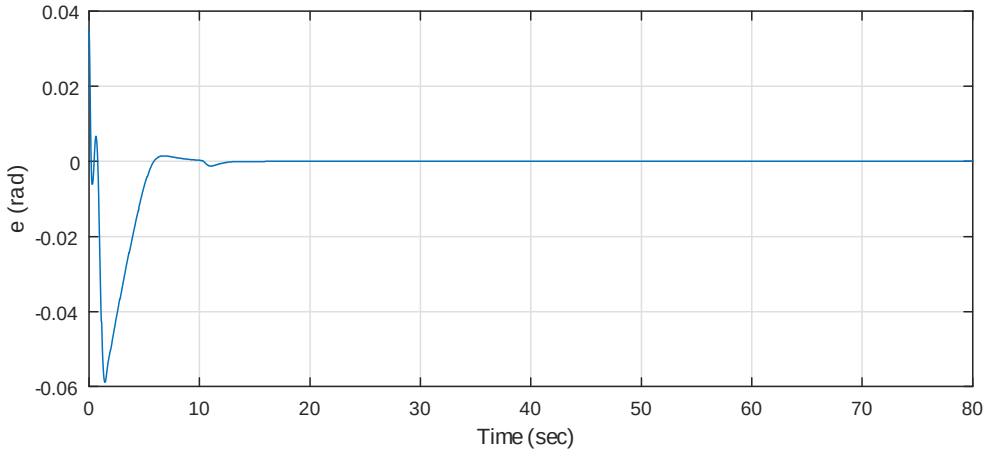

Figure 8.2: Tracking error $e\,(t)$.

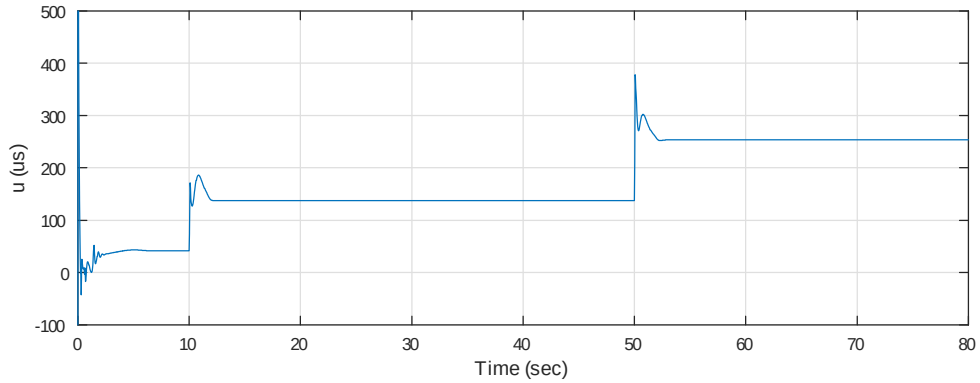

Figure 8.3: Control input $u\,(t)$.

Figure 8.4-8.6 present the parameter estimate $\hat{a}(t)$, the filter outputs $\xi_i(t)$, $i = 0, 1$, and the state estimate error $\tilde{w}(t)$, respectively. In Figure 8.4, the parameter estimate $\hat{a}(t)$ shows the convergence of some constant under the adaptation; In Figure 8.6, the state estimate error $\tilde{w}(t)$ yeilds an asymptotical convergence to zero.

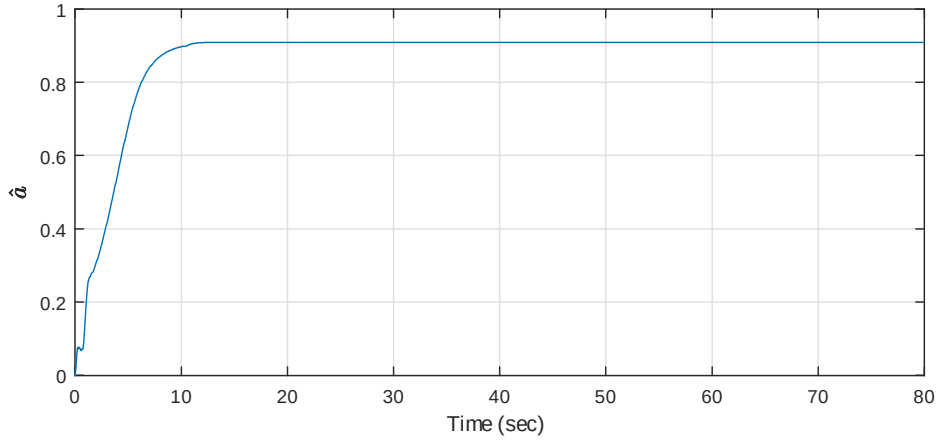

Figure 8.4: Parameter estimate $\hat{a}(t)$.

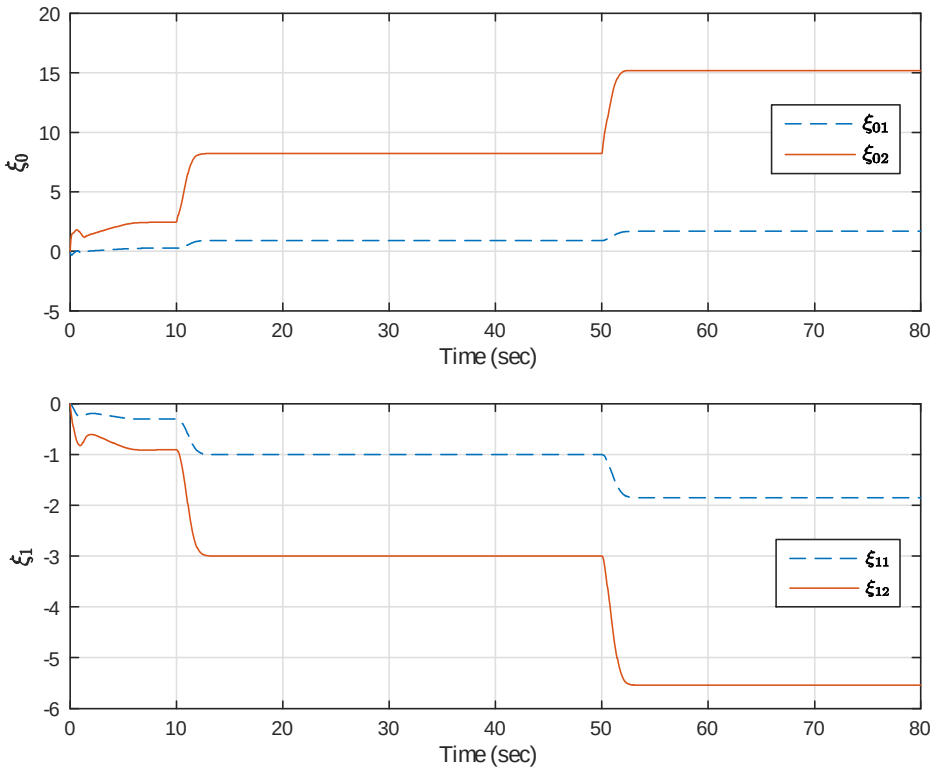

Figure 8.5: The filter outputs $\xi_0(t)$ and $\xi_1(t)$.

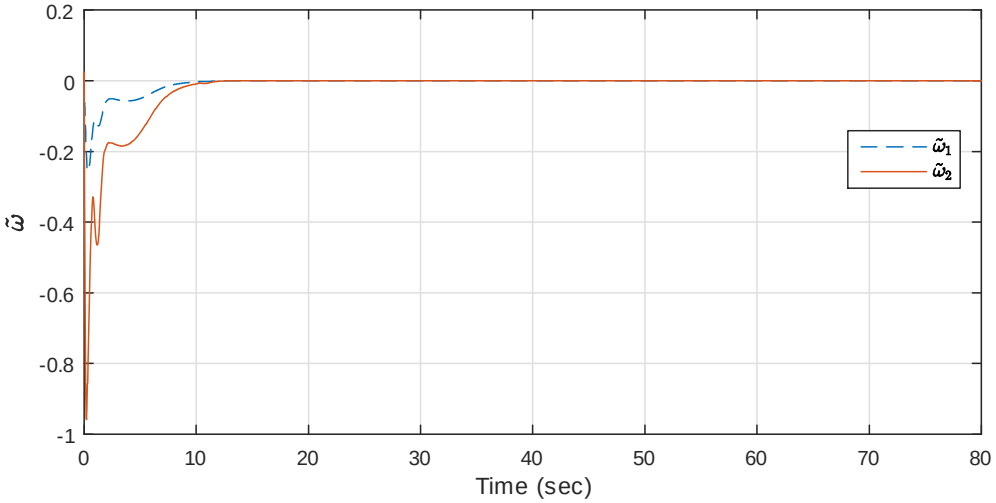

Figure 8.6: State estimate error $\tilde{w}\,(t)$.

Chapter 9 Conclusions and Future Work

This dissertation presented a class of feedback controllers for the NMES quadriceps muscle group-knee joint dynamics based on the backstepping technique and Lyapunov stability theory. Due to the complexity of the full-order system model, the controllers were based on simplified and/or reduced-order NMES models. Three levels of models were considered in this work. The first one was at the *torque level*, and only the mechanical passive dynamics were considered in the control design. In the second level, an *algebraic* relationship between torque and stimulation voltage was added to the first-level model, leading to a system with uncertainty in the control coefficient. The issue of voltage saturation was considered in this model. The third level considered a *dynamic* relationship between torque and stimulation voltage by including the muscle activation dynamics in the system model. This increased the order of the system model from two to three with the additional complexity that the third state is unmeasurable.

The controllers proposed in this work are building blocks for the control problem of the full-order system. That is, we introduced a set of control design tools applicable to subsets of the full-order system, which could be incorporated into other NMES control solutions. The main recommendation for future work is to translate the theoretical results proposed here to real-time implementations on a NMES testbed.

References

[1] J. Abbas and H. Chizeck. “Feedback control of coronal plane hip angle in paraplegic subjects using functional neuromuscular stimulation,” *IEEE Trans. Biomed. Eng.*, Vol. 38, No. 7, pp. 687-698, 1991.

[2] A. Ajoudani and A. Erfanian. "A neuro-sliding-mode control with adaptive modeling of uncertainty for control of movement in paralyzed limbs using functional electrical stimulation," *IEEE Trans. Biom. Eng.*, Vol. 56, No. 7, pp. 1771-1780, 2009.

[3] A. Alibeji, N. Kirsch, and N. Sharma. "An adaptive low-dimensional control for a hybrid neuroprosthesis," *Proc. IFAC Symp. Biological and Medical Systems*, pp. 303-308, Berlin, Germany, Sepetemper 2015.

[4] N. Alibeji, N. Kirsch, S. Farrokhi, and N. Sharma. "Further result on predictor-based control of neuromuscular electrical stimulation," *IEEE Trans. Neural Syst. Rehab. Eng.*, Vol. 23, No. 6, pp. 1095-1105, 2015.

[5] N. Alibeji, N. Kirsch, and N. Sharma. "Dynamic surface control of neuromuscular eletrical stimulation of a musculoskeletal system with activation dynamics and an input delay," *Proc. American Control Conf.*, pp. 631-636, Chicago, IL, 2015.

[6] N. Alibeiji, N. Kirsch, B. Dicianno, and N. Sharma. "A modified dynamic surface controller for delayed neuromuscular electrical stimulation," *IEEE/ASME Trans. Mechatronics*, Vol. 22, NO. 4, pp. 1755-1764, 2017.

[7] N. Alibeiji, N. Kirsch, and N. Sharma. "An adaptive low-dimensional control to compensate for actuator redundancy and FES-induced muscle fatigue in a hybrid neuroprosthesis," *Control Eng. Prac.*, Vol. 59, pp. 204-219, 2017.

[8] A. del Ama, Á. Gil-Agudo, J. Pons, and J. Moreno. “Hybrid FES-robot cooperative control of ambulatory gait rehabilitation exoskeleton,” *J. NeuroEng. Rehab.*, Vol. 11, No. 1, pp. 11-27, 2014.

[9] A. Annaswamy and S. Kárason. “Discrete-time adaptive control in the presence of input constraints,” *Automatica*, Vol. 31, No. 10, pp. 1421-1431, 1995.

[10] A. Annaswamy and J. Wong. “Adaptive control in the presence of saturation non-linearity,” *Intl. J. Adapt. Control Signal Process.*, Vol. 11, No. 1, pp. 3-19, 1997.

[11] A. Annaswamy, F. Skantze, and A. Loh. "Adaptive control of continuous time systems with convex/concave parameterization," *Automatica*, Vol. 34, No. 1, pp. 33-49, 1998.

[12] X. Bao, N. Kirsch, and N. Sharma. "Dynamic control allocation of a feedback linearized hybrid neuroprosthestic system," *Proc. American Control Conf.*, pp. 3976-3981, Boston, MA, 2016.

[13] L. Bernotas, P. Crago, and H. Chizeck. "Adaptive control of electrical stimulated muscle," *IEEE Trans. Biol. Eng.*, Vol. BME-34, No. 2, pp.140-147, 1987.

[14] F. Chaoui, F. Giri, L. Dugard, J. Dion, and M. M'Saad. "Adaptive tracking with saturating input and controller integral action," *IEEE Trans. Autom. Control*, Vol. 43, No. 11, pp. 1638-1643, 1998.

[15] F. Chaoui, F. Giri, and M. M'Saad. "Adaptive control of inputconstrained type-1 plants stabilization and tracking," *Automatica*, Vol. 37, No. 2, pp. 197-203, 2001.

[16] M. Chen, S. Ge, and B. Ren. "Adaptive tracking control of uncertain MIMO nonlinear systems with input constraints," *Automatica*, Vol. 47, No. 3, pp. 452-465, 2011.

[17] T. Cheng, Q. Wang, R. Kamalapurkar, H. Dinh, M. Bellman, and W. Dixon. "Identification-based closed-loop NMES limb tracking with amplitude-modulated control input," *IEEE Trans. Cybern.*, Vol. 46, No. 7, pp. 1679-1690, 2016.

[18] P. Crago, N. Lan, P. Veltink, J. Abbas, and C. Kantor. "New control strategies for neuroprosthetic systems," *J. Rehab. Res. Develop.*, Vol. 33, No. 2, pp. 158-172, 1996.

[19] G. Cybenko,"Approximations by superpositions of sigmoidal functions", *Mathematics of Control, Signals, and Systems*, Vol. 2, No. 4, pp. 303-314, 1989.

[20] D. Davy and M. Audu. "A dynamic optimization technique for predicting muscle force in the swing phase of gait," *J. Biomech.*, Vol. 20, No. 2, pp. 187-201, 1987.

[21] M. de Queiroz, D. Dawson, S. Nagarkatti, and F. Zhang, *Lyapunov-based control of mechanical systems*, Cambridge, MA: Birkhäuser, 2000

[22] B. Doll, N. Kirsch, and N. Sharma. "Optimization of a stimulation train based on a predictive model of muscle force and fatigue," *Proc. IFAC Symposium on Biological and Medical Syst.*, pp. 338-342, Berlin, Germany, 2015.

[23] S. Dorgan and M. O'Malley. "A nonlinear mathematical model of electrically stimulated skeletal muscle," *IEEE Trans. Rehab. Eng.*, Vol. 5, No. 2, pp. 179-194, 1997.

[24] W. Durfee and K. Palmer. "Estimation of force-activation, force-length, and force-velocity properties in isolated, electrically stimulated muscle," *IEEE Trans. Biom. Eng.*, Vol. 41, No. 3, pp. 205-216, 1994.

[25] W. Durfee. "Gair restoration by functional electrical stimulation," *Climbing and Walking Robots*, pp. 19-26, Springer, 2006.

[26] T. Edrich, R. Riener, and J. Quintern. "Analysis of passive elastic joint moments in paraplegics," *IEEE Trans. Biom. Eng.*, Vol. 47, No. 8, pp. 1058-1065, 2000.

[27] A. Esquenazi, M. Talaty, A. Packel, and M. Saulino. "The ReWalk powered exoskeleton to restore ambulatory function to individuals with thoracic-level motor-complete spinal cord injury," *Am. J. Phys. Med. Rehab.*, Vol. 91, No. 11, pp. 911-921, 2012.

[28] R. Farris, H. Quintero, and M. Goldfarb. "Preliminary evaluation of a powered lower limb orthosis to aid walking in paraplegic individuals," *IEEE Trans. Neural Syst. Rehab. Eng.*, Vol. 19, No. 6,

pp. 652-659, 2011.

[29] M. Ferrarin and A. Pedotti. "The relationship between electrical stimulus and joint torque: A dynamical model," *IEEE Trans. Rehab. Eng.*, Vol. 8, No. 3, pp. 342-352, 2000.

[30] M. Ferrarin, F. Palazzo, R. Riener, and J. Quintern. "Model-based control of FES-induced single joint movements," *IEEE Trans. Neural Syst. Rehab. Eng.*, Vol. 9, No. 3, pp. 245-257, 2001.

[31] G. Feng, C. Zhang, and M. Palaniswami. “Stability of input amplitude constrained adaptive pole placement control systems,” *Automatica*, Vol. 30, No. 6, pp. 1065-1070, 1994.

[32] N. Fisher, R. Kamalapurkar, and W. Dixon. "LaSalle-Yoshizawa corollaries for nonsmooth systems," *IEEE Trans. Autom. Control*, Vol. 58, No. 9, pp. 2333-2338, 2013.

[33] A. Fradkov, R. Ortega and G. Bastin. "Semi-adaptive control of convexly parametrized systems with application to temperature regulation of chemical reactors," *Int. J. Adapt. Control Signal Process*, Vol. 15, pp. 415-426, 2001.

[34] H. Franken, P. Veltink, and R. Henk. "Identification of passive knee joint and shank dynamics in paraplegics using quadriceps stimulation," *IEEE Trans. Rehab. Eng.*, Vol. 1, No. 3, pp. 154-164, 1993.

[35] H. Franken, P. Veltink, and H. Boom. "Restoring gait in paraplegics by functional electrical stimulation," *IEEE Eng. Med. Biol.*, Vol. 13, pp. 564-570, 1994.

[36] Y. Gao, X. Sun, C. Wen, and W. Wang. "Observer-based adaptive NN control for a class of uncertain nonlinear systems with nonsymmetric input saturation," *IEEE Trans. Neural Networks and Learning Syst.*, Vol. 28, No. 7, pp. 1520-1530, 2017.

[37] F. Gao, M. de Queiroz, and D. Dawson. "A new tuning function-based robust adaptive controller for parametric strict feedback systems," *Proc. IEEE Conf. Decision and Control*, pp. 3543-3548, New Orleans, LA, 2007.

[38] S. Ge, H. Fan, and T. Lee. "Adaptive neural control of nonlinear time-delay systems with unknown virtual control coefficients," *IEEE. Trans. Systems, Man, and Cybern.–Part B*, Vol. 34, No. 1, pp. 499-516, 2004.

[39] S. Ge and C. Wang. "Direct adaptive control of a class of nonlinear systems," *IEEE Trans. Neural Networks*, Vol. 13, No. 1, pp. 214-221, 2002.

[40] S. Ge and J. Wang. "Robust adaptive neural control for a class of perturbed strict feedback nonlinear systems," *IEEE Trans. Neural Networks*, Vol. 13, No. 6, pp. 1409-1419, 2002.

[41] J. Giuffrida and P. Crago. "Functional restoration of elbow extension after spinal-cord injury using a neural network-based synergistic FES controller," *IEEE Trans. Rehab. Eng.*, Vol. 1, No. 3, pp. 154-164, 1993.

[42] K. Ha, S. Murray, and M. Goldfarb. “An approach for the cooperative control of FES with a pow-

ered exoskeleton during level walking for persons with paraplegia," *IEEE Trans. Neural Syst. Rehab. Eng.*, Vol. 24, No. 4, pp. 455-466, 2016.

[43] J. Hamill and K. Knutzen. *Biomechanical basis of human movement*. New York, NY: Lippincott Williams & Wilkins, 3rd ed., 2008.

[44] H. Hatze. "A myocybernetic control model of skeletal muscle," *Biol. Cybernetics*, Vol. 25, pp. 103-119, 1977.

[45] H. Hatze. "A general myocybernetic control model of skeletal muscle," *Biol. Cybernetics*, Vol. 28, pp. 143-157, 1978.

[46] J. Hausdorff and W. Durfee. "Open-loop position control of the knee joint using electrical stimulation of the quadriceps and hamstrings," *Medical and Biological Eng. and Comp.*, Vol. 29, No. 3, pp. 269-280, 1991.

[47] A. Hill. "The heat of shortening and the dynamic constants of muscle," *Proc. Roy. Soc. London*, Vol. B126, pp. 136-195, 1938.

[48] J. Huang and Y. Chen. "A smooth switching adaptive controller for linearizable systems with improved transient performance," *Intl. J. Adaptive Control & Signal Proc.*, Vol. 20, No. 9, pp. 431-446, 2006.

[49] J. Huang. "Hybrid-based adaptive NN backstepping control of strict-feedback systems," *Automatica*, Vol. 45, No. 6, pp.1497-1503, 2009.

[50] N. Hung, H. Tuan, P. Apkarian, and T. Narikiyo. "General adaptive controls for nonlinearly parameterized systems under generalized matching condition." *Proc. IFAC World Congr.*, pp. 840-846, Barcelona, Spain, 2002.

[51] S. Jezernik, R. Wassink, and T. Keller. "Sliding mode closed loop control of FES: Controling the shank movement," *IEEE Trans. Biom. Eng.*, Vol. 51, No.2, pp. 263-272, 2004.

[52] R. Kamalapurkar, N. Fischer, S. Obuz, and W. Dixon. "Time-varying input and state delay compensation for uncertain nonlinear systems," *IEEE Trans. Autom. Control*, Vol. 61, No. 3, pp. 834-839, 2015.

[53] I. Kanellakopoulos, P. Kokotovic, and A. Morse. "Systematic design of adaptive controller for feedback linearizable systems," *IEEE Trans. Autom. Control*, Vol. 36, No. 11, pp. 1241-1253, 1991.

[54] A. Kantrowitz. "Electronic physiologic aid. A report of the ,aomonides Hospital," Brooklyn, NY, 1960.

[55] I. Karafyllis, M. Malisoff, M. de Queiroz, M. Krstic, and R. Yang. "Predictor-based tracking for neuromuscular electrical stimulation," *Int. J. Robust Nonlinear Control*, Vol. 25, pp. 2391-2419, 2015.

[56] S. Kárason and A. Annaswamy. “Adaptive control in the presence of input constraints,” *IEEE Trans. Autom. Control*, Vol. 39, No. 11, pp. 2325-2330, 1994.

[57] R. Kearney and I. Hunter. "System identification of human joint dynamics," *J. Biom. Eng.*, Vol. 18, No. 1, pp. 57-88, 1990.

[58] H. Khalil. *Nonlinear systems*, 3rd ed., Englewood Cliffs, New Jersey: Prentice Hall, 2002.

[59] N. Kirsch, N. Alibeji, L. Fisher, C. Gregory, and N. Sharma. "A semi-active hybrid neuroprosthesis for restoring lower limb function in paraplegics," *Proc. IEEE Intl. Conf. Eng. Med. Biol. Soc.*, pp. 2557-2560, 2014.

[60] N. Kirsch, N. Alibeji, B. Dicianno, and N. Sharma. "Switching control of functional electrical stimulation and motor assist for muscle fatigue," *Proc. American Control Conf.*, pp. 4865-4870, Boston, MA, July 2016.

[61] C. Klauer, T. Schauer, W. Reichenfelser, J. Karner, S. Zwicker, M. Gandolla, E. Ambrosini, S. Ferrante, M. Hack, A. Jedlitschka, A. Duschau-Wicke, M. Gföhler, and A. Pedrocchi. “Feedback control of arm movements using neuro-muscular electrical stimulation (NMES) combined with a lockable, passive exoskeleton for gravity compensation,” *Frontiers in Neuroscience*, Vol. 8, 2014.

[62] A. Kojic, A. Annaswamy, A. Loh, and R. Lozano. "Adaptive control of a class of nonlinear systems with with convex/concave parameterization," *Syst. Control Lett.*, Vol. 37, pp. 267-274, 1999.

[63] B. Koo, and A. Leonessa. "An adaptive block backstepping control design for functional electrical stimulation of agonist-antagonist muscles," *Proc. ASME Dynam. Syst. Control Conf.*, pp. 479-486, Arlington, VA, 2011.

[64] K. Kosmatopoulos and P. Ioannou. "Robust switching adaptive control of multi-input nonlinear systems," *IEEE Trans. Autom. Control*, Vol. 47, No. 4, pp. 610-624, 2002.

[65] A. Krailj and T. Bajd. *Functional electrical stimulation: Standing and walking after spinal cord injury*, Boca Raton, FL: CRC Press, 1989.

[66] J. Krevolin, M. Pandy, and J. Pearce. "Moment arm of the patellar tendon in the human knee," *J. Biomech.*, Vol. 37, pp. 785-788, 2004.

[67] M. Krstic, I. Kanellakopoulos, and P. Kokotovic. *Nonlinear and adaptive control design*, New York, NY: John Wiley & Sons, 1995.

[68] N. Lan, P. Crago, and H. Chizeck. “Control of end-point forces of a multijoint limb by functional neuromuscular stimulation,” *IEEE Trans. Biomed. Eng.*, Vol. 38, No. 10, pp. 953-965, 1991.

[69] N. Lan, P. Crago, and H. Chizeck. “Feedback control methods for task regulation by electrical stimulation of muscles,” *IEEE Trans. Biomed. Eng.*, Vol. 38, No. 12, pp. 1213-1223, 1991.

[70] M. Levy, J. Mizrahi, and Z. Susak. "Recruitment, force and fatigue characteristics of quadriceps muscles of paraplegics, isometrically activated by surface FES," *J. Biom. Eng.*, Vol. 12, No. 2, pp.

150-156, 1990.

[71] F. Lewis, S. Jagannathan, and A. Yesildirek. *Neural network control of robot manipulator and nonlinear systems*, London: Taylor and Francis, 1999.

[72] W. Liberson, H. Holmquest, D. Scott, and A. Dow. "Functional electrontherapy: Stimulation of the peroneal nerve synchronized with the swing phase of the gait in hemiplegic patients," *Arch. Phys. Med. Rehab.*, Vol. 42, pp. 101-105, 1961.

[73] T. Li, Y. Yang, J. Hu, and L. Yang. "Bobust adaptive fuzzy tracking control for a class of perturbed uncertain nonlinear systems with UVCGF," *Intl. J. Wavelets, Multiresolution and Information Proc.*, Vol. 5, No. 1, pp. 227-239, 2007.

[74] Y. Li, S. Tong, and T. Li. "Adaptive fuzzy output-feedback control for output constrained nonlinear systems in the presence of input saturation," *Fuzzy Sets and Systems*, No. 248, pp. 138-155, 2014.

[75] Y. Li, S. Tong, and T. Li. "Composite adaptive fuzzy output feedback control design for uncertain nonlinear strict-feedback systems with input saturation," *IEEE Trans. Cybern.*, Vol. 45, No. 10, pp. 2299-2308, 2015.

[76] D. Lin and W. Rymer. "A quantitative analysis of pendular motion of the lower leg in spastic human subjects," *IEEE Trans. Biom. Eng.*, Vol. 38, No. 9, pp. 906-918, 1991.

[77] A. Loh, A. Annaswamy, and F. Skantze. "Adaptation in the presence of a general nonlinear parameterization: an error model approach," *IEEE Trans. Autom. Control*, Vol. 44, No. 9, pp. 1634-1652, 1999.

[78] C. Lynch and M. Popovic. “A comparison of closed-loop control algorithms for regulating electrically stimulated knee movements in individuals with spinal cord injury,” *IEEE Trans. Neural Syst. Rehab. Eng*, Vol. 20, No. 4, pp. 539–548, 2012.

[79] J. Ma, Z. Zheng, and P. Li. "Adaptive dynamic surface control of a class of nonlinear systems with unknown direction control gains and input saturation," *IEEE Trans. Cybern.*, Vol. 45, No. 4, pp. 728-741, 2015.

[80] J. Mansour and M. Audu. "The passive elastic moment at the knee and its influence on human gait," *J. Biomech.*, Vol. 19, No. 5, pp. 369-373, 1986.

[81] E. Marsolais and R. Kobetic. "Functional electrical stimulation for walking in paraplegia." *The Journal of Bone and Joint Surgery*, Vol. 69, No. 5, pp. 728-733, 1987.

[82] D. McNeal, R. Nakai, P. Meadows, and W. Tu. "Open-loop control of the freely-swinging paralyzed leg," *IEEE Trans. Biol. Eng*, Vol. 36, No. 9, pp. 895–905, 1989.

[83] M. Merad, R. Downey, S. Obuz, and W. Dixon. "Isometric torque control for neuromuscular electrical stimulation with time-varying input delay," *IEEE Trans. Control Syst. Tech.*, Vol. 24, No. 3, pp. 971-978, 2016.

[84] J. Mortimer. "Motor prostheses," In *Handbook of physiology, nervous system II* (ed. V. Brooks), pp. 155-187, Bethesda, MD: American Physiological Society, 1981.

[85] K. Narendra and A. Annaswamy. *Stable adaptive systems*. Mineola, NY: Dover, 2005.

[86] M. Netto, A. Annaswamy, R. Ortega, and P. Moya. "Adaptive control of a class of nonlinearly parameterized systems using convexification," *Intl. J. Control*, Vol. 73, No. 14, pp. 1312-1321, 2000.

[87] M. Netto and A. Annaswamy. "Adaptive control of a class of multilinearly parameterized systems by using noncertainty equivalence control," *Proc. IEEE Conf. Dec. Control*, pp. 4829-4834, Maui, HI, 2012.

[88] P. Neuhaus, J. Noorden, T. Craig, T. Torres, J. Kirschbaum, and J. Pratt. "Design and evaluation of mina: A robotic orthosis for paraplegics," *IEEE ICORR*, pp. 1-8, 2011.

[89] B. Nigg and W. Herzog. *Biomechancis of The Musculo-skeletal System*. Chichester, England: Wiley, 1999.

[90] R. Nussbaum. " Some remarks on the conjecture in parameter adaptive control," *Syst. Contr. Lett.*, Vol. 3, pp. 243-246, 1983.

[91] R. Ortega. "Some remarks on adaptive neuro-fuzzy systems," *Intl. J. Adap. Control Sign. Proc.*, Vol. 10, No. 1, pp. 79-83, 1996.

[92] P. Peckham and D. Gray. "Functional neuromuscular stimulation," *J. Rehab. Res. Dev.*, Vol. 33, pp. 9-11, 1996.

[93] P. Peckham and J. Knutson. "Functional electrical stimulation for neuromuscular applications," *Annu. Rev. Biomed. Eng.*, Vol. 7, pp. 327-360, 2005.

[94] A. Pedotti, M. Ferrarin, J. Quintern, and R. Riener. *Neuroprosthetics: From basic research to clinical applications*. Berlin, Germany: Springer-Verlag, 1996.

[95] M. Polycarpou and P. Ioannou, "A robust adaptive nonlinear control design," *Automatica*, Vol. 32, No. 3, pp. 423-427, 1996.

[96] M. Polycarpou and M. Mears. "Stable adaptive tracking of uncertain systems using nonlinearly parameterized on-line approximators," *Intl. J. Control*, Vol. 70, No. 3, pp. 363-384, 1998.

[97] C. Qian and W. Lin. "Practical output tracking of nonlinear systems with uncontrollable unstable linearization," *IEEE Trans. Autom. Control*, Vol. 47, No. 1, pp. 21-36, 2002.

[98] T. Qiu, N. Alibeji, and N. Sharma. "Robust compensation of electromechanical delay during neuromuscular electrical stimulation of antagonistic muscles," *Proc. American Control Conf.*, pp. 4871-4876, Boston, MA, July 2016.

[99] Z. Qu and J. Xu. “Model-Based Learning Controls and Their Comparisons Using Lyapunov Direct

Method," *Asian J. Control*, Vol. 4, No.1, pp. 99-110, Mar. 2002.

[100] H. Quintero, R. Farris, W. Durfee, and M. Goldfarb. "Feasibility of a hybrid-FES system for gait restoration in paraplegics," *Proc. Intl. Conf. IEEE EMBC*, pp. 483–486, 2010.

[101] R. Riener, J. Quintern, and G. Schmidt. "Biomechanical model of the human knee evaluated by neuromuscular stimulation," *J. Biomech.*, Vol. 29, No. 9, pp. 1157-1167, 1996.

[102] R. Riener and T. Fuhr. "Patient-driven control of FES-supported standing up: A simulation study," *IEEE Trans. Rehab. Eng.*, Vol. 6, No. 2, pp. 113-124, 1998.

[103] R. Riener. "Model-based development of neuroprostheses for paraplegic patients," *Phil. Trans. R. Soc. Lond.*, Vol. B, pp. 877-894, 1999.

[104] J. Riess and J. Abbas. "Adaptive neural network control of cyclic movements using functional neuromuscular stimulation," *IEEE Trans. Rehab. Eng.*, Vol. 8, No. 1, pp. 42-52, 2000.

[105] O. Rutherford and D. Jones. "Measurement of fibre pennation using ultrasound in the human quadriceps in vivo," *Eur. J. Appl. Phys.*, Vol. 65, pp. 433–437, 1992.

[106] E. Ryan. "A universal adaptive stabilizer for a class of nonlinear systems," *Syst. Control Lett.*, Vol. 16, pp. 209–218, 1991.

[107] T. Schauer, N. Negard, F. Previdi, K. Hunt, M. Fraser, E. Ferchland, and J. Raisch. "Online identification and nonlinear control of the electrically stimulated quadriceps muscle," *Control Eng. Prac.*, Vol. 13, pp. 1207-1219, 2005.

[108] L. Schutte, M. Rodgers, F. Zajac, and R. Glaser. "Improving the efficacy of electrical stimulation-induced leg cycle ergometry: An analysis based on a dynamic musculoskeletal model," *IEEE Trans. Rehab. Eng.*, Vol. 1, No. 2, pp. 109-125, 1993.

[109] N. Sharma, P. Patre, C. Gregory, and W. Dixon. "Nonlinear control of NMES: Incorporating fatigue and calcium dynamics," *Proc. ASME Dym. Sys. Control Conf.*, Hollywood, CA, 2009.

[110] N. Sharma, K. Stegath, C. Gregory, and W. Dixon. "Nonlinear neuromuscular electrical stimulation tracking control of a human limb," *IEEE Trans. Neural Syst. Rehab. Eng.*, Vol. 17, No. 6, pp. 576-584, 2009.

[111] N. Sharma, C. Gregory, and W. Dixon. "Predictor-based compensation for electromechanical delay during neuromuscular electrical stimulation," *IEEE Trans. Neural Syst. Rehab. Eng.*, Vol. 19, No. 6, pp. 601-611, 2011.

[112] N. Sharma, C. Gregory, M. Johnson, and W. Dixon. "Closed-loop neural network-based NMES control for human limb tracking," *IEEE Trans. Control Syst. Tech.*, Vol. 20, No. 3, pp. 712-725, 2012.

[113] N. Sharma, V. Mushahwar, and R. Stein. "Dynamic optimization of FES and orthosis-based walking using simple models," *IEEE Trans. Neural Syst. Rehab. Eng.*, Vol. 22, No. 1, pp. 114-126,

2014.

[114] M. Sillen, C. Speksnijder, R. Eterman, P. Janssen, S. Wagers, E. Wouters, N. Uszko-Lencer, and M. Spruit. "Effects of neuromuscular electrical stimulation of muscles of ambulation in patients with chronic heart failure or COPD: A systematic review of the English-language literature," *CHEST Journal*, Vol. 136, No. 1, pp, 44-61, 2009.

[115] R. Stein, E. Zehr, M. Lebiedowska, D. Popovic, A. Scheiner, and H. Chizeck. "Estimating mechanical parameters of leg segments in individuals with and without physical disabilities," *IEEE Trans. Rehab. Eng.*, Vol. 4, No. 3, pp. 201-211, 1996.

[116] H. Sussmann, E. Sontag, and Y. Yang. "A general result on the stabilization of linear systems using bounded controls," *IEEE Trans. Autom. Control*, Vol. 39, No. 12, pp. 2411–2425, 1994.

[117] P. Veltink. "Control of FES-induced cyclical movements of the lower leg," *Med. Bio. Eng. Comput.*, Vol. 29, No. 6, pp. 8-12, 1991.

[118] P. Veltink. H. Chizeck, P. Crago, and A. El-Bialy. "Nonlinear joint angle control for artificially stimulated muscle," *IEEE Trans. Biom. Eng.*, Vol. 39, No. 4, pp. 368-380, 1992.

[119] C. Wang, D. Hill, S. Ge, and G. Chen. "An ISS-modular approach for adaptive neural control of pure-feedback systems," *Automatica*, Vol. 42, No. 5, pp. 723-731, 2006.

[120] Q. Wang, H. Dinh, M. Bellman, and W. Dixon. "Neuromuscular electrical stimulation with an uncertain muscle contraction model," *Proc. Dynam. Syst. Control Conf.*, pp. 519-528, Ft. Lauderdale, FL, 2012.

[121] Q. Wang, N. Sharma, M. Johnson, C. Gregory, and W. Dixon. "Adaptive inverse optimal neuromuscular electrical stimulation," *IEEE Trans. Cybern.*, Vol. 43, No. 6, pp. 1710-1718, 2013.

[122] C. Wen, J. Zhou, Z. Liu, and H. Su. "Robust adaptive control of uncertain nonlinear systems in the presence of input saturation and external disturbance," *IEEE Trans. Autom. Control*, Vol. 56, No. 7, pp. 1672-1678, 2011.

[123] J. M. Winters and L. Stark. "Muscle models: What is gained and what is lost by varying model complexity," *Biol. Cybern.*, Vol. 55, pp. 403–420, 1987.

[124] B. Xian, D. Dawson, M. de Queiroz, and J. Chen, "A continuous asymptotic tracking control strategy for uncertain nonlinear systems," *IEEE Trans. Autom. Control*, Vol. 49, No. 7, pp. 1206-1211, 2004.

[125] H. Xu, and P. Ioannou. "Robust adaptive control for a class of MIMO nonlinear systems with guaranteed error bounds," *IEEE Trans. Autom. Control*, Vol. 48, No. 5, pp. 728-742, 2003.

[126] R. Yang and M. de Queiroz. "Adaptive control of the nonlinearly parameterized limb dynamics with application to neuromuscular electrical stimulation," *Proc. American Control Conf.*, pp. 4883-4888, Boston, MA, 2016.

[127] R. Yang and M. de Queiroz. "Adaptive control with concave/convex parameterization for an electrically stimulated human limb," *Proc. Cyber-Physical & Human-Systems*, pp. 189-194, Florianopolis, Brazil, 2016.

[128] R. Yang and M. de Queiroz. "Robust adaptive control of the nonlinearly parameterized human shank dynamics for electrical stimulation applications," *ASME J. Dyn. Sys., Meas., and Control*, under review.

[129] X. Ye and J. Jiang. "Adaptive nonlinear design without a priori knowledge of control directions," *IEEE Transactions on Automatic Control*, Vol. 43, No. 11, pp. 1617-1621, 1998.

[130] A. Yesildirek, and F. Lewis. "Feedback linearization using neural networks," *Automatica*, Vol. 31, No. 11, pp. 1659-1664, 1995.

[131] K. Yokoi, N. Hung, H. Tuan, and S. Hosoe. "Adaptive control design for nonlinearly parametrized systems with a triangular structure," *Asian J. Control*, Vol. 9, No. 2, pp. 121-132, 2007.

[132] F. Zajac. "Muscle and tendon: Properties, models, scaling, and application to biomechanics and motor control," *Critical Reviews in Biomedical Engineering*, Vol. 17, No. 4, pp. 359-410.

[133] T. Zhang, S.S. Ge, and C.C. Huang. "Design and performance analysis of a direct adaptive controller for nonlinear systems," *Automatica*, Vol. 35, pp. 1809-1817, 1999.

[134] T. Zhang, S.S. Ge, C.C. Hang, "Adaptive neural network control for strict-feedback nonlinear systems using backstepping design," *Automatica*, Vol. 36, pp. 1835-1846, 2000.

[135] Y. Zheng, H. Hemami, and B. Stokes. “Muscle dynamics, size principle, and stability,” *IEEE Trans. Biomed. Eng.*, Vol. 31, pp. 489-497, 1984.

[136] Y. Zhong. “Globally stable adaptive system design for minimum phase SISO plants with input saturation,” *Automatica*, Vol. 41, No. 9, pp. 1539-1547, 2005.

[137] Q. Zhou, P. Shi, Y. Tian, and M. Wang. "Approximation-based adaptive tracking control for MIMO nonlinear systems with input saturation," *IEEE Trans. Cybern.*, Vol. 45, No. 10, pp. 2119-2128, 2015.

[138] Q. Zhou, L. Wang, C. Wu, H. Li, and H. Du. "Adaptive fuzzy control for nonstrict-feecback systems with input saturation and output constraint," *IEEE Transactions on Syst., Man, and Cybern.: Systems*, Vol. 47, No. 1, pp. 1-11, 2017.

Appendix A Lipschitz Bounding Functions

The calculation of the Lipschitz bounding functions $L_i(x_i)$, $i = 1, 2, 3$ is provided next. They are calculated by exploiting the convexity/concavity of the functions $f_i(x_i, \lambda_i)$ with respect to λ_i. For brevity, we only present the full derivation of $L_1(x_1)$. The other Lipschitz bounding functions can be derived using similar arguments.

Given that $f_1(x_1, \lambda_1) = f_1(q, k_2) = -q \exp(-k_2 q)$ is continuous and differentiable on some $\Theta_1 = [k_{2\min}, k_{2\max}]$, we can use the Mean Value Theorem to write

$$|f_1(q, k_2) - f_1(q, k_{2\min})| = \left| \frac{\partial f_1}{\partial k_2}(q, c) \right| |k_2 - k_{2\min}|, \tag{A.1}$$

where $k_2 \in \Theta_1$ and $c \in (k_{2\min}, k_2)$. According to Definition 2, f_1 is concave for $q > 0$ and convex for $q < 0$ on Θ_1. When f_1 is concave, we know from (3.6) that

$$\frac{\partial f_1}{\partial k_2}(q, k_{2\min}) \geq \frac{\partial f_1}{\partial k_2}(q, c). \tag{A.2}$$

Since $\partial f_1 / \partial k_2 = q^2 \exp(-k_2 q) \geq 0$ for all q and all $k_2 \in \Theta_1$, we have that

$$|f_1(q, k_2) - f_1(q, k_{2\min})| \leq \frac{\partial f_1}{\partial k_2}(q, k_{2\min}) |k_2 - k_{2\min}|. \tag{A.3}$$

Therefore, from (3.1), we can pick

$$L_1(q) = \frac{\partial f_1}{\partial k_2}(q, k_{2\min}). \tag{A.4}$$

When f_1 is convex, we know from (3.5) that

$$\frac{\partial f_1}{\partial k_2}(q, c) \leq \frac{\partial f_1}{\partial k_2}(q, k_{2\max}) = L_1(q). \tag{A.5}$$

When $q = 0$, since

$$\lim_{q \to 0^+} \frac{\partial f_1}{\partial k_2}(q, k_{2\min}) = \lim_{q \to 0^-} \frac{\partial f_1}{\partial k_2}(q, k_{2\max}) = 0, \tag{A.6}$$

the continuity of $L_1(q)$ is ensured.

Summarizing the above discussion, $L_1(q)$ can be calculated as follows

$$L_1(q) = \begin{cases} q^2 \exp\left(-k_{2\,\min} q\right) \text{ for } q > 0 \\ q^2 \exp\left(-k_{2\,\max} q\right) \text{ for } q \leq 0. \end{cases} \tag{A.7}$$

Similarly, we have that

$$L_2(q) = \begin{cases} q \exp\left(-k_{4\,\min} q\right) \text{ for } q > 0 \\ -q \exp\left(-k_{4\,\max} q\right) \text{ for } q \leq 0 \end{cases} \tag{A.8}$$

and

$$L_3(\dot{q}) = \begin{cases} \dot{q}\text{sech}^2\left(b_{3\,\min} \dot{q}\right) \text{ for } \dot{q} > 0 \\ -\dot{q}\text{sech}^2\left(b_{3\,\min} \dot{q}\right) \text{ for } \dot{q} \leq 0. \end{cases} \tag{A.9}$$

Appendix B Proof of Corollary 3

We only show the proof for the case of the convex function since the concave function proof follows from similar arguments. For any C^1 function $f(\lambda) : \mathbb{R} \to \mathbb{R}$ that is convex on $\Theta = [\lambda_{\min}, \lambda_{\max}]$ and for any $\lambda \in \Theta$, the following relation holds due to the Mean Value Theorem:

$$f'(\bar{\lambda}) = \frac{f(\lambda) - f(\lambda_{\min})}{\lambda - \lambda_{\min}} \quad \text{and} \quad f'(\breve{\lambda}) = \frac{f(\lambda_{\max}) - f(\lambda)}{\lambda_{\max} - \lambda}. \tag{B.1}$$

where $\bar{\lambda} \in (\lambda_{\min}, \lambda)$ and $\breve{\lambda} \in (\lambda, \lambda_{\max})$. From (3.5) and the facts that $\lambda - \lambda_{\min} \geq 0$ and $\lambda_{\max} - \lambda \geq 0$, we have

$$\begin{aligned} (\lambda - \lambda_{\min}) f'(\bar{\lambda}) &\geq (\lambda - \lambda_{\min}) f'(\lambda_{\min}) \\ (\lambda_{\max} - \lambda) f'(\breve{\lambda}) &\geq (\lambda_{\max} - \lambda) f'(\lambda_{\min}). \end{aligned} \tag{B.2}$$

After combining (B.1) and (B.2), we arrive at (3.7).

Vita

Ruzhou Yang was born in Cixi, Zhejiang Province, China. He received his bachelor's degree in mechanical engineering from Southwest Jiao Tong Unversity, China in 2011. In 2012, he entered the Mechanical Engineering Ph.D program at Louisiana State University as a direct Ph.D. student.